GREEN NANOCOMPOSITE HYDROGELS AS NOVEL MATERIALS FOR INVESTIGATION OF TOXIC DYES AS ENVIRONMENTAL POLLUTANTS

Thesis Submitted for the Award of the Degree of

DOCTOR OF PHILOSOPHY

in

Forensic Sciences

By

Anuradha

Registration Number: 12020483

Supervised By
Dr. Tejasvi Pandey (25999)
Department of Forensic science (Head of Department)
Assistant Professor



LOVELY PROFESSIONAL UNIVERSITY, PUNJAB 2025

DECLARATION

I, hereby declared that the presented work in the thesis entitled "Green nanocomposite

hydrogels as novel materials for investigation of toxic dyes as environmental

pollutants" in fulfilment of degree of Doctor of Philosophy (Ph. D.) is outcome of

research work carried out by me under the supervision of Dr. Tejasvi Pandey, working

as Assistant Professor, in the Department of Forensic Science, School of

Bioengineering and Biosciences of Lovely Professional University, Punjab, India. In

keeping with general practice of reporting scientific observations,

acknowledgements have been made whenever work described here has been based on

findings of other investigator. This work has not been submitted in part or full to any

other University or Institute for the award of any degree.

Juraella

(Signature of Scholar)

Name of the scholar: Anuradha

Registration No.: 12020483

Department/school: Department of Forensic science, School of Bioengineering and

Biosciences

Lovely Professional University,

Punjab, India

i

CERTIFICATE

This is to certify that the work reported in the Ph. D. thesis entitled "Green

nanocomposite hydrogels as novel materials for investigation of toxic dyes as

environmental pollutants" submitted in fulfillment of the requirement for the award of

degree of **Doctor of Philosophy** (Ph.D.) in the Department of Forensic Science, School

of Bioengineering and Biosciences is a research work carried out by Anuradha,

12020483, is bonafide record of his/her original work carried out under my supervision

and that no part of thesis has been submitted for any other degree, diploma or equivalent

course.

(Signature of Supervisor)

Name of supervisor: Dr. Tejasvi Pandey

Designation: Assistant Professor

Department/school: Department of Forensic science, School of Bioengineering and

Biosciences

University: Lovely Professional University

ii

ABSTRACT

This study presents the design, synthesis, characterization, and application of green nanocomposite hydrogels as innovative materials for the remediation of toxic dyes from aqueous environments. Environmental pollution from synthetic dyes poses a serious threat to water resources, necessitating sustainable remediation technologies. This work aimed to develop green nanocomposite hydrogels as novel adsorbent materials for the removal of toxic dye pollutants from aqueous solutions. A renewable plant-based polysaccharide, Butea monosperma gum (BM), was utilized as the natural polymer matrix to impart biodegradability and abundant functional groups, while a synthetic poly(ethylene glycol) (PEG) matrix provided a performance baseline for comparison. The research focused on grafting acrylic acid (AA) onto these backbones and crosslinking them into three-dimensional networks. A rapid, microwave-assisted polymerization route was employed as a green alternative to conventional thermal and chemical (redox) initiation methods, guided by the hypothesis that microwave irradiation would enhance grafting efficiency and hydrogel performance by providing rapid, uniform heating, notably reducing reaction times to mere seconds compared to the several hours required by conventional methods. The scope of the study also encompassed comparing the microwave technique with traditional polymerization routes to evaluate improvements in network formation, swelling capacity, and adsorption efficacy. It was further hypothesized that incorporating zinc oxide (ZnO) nanoparticles into the hydrogel matrix would yield hydrogel nanocomposites with superior adsorption of anionic dyes due to increased surface area and additional binding interactions.

Methodologically, BM-g-poly(AA) and PEG-g-poly(AA) hydrogels were synthesized under various conditions to optimize their structure and properties. Key parameters (monomer, initiator, cross-linker concentrations, and reaction time) were systematically varied, and the resulting swelling capacity (%Ps) of each hydrogel was measured to identify optimal formulation conditions. The microwave approach enabled hydrogel formation in as little as 40–120 seconds, in contrast to the 5–6 hours required for analogous thermal and redox processes, underscoring its efficiency and energy savings. The optimized BM-based hydrogel achieved a swelling degree of approximately 448%,

markedly higher than the maximum ~312% swelling obtained via conventional thermal polymerization and ~278% via redox initiation under similar formulations. In contrast, the optimized PEG-based hydrogel showed a lower maximum swelling of about 246%, highlighting the superior water absorbency of the natural BM gum network over the synthetic PEG. Notably, introduction of ZnO nanoparticles into the hydrogel matrices further enhanced water uptake. The ZnO-BM-g-poly(AA) nanocomposite exhibited an impressive ~515% swelling at optimal conditions, while the ZnO-PEG-g-poly(AA) counterpart reached ~280%. These enhancements are attributed to the hydrophilicity of ZnO and its strong hydrogen-bonding and electrostatic interactions with the polymer network, which increase free volume and water affinity. Overall, the microwave-synthesized hydrogels displayed significantly higher swelling capacities than those produced by conventional methods, confirming the advantage of the green microwave approach in creating highly superabsorbent networks.

Comprehensive characterization verified the successful fabrication of the hydrogels and nanocomposites. Fourier-transform infrared (FTIR) spectroscopy confirmed effective grafting of AA onto both BM and PEG backbones, with new peaks for carbonyl (C=O) groups around 1700 cm⁻¹ and other characteristic bonds, as well as Zn–O vibration bands (≈400–600 cm⁻¹) in the nanocomposites. Thermogravimetric analysis (TGA) revealed improved thermal stability in the ZnO-containing hydrogel nanocomposites compared to the neat hydrogels, evidenced by reduced weight loss at elevated temperatures due to the presence of thermally stable ZnO nanoparticles. X-ray diffraction (XRD) patterns showed the BM gum to be largely amorphous, whereas the incorporation of crystalline ZnO imparted semi-crystalline character to the nanocomposite (displaying ZnO's oval phase peaks). Field-emission scanning electron microscopy (FE-SEM) illustrated the morphological transformation from the smooth, amorphous surface of raw BM gum to a cross-linked porous network in the BM-gpoly(AA) hydrogel, and further confirmed the formation of a well-distributed nanocomposite structure upon ZnO addition. Discrete ZnO nanoparticles (nanometersized, oval structures) were observed embedded within the hydrogel matrix, contributing to a rougher, globular morphology relative to the base hydrogel. Collectively, these analyses substantiated the formation of interpenetrating polymer

networks and the successful integration of nanoparticles, validating the proposed synthesis strategies.

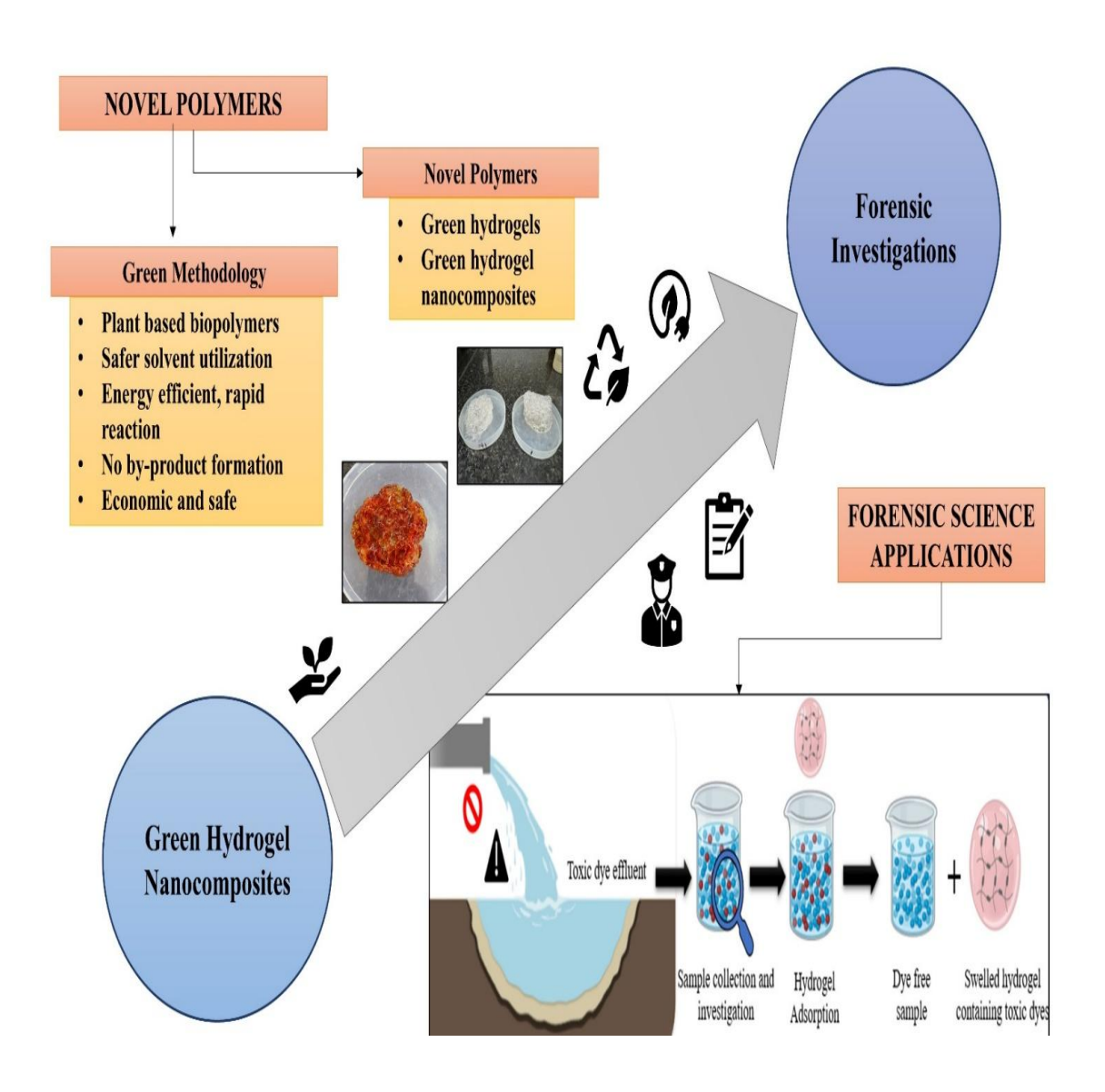
The adsorption performance of the synthesized materials was evaluated using two model azo dyes, Amaranth (AR) and Methyl Orange (MO), which are common toxic anionic pollutants in wastewater. Batch adsorption experiments investigated the effects of contact time, initial dye concentration, pH, and adsorbent dosage on removal efficiency. Owing to their high swelling and abundance of functional groups (-COOH from poly(AA) and hydroxyls from BM), the hydrogels rapidly absorbed water and facilitated diffusion of dye molecules into the network. The BM-g-poly(AA) hydrogel achieved appreciable dye uptake, with Amaranth removal increasing from ~48% to ~78% as the dye concentration rose from 6 to 10 mg/L. At optimal conditions (nearneutral pH ~7 and sufficient contact time), the hydrogel removed up to 77–84% of the dyes from solution. The ZnO-BM-g-poly(AA) nanocomposite, however, consistently outperformed the base hydrogel. It reached ~87% removal of Amaranth at 10 mg/L initial concentration and maintained high efficiency (~85-89%) even at higher concentrations up to 14 mg/L. Similarly, for Methyl Orange, the nanocomposite showed a maximum removal of about 89-90% under optimal pH and contact time, surpassing the ~84% maximum by the hydrogel. The enhanced dye uptake by the nanocomposite is ascribed to the increased surface area and active sites provided by the embedded ZnO nanoparticles, which promote stronger dye binding (via hydrogen bonding, coordination to Zn²⁺, and electrostatic attraction) compared to the hydrogel alone. Kinetic studies indicated that the nanocomposite also adsorbed dyes at a faster rate, attaining equilibrium removal more rapidly than the non-nanocomposite hydrogel, likely due to more efficient diffusion and binding site accessibility. Both materials exhibited pH-dependent behaviour, with optimum adsorption at pH~7 where electrostatic interactions between the negatively charged dye molecules and the protonated polymer network are most favorable; more acidic or alkaline conditions led to decreased removal due to either reduced dye affinity or competition with counterions. These results demonstrate that the green-synthesized hydrogels, particularly the ZnO nanocomposite, are highly effective in sequestering toxic anionic dyes from water.

In summary, this thesis presents a comprehensive investigation of green nanocomposite hydrogels as efficient adsorbents for environmental dye pollutants. The research successfully met its objectives by establishing a microwave-assisted synthesis route for natural gum-based and synthetic polymer-based hydrogels, and by demonstrating that this route yields materials with superior swelling and adsorption capabilities compared to conventional methods. The ZnO-incorporated BM hydrogel emerged as a particularly promising material, achieving near-complete dye removal (~90%) in both Amaranth and Methyl Orange tests. The findings provide insight into the mechanisms of free-radical grafting and nanoparticle-polymer interactions that underpin the enhanced performance, highlighting how a biopolymer matrix and inorganic nanoparticles can synergistically improve water remediation efficacy. The novelty of this work lies in the combination of a sustainable plant-derived polymer, an eco-friendly fabrication technique, and nanotechnology to create high-performance adsorbents. These outcomes contribute to knowledge by offering a viable green material platform for wastewater treatment and for detecting of illegal toxic dyes that can be utilized for forensic purposes, demonstrating that microwave-synthesized BM-based hydrogel nanocomposites can serve as robust and effective agents for removing toxic dyes. Furthermore, the use of a naturally derived polymer and a solvent-based, initiatordriven microwave process aligns with green chemistry principles, potentially reducing secondary pollution and providing a more sustainable solution than conventional adsorbents.

Overall, this study establishes microwave-assisted green nanocomposite hydrogels particularly those based on *Butea monosperma* (BM) gum as highly efficient and ecofriendly adsorbents for the remediation of hazardous dyes. This aligns with the goals of sustainable materials development for environmental protection and extends to the forensic detection and removal of illegal dyes, thereby highlighting the multidisciplinary significance of the work.

Keywords: Hydrogel, nanocomposite, forensic dyes, adsorption kinetics.

GRAPHICAL ABSTRACT



ACKNOWLEDGMENT

The journey of completing a doctoral thesis is never a solitary endeavour. It is the product of intellectual collaboration, emotional resilience, and the unwavering presence of those who walk beside you, often quietly, yet impactfully. With immense humility and gratitude, I wish to acknowledge all those who have contributed to the realization of this work.

I extend sincere appreciation to the academic and administrative leadership of **Dr. Ashok Kumar Mittal [Chancellor], Dr. Rashmi Mittal [Pro-Chancellor]** and **Dr Neeta Raj Sharma [Dean, School of Bioengineering and Biosciences]**. The environment of inquiry and collaboration, along with access to resources and facilities, was crucial to nurturing the ideas that eventually took shape in this thesis.

At the core of this academic voyage, I owe heartfelt thanks to my research mentor **Dr. Tejasvi Pandey [Head of Department]**, whose insightful guidance, critical perspectives, and steady encouragement provided the scaffolding for both my research and personal growth. Her thoughtful questions often led me to unexpected clarity, and her patience was the silent fuel that kept this project in motion.

I am deeply grateful to my best friends **Inderpal Devgon**, **Aditi Sharma** and **Simran Kauts** for the brainstorming sessions, for offering technical expertise, and for being part of this shared journey of discovery. Every conversation, challenge, and breakthrough has contributed to the texture of this work in ways words can scarcely capture.

To my grandparents Mr. Ram Murti Sandhu and Mrs. Surinder Kaur and parents Mr. Ramanjit and Mrs. Rajinder Kaur, I owe a debt of love that no acknowledgment can fully express. I would also thank my brothers Varun, Rahul, Sehaj, Prince and little sister Upasana whose faith in me remained unshaken, even when mine wavered. Their patience during the silences, their joy during small victories, and their strength during setbacks have been a quiet but vital undercurrent in this journey.

Lastly, I thank the divine presence of God that has been my silent companion in moments of stillness, struggle, and celebration. This work, while academic in form, is also a testament to perseverance, gratitude, and faith.

TABLE OF CONTENTS

CHAPTER	CHAPTER CONTENT	
		NO.
CHAPTER 1	INTRODUCTION	1-17
1.1	Hydrogels	1-4
1.2	Hydrogel nanocomposites	4-11
1.3	Forensic Applications of Hydrogels and Hydrogel Nanocomposites	11-17
CHAPTER 2	REVIEW OF LITERATURE	18-33
2.1	Today's World Green hydrogel nanocomposites	18-19
2.2	Historical Development of Hydrogels and Nanocomposite Hydrogels	19-24
2.3	Role of Green Natural Gums in Environmentally Friendly Hydrogels	24-27
2.4	Pollution by Dyes: Environmental and Forensic Perspectives	27-31
2.5	Advantages of Utilizing Green Nanocomposite Hydrogels	31-33
CHAPTER 3	RESEARCH OBJECTIVES AND HYPOTHESES	34-36
CHAPTER 4	MATERIALS AND METHODOLOGY	37-50
4.1	Materials	37-39
4.2	Methodology	40-50

CONFERENCES		
APPENDIX:	RESEARCH PUBLICATIONS AND	137-149
BIBLIOGRAP	122-136	
CHAPTER 6	SUMMARY AND CONCLUSION	117-121
5.6	Desorption studies	113-116
5.5	Adsorption kinetics	92-113
5.4	Instrumentational Analysis	82-92
5.3	Swelling and Optimization Studies	61-82
5.2	Hydrogel Nanocomposite Formation Mechanism	57-61
5.1	Natural hydrogel synthesis via Various routes	51-57
CHAPTER 5	RESULTS AND DISCUSSION	51-116
4.6	Desorption experiments	49-50
4.5	Adsorption kinetics	48-49
4.4	Instrumentation and Characterization	45-48
	hydrogel nanocomposites	
4.3	Swelling studies of synthesised hydrogels and	45
4.2.3	Hydrogel nanocomposite synthesis	43-45
4.2.2	Synthetic hydrogel Synthesis	42
4.2.1	Natural Hydrogel Synthesis Via Various Routes	40-42

LIST OF FIGURES

Sr. No.	Title	Page No.
Figure 1.1	Hydrogel classification	03
Figure 1.2	Hydrogels in forensic science	17
Figure 4.1	A schematic for hydrogel preparation	41
Figure 4.2	Schematic of hydrogel nanocomposite formation	44
Figure 5.1	Synthesized BM-g-poly(AA) hydrogel	52
Figure 5.2	Process of chain initiation, propagation and termination	53
	during formation of hydrogel	
Figure 5.3	Bond Formation during Radical polymerization	54
Figure 5.4	Hydrogel formed via Thermal polymerization	55
Figure 5.5	Hydrogel formed via Chemical (redox) initiation	56
Figure 5.6	Synthesized PEG-g-poly(AA) hydrogel	57
Figure 5.7	Prepared ZnO nanoparticles	57
Figure 5.8	ZnO-BM-g-poly (AA) hydrogel nanocomposite	59
Figure 5.9	ZnO-PEG-g-poly(AA) hydrogel nanocomposites	60
Figure 5.10	Variation in swelling percentage (%P) with respect to (A)	66-67
	Initiator concentration, (B) Solvent, (C) Monomer, (D)	
	Cross-linker and (E) Time of BM-g-poly (AA) hydrogel	
Figure 5.11	Optimized reaction conditions with maximum %P for	71
	ZnO-BM-g-poly-(AA) hydrogel nanocomposite	
Figure 5.12	Swelling studies for hydrogel nanocomposite	71

Figure 5.13	Variation in swelling percentage (%P) with respect to (A) Initiator concentration, (B) Solvent, (C) Monomer, (D) Cross-linker and (E) Time of PEG-g-poly (AA) hydrogel	78-79
Figure 5.14	Optimized reaction conditions with maximum %P for ZnO-PEG based hydrogel nanocomposite	81
Figure 5.15	X-ray diffraction pattern of BM gum, ZnO nanoparticles, BM-g-poly (AA) hydrogel, ZnO-BM-g-poly (AA) hydrogel nanocomposite, PEG-g-poly (AA) hydrogel and ZnO-PEG-g-poly(AA) hydrogel nanocomposite	83-84
Figure 5.16	FTIR-spectra of BM gum, ZnO nanoparticles, BM-g-poly (AA) hydrogel, ZnO-BM-g-poly (AA) hydrogel nanocomposite, PEG-g-poly (AA) hydrogel and ZnO-PEG-g-poly(AA) hydrogel nanocomposite	87-88
Figure 5.17	Thermogravimetric analysis	89
Figure 5.18	FE-SEM micrographs of a) BM gum, b) BM-g-poly (AA) hydrogel, c) ZnO-BM-g-poly (AA) hydrogel nanocomposite, d) ZnO nanoparticles and e) ZnO-PEG-g-poly (AA) nanocomposite.	90-91
Figure 5.19	Standard curve of Amaranth absorption in U.V spectrophotometer	93
Figure 5.20	Standard curve of Methyl orange absorption in U.V spectrophotometer	94
Figure 5.21	Amaranth removal efficiency of hydrogel and nanocomposite with respect to time	97
Figure 5.22	Amaranth removal efficiency of hydrogel and nanocomposite with respect to Adsorbent Dosage	99

Figure 5.23	Amaranth removal efficiency of hydrogel and	101
	nanocomposite with respect to pH	
Figure 5.24	Amaranth removal efficiency of hydrogel and	103
	nanocomposite with respect to Initial concentration	
Figure 5.25	MO removal efficiency of hydrogel and nanocomposite	106
	with respect to time	
Figure 5.26	MO removal efficiency of hydrogel and nanocomposite	108
	with respect to pH	
Figure 5.27	MO removal efficiency of hydrogel and nanocomposite	110
	with respect to Adsorbent dosage	
Figure 5.28	MO removal efficiency of hydrogel and nanocomposite 112	
	with respect to initial concentration	
Figure 5.29	Desorption of Amaranth and methyl orange from ZnO-	116
	BM-g-poly(AA) hydrogel nanocomposite	

LIST OF TABLES

Table No.	Title	Page No.
Table 1.1	Hydrogels and their application in forensic sciences	15-17
Table 4.1	Materials used for the preparation of hydrogels and	38-39
	nanocomposites	
Table 5.1	Initiator optimization of natural hydrogel	61
Table 5.2	Solvent optimization of natural hydrogel	62
Table 5.3	Monomer Optimization of natural hydrogel	63
Table 5.4	Cross-linker optimization of natural hydrogel	64
Table 5.5	Time of reaction optimization of natural hydrogel	65
Table 5.6	Optimized swelling of Natural Hydrogel Synthesized via	69
	different routes	
Table 5.7	Optimized reaction conditions for ZnO-BM-g-poly-(AA)	70
	hydrogel nanocomposite	
Table 5.8	Initiator optimization of synthetic hydrogel	72
Table 5.9	Solvent optimization of synthetic hydrogel	73
Table 5.10	Monomer Optimization of synthetic hydrogel	74
Table 5.11	Cross-linker optimization of synthetic hydrogel	75
Table 5.12	Time of reaction optimization of synthetic hydrogel	77
Table 5.13	Optimized reaction conditions for ZnO-PEG-poly (AA)	80
	hydrogel nanocomposite	
Table 5.14	Standard working solutions for AR	92

Table 5.15	Standard working solutions for MO	93
Table 5.16	Amaranth removal efficiency of hydrogel with respect to time	95
Table 5.17	Amaranth removal efficiency of nanocomposite with respect to time	96
Table 5.18	Amaranth removal efficiency of hydrogel with respect to dosage	98
Table 5.19	Amaranth removal efficiency of nanocomposite with respect to dosage	99
Table 5.20	Amaranth removal efficiency of hydrogel with respect to pH	100
Table 5.21	Amaranth removal efficiency of nanocomposite with respect to pH	101
Table 5.22	Amaranth removal efficiency of hydrogel with respect to initial concentration	102
Table 5.23	Amaranth removal efficiency of nanocomposite with respect to initial concentration	103
Table 5.24	Methyl orange removal efficiency of hydrogel with respect to time	104
Table 5.25	Methyl orange removal efficiency of nanocomposite with respect to time	105
Table 5.26	Methyl orange removal efficiency of hydrogel with respect to pH	107
Table 5.27	Methyl orange removal efficiency of nanocomposite with respect to pH	107

Table 5.28	Methyl orange removal efficiency of hydrogel with respect to dosage	109
Table 5.29	Methyl orange removal efficiency of nanocomposite with respect to dosage	109
Table 5.30	Methyl orange removal efficiency of hydrogel with respect to initial concentration	111
Table 5.31	Methyl orange removal efficiency of nanocomposite with respect to initial concentration	112
Table 5.32	Screening of different desorbing media for AR and MO loaded ZnO-BM-g-poly(AA) hydrogel nanocomposite	113
Table 5.33	Desorption of Amaranth (AR) from ZnO–BM-g-poly(AA) hydrogel nanocomposite	114
Table 5.34	Desorption of Methyl Orange (MO) from ZnO–BM-g-poly(AA) hydrogel nanocomposite	115

CHAPTER 1 INTRODUCTION

1.1 Hydrogels

Hydrogels are hydrophilic polymeric materials characterized by a three-dimensional cross-linked network capable of absorbing and retaining large volumes of water or biological fluids without dissolving. Their high water content and soft, elastic nature make them structurally and functionally similar to natural tissue, rendering them highly suitable for a broad spectrum of scientific and technological applications. The hydrophilicity of hydrogels arises from the presence of functional groups such as hydroxyl (–OH), carboxyl (–COOH), amide (–CONH₂), amine (–NH₂), sulfonic acid (–SO₃H), and other polar moieties along the polymer backbone. This affinity for water is further enhanced by osmotic pressure and capillary effects, which facilitate fluid uptake and retention. Despite their high swelling capacity, hydrogels maintain structural integrity due to crosslinking within the polymer matrix, which prevents dissolution and supports network expansion (Ullah et al., 2015; Madduma-Bandarage et al., 2021).

The origin of hydrogel research dates back to the 1960s, with the first synthetic hydrogel, poly(2-hydroxyethyl methacrylate) (PHEMA), being developed for biomedical use. Since then, significant advances in polymer chemistry have led to the design of a wide range of hydrogels with tailored properties. Hydrogels are typically classified based on their origin (natural or synthetic), crosslinking mechanism (physical or chemical), and responsiveness to environmental stimuli (conventional or smart hydrogels). Natural hydrogels are derived from polysaccharides and proteins such as starch, guar gum, cellulose, alginate, chitosan, psyllium, gelatin, and hyaluronic acid (Gyles et al., 2017). These biopolymers are favored for their biocompatibility, biodegradability, and low toxicity. In contrast, synthetic hydrogels, fabricated from polymers such as poly(acrylamide) (PAAm), poly(ethylene glycol) (PEG), poly(vinyl alcohol) (PVA), and poly(acrylic acid) (PAA), offer precise control over physicochemical properties and are often used when mechanical strength or reproducibility is critical (Madduma-Bandarage et al., 2021).

Crosslinking plays a fundamental role in determining the mechanical and functional characteristics of hydrogels. Physical crosslinking relies on non-covalent interactions

such as hydrogen bonding, ionic interactions, crystallization, and entanglements, which are reversible and environmentally sensitive. Chemical crosslinking, on the other hand, involves covalent bond formation between polymer chains using crosslinking agents like glutaraldehyde, formaldehyde, or N,N'-methylenebisacrylamide (BIS), resulting in permanent network structures with higher mechanical stability and resistance to degradation. The choice of crosslinking method is guided by the intended application, with chemically crosslinked hydrogels being more suited for load-bearing biomedical implants, while physically crosslinked hydrogels are advantageous in drug delivery systems where reversibility and environmental responsiveness are desired (Xiang et al., 2021). Different types of hydrogels are shown in figure 1.1.

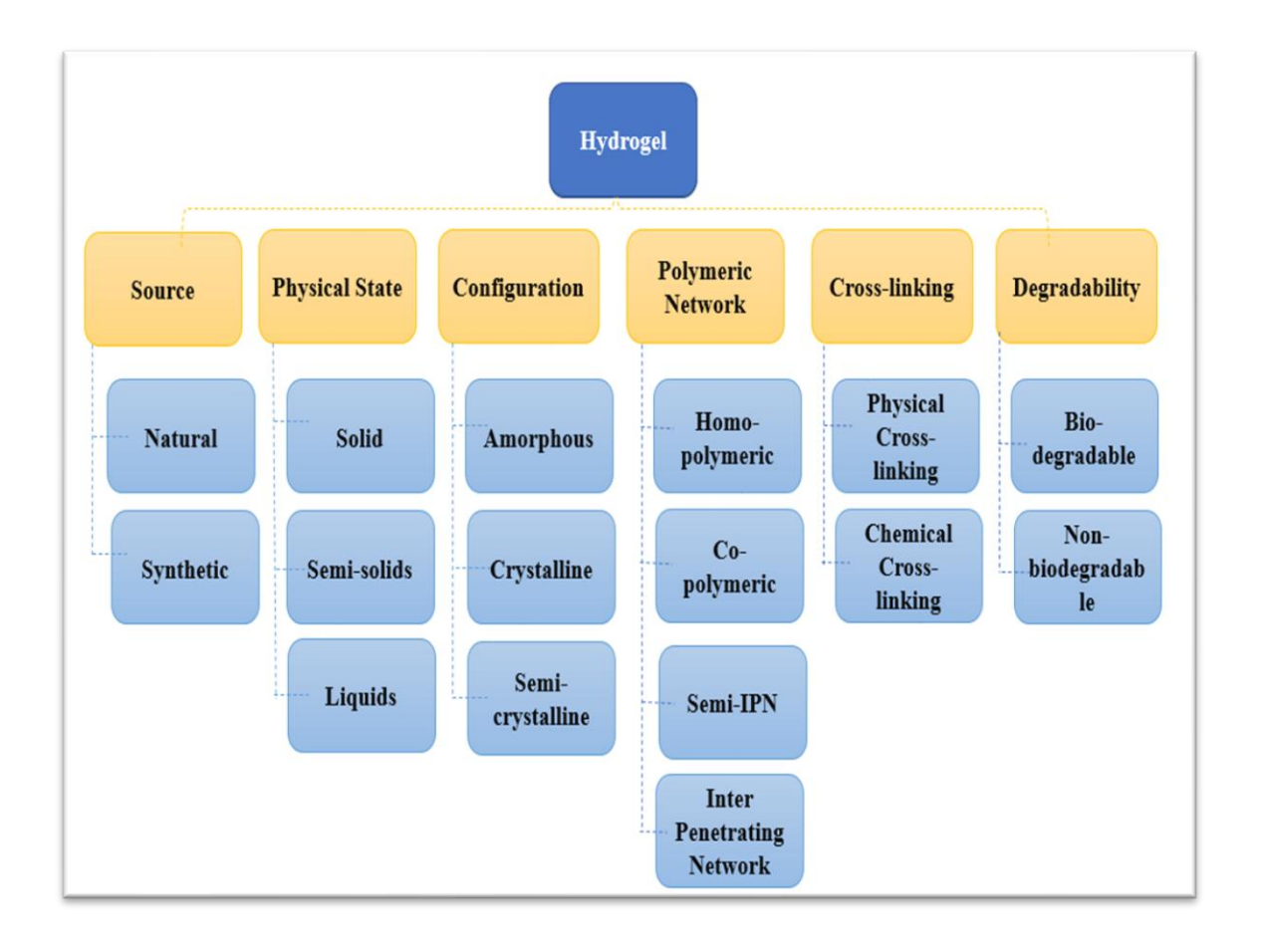


Figure 1.1: Hydrogel classification

Hydrogels have found widespread significance in diverse scientific fields. In biomedicine, they serve as wound dressings, drug delivery vehicles, surgical sealants, tissue engineering scaffolds, and biosensors due to their excellent biocompatibility and tunable properties. In agriculture, hydrogels function as soil conditioners and controlled-release carriers for fertilizers and pesticides, enhancing water retention and resource efficiency (Varaprasad et al., 2017). In environmental sciences, hydrogels are employed for water purification, heavy metal adsorption, and dye removal due to their high porosity, absorbency, and customizable surface chemistry. Furthermore, smart hydrogels, which respond to stimuli such as pH, temperature, ionic strength, or light, are being extensively studied for next-generation applications in responsive drug release, soft robotics, and bio-actuators (Deng et al., 2021).

Notably, the application of hydrogels in environmental forensics has garnered attention, especially for addressing complex contamination problems. For example, superabsorbent hydrogels have been employed to sequester toxic dyes from textile effluents and to capture explosive residues like picric acid, which are otherwise persistent in aquatic ecosystems. Their biocompatibility, affordability, and reusability make them sustainable alternatives to conventional remediation tools (Kaith et al., 2012; Priya et al., 2020).

Hydrogels represent a highly versatile and dynamic class of materials with profound implications across multiple scientific domains. Their design, governed by the interplay between polymer selection, crosslinking strategy, and network architecture, allows for the creation of application-specific solutions ranging from biomedical devices to environmental remediation technologies. As research continues to advance, hydrogels are poised to play an increasingly pivotal role in addressing complex biological, environmental, and industrial challenges.

1.2 Hydrogel nanocomposites

Hydrogel nanocomposites are an emerging class of multifunctional materials that synergistically integrate the three-dimensional, hydrophilic polymeric network of hydrogels with nanoscale fillers to enhance and expand their physicochemical and biological performance. The convergence of hydrogel matrices with nanomaterials results in hybrid systems that exhibit superior mechanical integrity, tailored responsiveness to environmental cues, and a broadened spectrum of functional applications. These materials have increasingly attracted attention due to their dynamic

behavior, tunability, and biocompatibility, making them suitable for interdisciplinary applications ranging from regenerative medicine to soft robotics and environmental monitoring (Kabiri et al., 2011).

One of the central advantages of hydrogel nanocomposites lies in their tunable structural characteristics and improved mechanical properties. While conventional hydrogels often suffer from brittleness, low tensile strength, and poor load-bearing capacity, the integration of nanoscale reinforcements significantly ameliorates these deficiencies. Nanomaterials such as graphene oxide, carbon nanotubes, silica nanoparticles, and nano clays can form physical or chemical interactions with the hydrogel polymer chains, resulting in improved elasticity, compressive strength, and toughness. These improvements are critical in applications such as tissue engineering, where scaffolds must mimic the mechanical properties of native tissues (Radia et al., 2024).

In addition to mechanical reinforcement, hydrogel nanocomposites offer enhanced responsiveness to external stimuli, enabling the development of "smart" materials. Stimuli-responsive nanomaterials can imbue the hydrogel with the ability to undergo reversible physical or chemical changes in response to specific environmental triggers. For example, thermoresponsive nanogels can expand or contract with temperature changes, while pH-responsive nanoparticles can alter the swelling behavior of the hydrogel in different biological environments. These adaptive responses are highly desirable for applications in targeted drug delivery, biosensing, and actuators in soft electronics (Cha et al., 2020; Abdollahi et al., 2024).

Moreover, the functionalization of hydrogel nanocomposites extends to their surface chemistry and biological interactions. Nanomaterials can be engineered to provide specific biological cues or to interact selectively with cells, proteins, or nucleic acids. This level of control enables applications in bio adhesion, cell proliferation, and gene therapy (Bakhshi et al., 2024). For instance, nanocomposites incorporating magnetic nanoparticles can be externally guided using magnetic fields, allowing for spatially controlled drug release or the remote modulation of biological processes in vivo.

Environmental applications of hydrogel nanocomposites are also expanding rapidly. Their high water retention capacity and porous structure, combined with the adsorptive properties of embedded nanomaterials, make them ideal for removing heavy metals, dyes, and organic pollutants from aqueous systems. Functionalized nanocomposites can also act as selective sensors for detecting environmental contaminants, leveraging the optical or electrochemical responsiveness of the nanofillers (Moharrami et al., 2020; Kumar et al., 2023).

Overall, hydrogel nanocomposites represent a significant advancement in materials science, offering a versatile platform for innovation across multiple domains. Their design can be precisely tailored through the choice of nanofillers, crosslinking strategies, and polymer backbones, allowing for the development of application-specific solutions. Continued interdisciplinary research in nanotechnology, polymer science, and biomedical engineering is expected to unlock the full potential of these hybrid systems, positioning them as key materials in the future of smart and sustainable technologies.

1.2.1 Classification of hydrogel nanocomposites

Hydrogel nanocomposites can be broadly categorized based on the type of nanomaterial incorporated into the hydrogel matrix, the nature of interactions between the hydrogel and the nanofillers, and the intended functionality of the final material. These classifications reflect the diversity and tunability of hydrogel nanocomposites, which originate from the convergence of polymer chemistry, nanotechnology, and materials science. Their development was driven by the need to overcome the inherent limitations of traditional hydrogels, such as poor mechanical strength and limited functionality, while extending their utility to a wider array of advanced applications (Karchoubi et al., 2024).

1.2.1.1 Polymer-based Nanocomposite Hydrogels: These nanocomposites are formed by integrating nanostructured polymers such as dendrimers, hyperbranched polymers, or polymeric micelles into the hydrogel network. These nano polymers can enhance the mechanical stability and provide additional functionalities such as drug loading capacity or surface functionalization. The compatibility of polymeric

nanofillers with hydrogel matrices also facilitates homogeneous dispersion and synergistic interactions at the molecular level (Sofini et al., 2024).

- **1.2.1.2 Inorganic Nanoparticle-based Hydrogels:** This category includes hydrogels embedded with inorganic nanoparticles such as silver (Ag), gold (Au), titanium dioxide (TiO₂), zinc oxide (ZnO), and iron oxide (Fe₃O₄). These nanofillers introduce unique optical, magnetic, or antimicrobial properties to the hydrogel (Shabalina et al., 2024). For example, silver nanoparticles impart antimicrobial activity, making such hydrogels useful for wound healing and infection control. Magnetic nanoparticles, on the other hand, allow remote manipulation and magnetically guided drug delivery (Karchoubi et al., 2024).
- **1.2.1.3** Carbon-based Nanocomposite Hydrogels: Carbon nanomaterials such as graphene oxide (GO), carbon nanotubes (CNTs), and fullerenes are widely used in hydrogel nanocomposites due to their exceptional electrical conductivity, mechanical strength, and high surface area. These materials are particularly significant in biosensing, tissue engineering, and flexible electronics. The inclusion of carbon nanostructures enables the design of electroconductive hydrogels capable of interfacing with electrically active tissues such as nerves or cardiac muscle (Shin et al., 2024).
- **1.2.1.4 Clay-based Nanocomposite Hydrogels:** Clay minerals such as montmorillonite, laponite, or halloysite nanotubes serve as reinforcing agents that improve the rheological and mechanical properties of hydrogels. These nanoclays can form ionic or hydrogen bonds with the polymer network, resulting in enhanced viscosity, gelation behavior, and mechanical integrity. They are also used for their adsorptive properties in environmental remediation and controlled drug release systems (Huang et al., 2024).
- **1.2.1.5** Nanocellulose-based Hydrogels: Nanocellulose, including cellulose nanofibers (CNFs) and cellulose nanocrystals (CNCs), is a sustainable and biodegradable nanomaterial derived from plant biomass. Its incorporation into hydrogels improves mechanical strength, biocompatibility, and water retention capacity. Nanocellulose-based hydrogels are particularly significant in tissue

scaffolding, as they mimic the fibrous architecture of native extracellular matrices (Rana et al., 2024).

1.2.2 Origin and Development

The concept of hydrogel nanocomposites emerged in the early 2000s as a response to the limitations of traditional hydrogels, particularly in high-performance biomedical and engineering applications (Schexnailder et al., 2009). The inspiration stemmed from natural composite materials such as cartilage and bone, which achieve remarkable mechanical and functional properties through hierarchical structures that combine organic and inorganic components. By replicating this strategy at the nanoscale, researchers began to incorporate nanomaterials into hydrogels to produce composites with superior properties.

Advancements in nanotechnology, particularly the synthesis and functionalization of nanomaterials, played a pivotal role in the evolution of hydrogel nanocomposites. The availability of various nanofillers with well-defined size, shape, and surface chemistry enabled precise tailoring of composite properties (Shabalina et al., 2024). Concurrently, innovations in hydrogel design, including new polymerization techniques and crosslinking strategies, facilitated better integration and dispersion of nanomaterials within the hydrogel matrix.

1.2.3 Significance of Hydrogel Nanocomposites

The significance of hydrogel nanocomposites lies in their multifunctionality, tunability, and broad application scope. These materials address critical challenges in biomedicine, such as the need for biocompatible scaffolds with mechanical resilience, responsive drug delivery systems, and antimicrobial surfaces. In environmental science, hydrogel nanocomposites offer solutions for water purification, pollutant detection, and resource recovery. In soft robotics and wearable electronics, their flexibility, conductivity, and responsiveness to stimuli make them ideal for next-generation devices. Moreover, the interdisciplinary nature of hydrogel nanocomposite research fosters innovation at the intersection of biology, chemistry, materials science, and engineering. These materials are not merely improved hydrogels; they represent a paradigm shift toward intelligent,

adaptive, and multifunctional systems capable of performing complex tasks in real-world environments. Their continued development is poised to have a profound impact on healthcare, sustainability, and advanced manufacturing (Karchoubi et al., 2024).

1.2.4 Synthesis Strategies of Hydrogels and Hydrogel Nanocomposites

The synthesis of hydrogels and hydrogel nanocomposites is rooted in the controlled assembly of polymeric structures capable of retaining large quantities of water, with or without the integration of nanoscale materials. These synthetic processes are defined not only by the chemistry of the polymers and nanofillers but also by the specific physicochemical conditions employed to construct mechanically robust, responsive, and functionally versatile networks (Li et al., 2022). The selection of synthesis method profoundly influences the morphology, porosity, mechanical strength, and responsiveness of the final hydrogel. The principal synthesis strategies include (Qin et al., 2024):

- **1.2.4.1 Free Radical Polymerization (FRP):** This is the most conventional approach, wherein vinyl monomers such as acrylamide, acrylic acid, or methacrylates are polymerized using radical initiators like ammonium persulfate (APS) or potassium persulfate (KPS). A crosslinker, often N,N'-methylenebisacrylamide (BIS), is incorporated to bridge polymer chains and form a permanent network. The polymerization can occur in bulk, solution, or within molds, enabling design flexibility for thin films, beads, or bulk gels (More et al., 2024; Zhang et al., 2024).
- **1.2.4.2 Ionic Crosslinking:** Hydrogels based on natural polyelectrolytes such as alginate and chitosan can be formed through electrostatic interactions between oppositely charged species. For instance, divalent cations like Ca²⁺ ionically crosslink alginate chains, creating a network structure without the need for chemical reagents, which is advantageous for biocompatibility and in situ gelation (Ji et al., 2021).
- **1.2.4.3 Physical Crosslinking:** In this method, non-covalent forces such as hydrogen bonding, crystallization, host–guest interactions, or hydrophobic associations drive gel formation. These physically crosslinked hydrogels offer reversibility and stimuli-responsive behavior, making them ideal candidates for applications requiring controlled

sol-gel transitions, such as injectable systems or self-healing materials (Nasution et al., 2022).

1.2.4.4 Hydrogel Nanocomposite Synthesis: Integration of Nanostructures

Hydrogel nanocomposites are formulated by incorporating nanomaterials into hydrogel matrices to impart new functionalities or reinforce existing ones. The presence of nanoscale fillers can profoundly enhance properties such as mechanical strength, conductivity, antimicrobial activity, or environmental responsiveness. Their synthesis commonly follows one of several strategic methodologies (Barrett-Catton et al., 2021):

- **1.2.4.5 Direct Dispersion (Physical Blending):** Nanomaterials (e.g., carbon nanotubes, metal nanoparticles, nanoclays) are dispersed directly into the hydrogel precursor solution. Uniform dispersion is often aided by ultrasonication or high-shear mixing. This method is straightforward but may suffer from nanoparticle aggregation without appropriate surfactants or stabilizers (Sharma et al., 2021).
- **1.2.4.6** In Situ Nanoparticle Formation: This approach involves the generation of nanoparticles within the hydrogel network during or after gel formation. For example, metal ions can be reduced chemically in situ to form nanoparticles that are spatially confined within the gel. This method ensures homogenous nanoparticle distribution and enhances interfacial interactions between nanofillers and the hydrogel matrix (García Schejtman et al., 2022).
- **1.2.4.7 Layer-by-Layer (LbL) Assembly**: In this method, alternating layers of oppositely charged or functionally modified nanoparticles are sequentially adsorbed onto a pre-formed hydrogel surface. This allows for nanoscale precision in the spatial arrangement of functional layers, making it highly effective for sensor development or stimuli-responsive coatings (Ivanov et al., 2021).
- **1.2.4.8 Electrospinning-Assisted Integration:** Nanofibers embedded with nanoparticles are electro spun and subsequently embedded or hybridized with hydrogel matrices. This method produces fibrous nanocomposite structures with enhanced mechanical and structural integrity, especially relevant in scaffold fabrication for tissue engineering and drug delivery systems (Ghosh et al., 2021).

The final architecture and function of both hydrogels and hydrogel nanocomposites are heavily influenced by the fabrication techniques employed post-synthesis. Methods such as 3D bioprinting, microfluidic molding, freeze-thaw cycling, or lyophilization allow for customized structuring, porosity control, and spatial localization of nanocomponents (Cha et al., 2020). These features are crucial when designing materials for niche applications such as load-bearing tissue scaffolds, smart drug release platforms, or multifunctional biosensors.

In essence, the synthesis of hydrogels and their nanocomposites is a nuanced interplay between polymer chemistry, nanotechnology, and processing techniques. The polymerization mechanism, crosslinking strategy, and nanomaterial integration must be selected based on the desired structural and functional attributes of the final material (Ghosh et al., 2021).

1.3 Forensic Applications of Hydrogels and Hydrogel Nanocomposites

Hydrogels and hydrogel nanocomposites are emerging as versatile tools in forensic science, owing to their unique capacity to absorb and immobilize various substances. These soft, water-swollen polymer networks have found use in environmental forensics and food safety investigations, particularly for capturing dye-based contaminants, as well as in other areas ranging from trace evidence collection to sensor technologies.

1.3.1 Absorption of Textile and Food Dyes

One of the primary forensic applications of hydrogels is the adsorption of synthetic dyes, especially in environmental and food-related cases. Textile dyes (e.g. azo dyes) and food colorants can be significant pollutants or adulterants, and their presence often warrants forensic investigation. Many of these dyes are complex, highly water-soluble aromatic compounds that do not biodegrade easily (Blachnio et al., 2024).

They are widely used in industries such as textiles and food processing, leading to a high likelihood of environmental contamination in water bodies (Blachnio et al., 2024). In environmental forensics, hydrogel-based adsorbents can be deployed to capture dye pollutants from water samples, aiding in both remediation and the tracing of pollution sources. Traditional adsorbents like activated carbon have limitations (micropores

causing slow uptake of large dye molecules), whereas hydrogels can be engineered with mesoporous structures that enable faster diffusion and adsorption of bulky dye molecules .For instance, chitosan–silica composite hydrogels with tailored mesopores have been shown to rapidly uptake anionic azo dyes (like Acid Red 88 and Basic Red 46) from water, offering improved kinetics and capacity over conventional sorbents. Incorporating nanomaterials can further enhance performance; adding graphene oxide into an alginate hydrogel matrix, for example, markedly increases the surface area and mechanical stability of the hydrogel, boosting its dye uptake efficiency (Ferfera-Harrar et al., 2022).

In food forensic investigations, hydrogels similarly serve to extract or detect illicit dyes used in adulteration. A striking example is the use of a poly(vinyl alcohol) (PVA) hydrogel "slime" as a flexible sampling substrate for colorimetric detection of banned food dyes. Researchers demonstrated that a PVA hydrogel pad doped with plasmonic nanoparticles could be pressed onto a fruit's surface to collect and detect Sudan III dye (a toxic, non-permitted food colorant) via surface-enhanced Raman spectroscopy (SERS) (Gong et al., 2016).

This hydrogel-based SERS method enabled on-site identification of Sudan dye on tainted fruit peel at levels of only tens of parts per billion, even after several weeks. The ease of use (simply pressing the gel on the surface) and high sensitivity illustrate how hydrogel nanocomposites can function as forensic samplers for food safety, concentrating trace dyes for rapid analysis. Such applications underscore the value of hydrogels in both removing unwanted dyes from samples and preserving them for evidentiary analysis in environmental and food forensics (Gao et al., 2022).

Small cationic dyes such as Methylene Blue (blue spheres, MB) may bind via ion exchange or electrostatic interactions, while larger aromatic dyes (yellow spheres, e.g. Rhodamine B, Congo Red, Eosin Y) can chelate or coordinate with polymer functional groups, resulting in stronger chemisorption (Shi et al., 2022).

The effectiveness of hydrogels in absorbing dyes is attributable to several key physicochemical features. First, hydrogels possess a highly porous three-dimensional network that swells with water, providing a large internal surface area and numerous microenvironments for dye molecules to occupy. This high surface area and porosity create ample active sites for adsorption and facilitate diffusion of dye molecules into the matrix. Second, hydrogels can be imbued with various functional groups (depending on their polymer composition and cross-linkers) that interact with dye molecules. Functional moieties such as carboxylates (–COO⁻), sulfonates (–SO₃⁻), hydroxyls (–OH), and amines (–NH₂) on the polymer chains can bind dyes through hydrogen bonding, van der Waals forces, and electrostatic attractions. For example, a starch-based hydrogel functionalized with amino and phosphate groups showed enhanced uptake of cationic Methylene Blue due to additional hydrogen-bonding and ionic interactions with the dye (Akhtar et al., 2024).

In other cases, charged hydrogels act as ion-exchangers, sequestering oppositely charged dye ions from solution. Additionally, if a hydrogel nanocomposite contains aromatic or graphitic components (such as graphene or carbon nanotubes), it can engage in π – π stacking with aromatic dye molecules (Sethi et al., 2023), further strengthening adsorption. The combination of these mechanisms like extensive surface area, tailored porosity, and specific chemical interactions allows hydrogels to effectively capture a wide range of dye molecules. Notably, adsorption studies often find that dyes form monolayer coverage on hydrogel adsorbents following Langmuir-type isotherms, indicating strong affinity and saturable binding sites within the gel matrix (Blachnio et al., 2024)

1.3.2 Trace Evidence Collection

Hydrogels can be used to collect microscopic residues and particulates from crime scenes in a non-destructive manner. For example, a gelatin-based hydrogel swab has been developed to recover inorganic explosive residues (such as ammonium nitrate from post-blast debris) by applying the gel to a surface and peeling it off after gelling (Amaral et al., 2020).

The hydrogel encapsulates the residue, which can later be dissolved out and analyzed, offering an alternative to traditional solvent swabbing. Similarly, "soft" hydrogels have been utilized to lift trace evidence like gunshot residue or drug particles from delicate surfaces without damaging them, thereby preserving the evidence integrity.

1.3.3 Latent Fingerprint Development

In forensic fingerprinting, hydrogels provide novel means to visualize or analyze prints, especially on challenging substrates. Viscous hydrogel formulations (with high viscosity ≥2000 cP) have shown promise as green replacements for conventional fingerprint reagents on porous materials like paper, preventing diffusion of sweat components and thus preserving ridge details. Hydrogels can also serve as non-marking collection media for chemical constituents of fingerprints. For instance, cross-linkable dextran-methacrylate hydrogels can be cast over a fingerprint to absorb amino acids and other water-soluble fingerprint residues, which are then extracted for amino acid profiling via LC-MS. Importantly, this process does not visibly alter the print, so the same fingerprint can still be developed later (e.g. by cyanoacrylate fuming) for identification. Such techniques enhance the information yield from fingerprints by coupling chemical analysis with traditional pattern matching (van Helmond et al., 2019).

1.3.4 Drug and Toxin Detection

Hydrogels have gained traction as components of biosensors for illicit drugs and toxic chemicals. Owing to their biocompatibility and ability to incorporate recognition elements, hydrogel matrices are used in colorimetric and electrochemical sensor platforms. For example, hydrogel microparticles impregnated with reagents or nanoparticles can selectively absorb drugs from biological fluids and produce a detectable signal. A recent study demonstrated a wearable hydrogel-based SERS patch that could detect trace levels of a methamphetamine analogue in simulated sweat, showing the potential for on-site drug screening via an optical signal (Rosendo et al., 2023).

In another approach, molecularly imprinted hydrogels (polymers cast with target molecules as templates) have been designed to bind specific drugs or toxins, allowing their detection through changes in the hydrogel's swelling or optical properties. These hydrogel sensors can provide rapid, in-field screening tests for substances ranging from narcotics to environmental toxins.

1.3.5 Sensor Technology

More broadly, hydrogel nanocomposites serve as adaptable platforms in various forensic analytical devices. Their stimuli-responsive swelling behavior (e.g. responding to pH, temperature, or chemical binding) can transduce the presence of analytes into measurable signals. For instance, hydrogels incorporating conductive nanomaterials have been used in electrochemical sensors where the uptake of an explosive or poison changes the gel's electrical properties, triggering an alarm. Likewise, enzyme-loaded hydrogels have been employed in biosensors to detect metabolites (like alcohol or drugs) relevant to forensic toxicology, producing a color change or fluorescence in the presence of the target. In all these cases, the hydrogel provides a stable, inert matrix that can host sensing reagents and intimately interact with samples. This versatility has made hydrogels a foundation for developing portable forensic sensors that are sensitive, selective, and able to operate in situ (Rosendo et al., 2023).

Overall, the use of hydrogels and hydrogel nanocomposites in forensic science is a rapidly developing area. Their high absorbency and tunable chemistry make them ideal for capturing evidence from dyes in polluted water or tainted food, to trace residues and latent fingerprints at crime scenes. In tandem with these practical applications, a solid scientific understanding of how hydrogels interact with analytes (through surface area effects and functional group chemistry) guides the design of even more effective hydrogel-based forensic tools. As research progresses, we can expect hydrogels to play an increasingly prominent role in eco-friendly, innovative forensic techniques, improving both the detection of clandestine substances and the preservation of crucial evidence. Hydrogels prepared from green route and their applications in forensic have been discussed in table 1.1 and their importance in sustainable investigations in figure 1.2.

Table 1.1: Hydrogels and their application in forensic sciences (Sandhu et al., 2023)

Target Area	Green Hydrogels utilized	Forensic Applications

Nanotechnology	Cellulose, Chitin, Poly vinyl alcohol (PVA), alginate, nanofibers, nanorods, nanoparticles, quantum dots	 Data security Biometrics Nano-drug delivery Nano-forensic
Fingerprint technology	Chitosan, cellulose, alginate, DNA hydrogels, starch, xanthan gum, polyethylene glycol (PEG)	 Fingerprint development Collection Latent fingerprint detection Fingerprint spoofing
Trace evidence collection and detection	Gelatin, PVA, alginate, elastomer based,	 Gunshot residues, paint, glass, explosives detection Drugs and its metabolites Blood, saliva, semen, urine, sweat On-site detection
Dye removal	Sodium alginate, chitosan, polysaccharide, green aerogels, nanocrystalline cellulose	 Removal and detection of toxic food dyes Textile dyes detection Illegal adulterants detection Heavy metal absorption
Environmental forensic solutions	Chitosan, PVA, polyolefin, hydrocarbon based gels	 Detection of oil spills Chemical and petroleum spills Toxicants from natural water bodies and soil Tracking and detection
Sensing technology	Chitosan, quantum dots, nanoparticles, DNA	 Nitroaromatic explosive detection TNT, TNP, 4-NP, adenosine, glucose, metal ion sensing Target specific detection, quantification, sampling and sensing

Ballistic	Gelatin, amine, metal	Ballistic simulants
simulants	organic frameworks,	Gunshot injury detection
	calcium, alginate	Trajectory projection
		Chemical warfare agents' detection
		Muscle regeneration
		• 3-D bioprinting
Forensic DNA	Alginate, DNA hydrogels,	Forensic biology
	nanoparticles based	Tissue mimetics
	hydrogels	DNA nanotechnology
		Nucleic acid biosensor

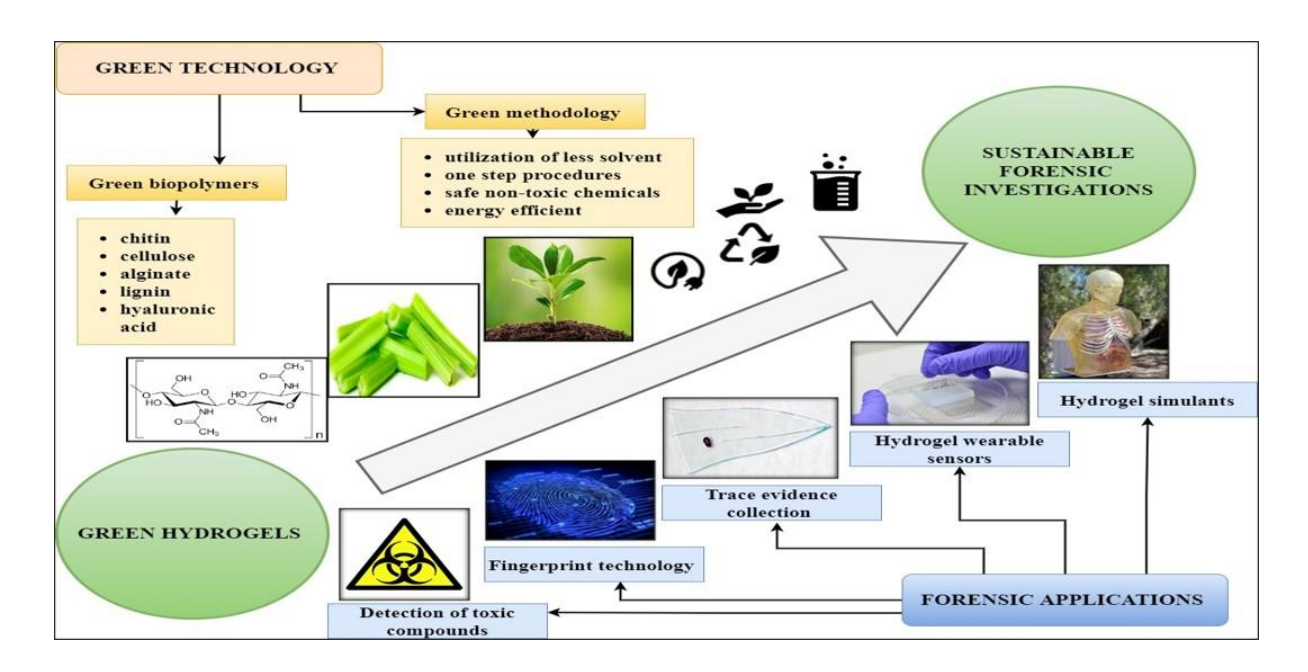


Figure 1.2: Hydrogels in forensic science

CHAPTER 2 REVIEW OF LITERATURE

2.1 Today's World Green hydrogel nanocomposites

Green nanocomposite hydrogels are a class of advanced materials composed of polymer hydrogel networks integrated with nanoscale fillers or particles, designed with an emphasis on environmental friendliness and sustainability. A hydrogel is a three-dimensional, hydrophilic polymer network capable of absorbing large amounts of water while maintaining its structure (Kopecek et al., 2009). When nanoparticles or nanostructures are incorporated into such networks, the result is a nanocomposite hydrogel (often termed a hybrid hydrogel) with enhanced or novel properties (Gaharwar et al., 2014). These hydrogels can be formulated from natural, "green" polymers (e.g. polysaccharides, biopolymers) and benign crosslinkers, reducing the use of toxic chemicals in their synthesis. The "green" aspect signifies that the materials are biocompatible, biodegradable, and derived from renewable resources, aligning with the principles of sustainability and minimizing secondary pollution (Ge et al., 2022).

The relevance of green nanocomposite hydrogels in today's context is two-fold. First, they offer a promising solution for environmental remediation, particularly for water pollution by toxic dyes. Synthetic dyes from textile, food, and other industries have become persistent pollutants in water bodies, posing serious ecological and health risks (Kant et al., 2011; Periyasamy 2024; Rando et al., 2024). Traditional wastewater treatments often struggle to completely remove or detect these dye contaminants. Green nanocomposite hydrogels, with their high water affinity and customizable chemistry, can adsorb and immobilize dye molecules efficiently, acting as advanced adsorbents or even catalysts for dye degradation

Second, these materials open up new possibilities in forensic environmental analysis. By capturing dye pollutants from water or soil, hydrogels can concentrate trace contaminants, facilitating their detection and forensic identification. In fact, analysts note that the prevalence of synthetic dyes in the environment can "help to solve crimes and pollution problems if detection techniques are proper," underscoring the forensic value of identifying dye residues in complex samples (Teran et al., 2021). Thus, green nanocomposite hydrogels represent a novel intersection of environmental science and

forensic investigation, providing a tool to both clean up pollutants and preserve evidence of illegal dye use or discharge.

In the following sections of literature review, we review the development of hydrogels and hydrogel nanocomposites, highlight recent research trends, discuss the role of natural "green" gums in creating eco-friendly hydrogels, examine the pollution issues caused by toxic dyes, and explore how these hydrogels can be utilized to detect and investigate dye pollutants in environmental and forensic contexts.

2.2 Historical Development of Hydrogels and Nanocomposite Hydrogels

2.2.1 Origins of Hydrogels

The concept of synthetic hydrogels dates back to the mid-20th century. In the early 1950s, Otto Wichterle and Drahoslav Lím pioneered the development of hydrophilic polymer networks for biomedical use, aiming to create materials with tissue-like softness and biocompatibility. Their efforts led to the first crosslinked poly(2-hydroxyethyl methacrylate) (poly-HEMA) hydrogel, which was reported in a seminal 1960 paper (Winchterle & Lim, 1960). This material, used for soft contact lenses, is often regarded as the first modern hydrogel designed for clinical application. Indeed, hydrogels became "the first biomaterials designed for clinical use," initially in ophthalmic devices. Throughout the 1960s and 70s, hydrogel research expanded to other polymers (e.g. polyacrylamide, polyvinylpyrrolidone, polyvinyl alcohol) and applications such as drug delivery and tissue engineering. These early hydrogels were typically single-polymer networks crosslinked either covalently or by other means, and while they offered high water content and biocompatibility, they often lacked mechanical strength and chemical functionality (Kopecek et al., 2009).

2.2.2 Advent of Hydrogel Nanocomposites

By the late 20th and early 21st century, scientists began to enhance hydrogel performance by incorporating nanomaterials. A landmark development came in 2002, when Haraguchi and Takehisa introduced the concept of the nanocomposite hydrogel – a hybrid organic–inorganic network in which polymer chains are integrated with inorganic nanoparticle fillers. In their work, a clay (silicate) was dispersed in a

polymerizing hydrogel matrix, creating a crosslinked network where the clay nanosheets served as multifunctional crosslinkers. The resulting material, termed an "NC gel", exhibited extraordinary improvements in mechanical strength, elasticity, and swelling behavior compared to conventional hydrogels (Haraguchi & Takehisa, 2002; Haraguchi & Takehisa, 2005).

This 2002 report is widely recognized as a breakthrough that extended the concept of polymer nanocomposites into the hydrogel field. Following this, a variety of nanocomposite hydrogels were developed through the 2000s and 2010s, using nanofillers such as silica, graphene oxide, carbon nanotubes, metal nanoparticles, nanocellulose, and clay, among others (Gaharwar et al., 2014). These nanofillers imparted properties like higher mechanical toughness, electrical conductivity, magnetic responsiveness, and enhanced adsorption capacity, depending on their nature (Tipa et al., 2020).

2.2.3 Latest Research Trends in Hydrogel Nanocomposites

Publication trends reflect this expansion: there has been a steady rise in research output on "nanocomposite hydrogels" each year. Hydrogels progressed from simple passive materials to active systems capable of responding to stimuli or interacting with contaminants. For instance, hybrid hydrogels with carbon nanotubes enabled electrically conductive tissue scaffolds and those with magnetic nanoparticles allowed remote manipulation and easy recovery from solutions. By integrating functional nanomaterials, hydrogels could be tailored to address specific challenges including the adsorption of toxic dye molecules from wastewater, a focus of growing interest in the past decade.

Contemporary research on hydrogel nanocomposites is marked by an emphasis on multifunctionality, smart response, and targeted applications. Several notable trends can be identified. Recent advances have led to "smart" nanocomposite hydrogels that can respond to environmental triggers (pH, temperature, light, magnetic fields) by changing their behavior. For example, incorporating iron-oxide nanoparticles yields hydrogels that respond to magnetic fields, and coupling light-sensitive moieties or photocatalytic nanoparticles can make hydrogels photo-responsive (Rando et al., 2024).

Self-healing nanocomposite hydrogels, which can autonomically repair their network after damage, have also emerged by using reversible bonds or dynamic interactions at the nano-additive/polymer interface. These features enhance the longevity and reusability of hydrogels in applications like water treatment and sensors.

A significant trend is the development of hydrogel nanocomposites for water purification, targeting pollutants such as dyes, heavy metals, pharmaceuticals, and oils (Rando et al., 2024). Researchers are designing hydrogels that act as high-capacity adsorbents, often combining multiple functions like adsorption and photocatalytic degradation. For instance, composite hydrogels embedding photocatalysts (e.g. TiO₂, ZnO) can both adsorb dye molecules and then degrade them under light, offering a one-two punch for pollutant removal. Similarly, hydrogels containing magnetic nanoparticles can be easily removed from treated water along with the absorbed pollutants by applying a magnet, simplifying cleanup. The latest studies report exceptional adsorption capacities for certain nanocomposite hydrogels: e.g., a graphene oxide-infused bio hydrogel adsorbing over 1400 mg/g of methylene blue dye (Santoso et al., 2021; El-saied et al., 2021; Ge et al., 2022) far outperforming many traditional adsorbents. Such high uptake is attributed to the synergistic effect of the porous polymer network and the high surface area of nanofillers.

Concurrently, hydrogel nanocomposites continue to advance in biomedical domains (wound dressings, drug delivery systems, tissue engineering) and as sensors. Nanocomposite hydrogels can be engineered to immobilize biomolecules or change optical/electrical signals in the presence of specific analytes. This has led to biosensors for glucose, enzymes, or toxins. Translating this to environmental monitoring, researchers have begun developing hydrogel-based sensors for pollutants. Notably, hydrogel-based sensors for dyes and other contaminants are being explored, where the hydrogel might swell or change color/fluorescence upon absorbing a target pollutant, thereby signalling its presence (Rando et al., 2024). Such dual sorbent-sensor systems are highly attractive, as they can both capture a pollutant and instantly report its detection. This trend aligns with the needs of environmental forensics, where on-site indication of a contaminant can guide quick action.

There is growing interest in ensuring that the hydrogels themselves are environmentally benign. Researchers are increasingly using bio-based polymers and green chemistry techniques to fabricate hydrogels (El-saied et al., 2021; Ge et al., 2022). For example, plant-derived polymers or waste biomass are used as hydrogel matrices, and natural crosslinkers (like citric acid or enzymes) replace toxic reagents (Nguyen et al., 2022). This not only reduces the environmental footprint of hydrogel production but also ensures that if the hydrogel is used in environmental applications, it will not introduce new persistent pollutants. The latest hydrogel studies often emphasize facile, low-energy synthesis methods (such as microwave-assisted polymerization or UV-curing) and the elimination of harmful solvents. The result is an "eco-friendly" nanocomposite hydrogel that aligns with the broader goals of green chemistry while delivering high performance in use.

A cutting-edge development in this field is the use of microwave irradiation to synthesize hydrogels and grafted polymer networks. Traditional hydrogel synthesis (thermal or chemical initiation) can be time-consuming (several hours) and may yield uneven network structures. Microwave-assisted synthesis, by contrast, rapidly delivers energy throughout the reaction mixture, drastically reducing polymerization time to minutes and often improving the material's properties. For example, polyacrylamide—chitosan hydrogels prepared with microwave heating achieved a higher product yield in a fraction of the time compared to conventional heating. Interestingly, while one study noted that initial dye removal rate of a microwave-synthesized hydrogel was slightly lower than that of a conventionally made hydrogel, the microwave product exhibited a much higher maximum adsorption capacity for the dye. This suggests microwaves can create a more porous or better-crosslinked network that ultimately binds more dye. Microwave techniques have also been reported to improve grafting efficiency and hydrogel stability (Batouti et al., 2023).

Additionally, microwave synthesis is often a cleaner process (using water as a solvent and fewer additives) and is considered energy-efficient and easily scalable. Despite these advantages, microwave-synthesized hydrogels for dye remediation are still an emerging area. Few studies to date have systematically compared microwave versus conventional hydrogel preparation in terms of adsorption performance, especially for

complex dye mixtures or real wastewater. This represents a novel avenue to pursue, bridging materials science and forensic needs (e.g. creating adsorbents quickly for onsite pollutant clean-up or evidence collection).

Modern hydrogel nanocomposites are characterized by tailored functionality. Researchers can mix and match polymer backbones, crosslinking chemistry, and nanomaterials to obtain a desired set of properties. Whether the goal is to create a robust adsorbent for toxic dyes, a reusable catalytic sponge, or a sensitive detector, the hydrogel toolbox is rich and continually expanding. This versatility makes nanocomposite hydrogels particularly exciting for tackling complex problems like dye pollution, where a combination of high capacity, selectivity, reusability, and safeness is required.

2.3 Role of Green Natural Gums in Environmentally Friendly Hydrogels

A major thrust in "green" hydrogel research is the use of natural plant gums and polysaccharides as the polymer matrix. These natural gums such as guar gum, xanthan gum, gellan gum, and gum arabic are biopolymers extracted from plants or microbial fermentation, known for their gel-forming abilities, abundance, and benign nature (Elsaied et al., 2021; Sandhu & Pandey, 2023).

They offer a renewable alternative to synthetic polymers (like polyacrylamide or polyacrylate) and inherently possess functional groups (hydroxyl, carboxyl, etc.) that can be leveraged for crosslinking and pollutant binding. In forming hydrogels, these gums can be used alone or grafted with synthetic polymer segments to improve strength (Sandhu et al., 2023).

Examples of several natural gums in creating eco-friendly hydrogel nanocomposites:

2.3.1 Guar Gum: Derived from the guar bean, guar gum is a galactomannan polysaccharide that is water-soluble and gel-forming. Guar gum has plentiful hydroxyl groups (making it a neutral polysaccharide) which allow it to be chemically crosslinked or grafted with ease. Hydrogels based on guar gum have been widely studied for adsorbing pollutants. For example, crosslinked guar gum hydrogels (sometimes grafted with acrylic monomers for strength) have achieved high adsorption capacities for dye

molecules. In one study, a biodegradable guar-gum nanocomposite hydrogel showed capacities of 781 mg/g for malachite green and 282 mg/g for safranin dyes exceptionally high values, demonstrating the efficacy of guar-based networks. Another composite of carboxymethyl cellulose, guar gum, and graphene oxide removed malachite green with ~88% efficiency (adsorption ~17.6 mg/g), while guar gum combined with activated carbon could adsorb ~64.5 mg/g of Congo Red (an anionic dye) and be reused for multiple cycles (El-saied et al., 2021). These examples underscore that guar gum, especially when reinforced with nanoparticles or functionalized (e.g. sulfonated guar gum), can serve as a high-performance and recyclable adsorbent in hydrogels (Chauhan et al., 2025)

2.3.2 Xanthan Gum: Xanthan is an extracellular polysaccharide from bacteria (Xanthomonas species) and contains a cellulose-like backbone with branching sugars and carboxylate groups (it is an anionic polysaccharide). Xanthan gum-based hydrogels are attractive due to xanthan's excellent viscosifying and film-forming properties and its inherent charges that can bind cationic pollutants. Studies report that xanthan gum composites are very effective for toxic dye removal, and also environmentally friendly in composition. For instance, a semi-interpenetrating network hydrogel of xanthan gum and poly(acrylic acid) with hydroxyapatite nanoparticles could adsorb cationic dyes like methylene blue and crystal violet with capacities of 63 and 87 mg/g respectively (Ge et al., 2022). Such composites leverage xanthan's bio-derived network and the added functionality of synthetic/polymeric components and nanofillers. Xanthan gum hydrogels have also been used to remove anionic dyes and heavy metals, often by modifying the gum (e.g., grafting acrylamide or embedding clays) to introduce more binding sites. The literature consistently notes that xanthan-based adsorbents are "environmentally friendly and have great potential to effectively remove toxic dyes from industrial wastewater" (Njuguna et al., 2021; Dutta et al., 2023).

2.3.3 Gellan Gum: Gellan gum is a linear anionic polysaccharide produced by bacteria (Sphingomonas) and is known for forming clear, firm gels in the presence of divalent cations. Gellan gum hydrogels have gained attention for water treatment due to their strength and tunable porosity. When crosslinked (either chemically or by ionic crosslinkers), gellan gum hydrogels can act as robust adsorbents. A notable example is

a gellan gum-clay hybrid hydrogel that achieved ~99% removal of malachite green and ~95% of methylene blue from aqueous solutions (initial dye 50 mg/L) within 6 hours (Choudhary et al., 2020). This hydrogel was synthesized via a green method (microwave-assisted grafting of acrylic monomers onto gellan, using a benign initiator) and demonstrated outstanding efficiency at low dye concentrations. In another study, a fully green composite hydrogel made of gellan gum and bacterial cellulose crosslinked with citric acid (a non-toxic crosslinker) showed good adsorption of cationic dyes: it could uptake ~17.6 mg/g of safranin and 13.5 mg/g of crystal violet at optimum conditions (Nguyen et al., 2022).

While these capacities are moderate, the entirely bio-based nature of the hydrogel and its facile degradability after use make it appealing for deployable environmental cleanup. Gellan-based hydrogels can also be reinforced with inorganic particles (like activated carbon or layered double hydroxides) to improve their adsorption. For example, incorporating a Cu–Al layered double hydroxide into a gellan matrix yielded a nanohydrogel that efficiently adsorbed crystal violet (90.9 mg/g capacity) (El-saied et al., 2021). Such results demonstrate that gellan gum can serve as a versatile platform for building composite hydrogels that are both effective and green.

2.3.4 Gum Arabic: Gum arabic (acacia gum) is a complex branched polysaccharide exudate from Acacia trees, containing both neutral and acidic sugar units. It has been used historically as a natural binder and is edible, making it an attractive component for eco-friendly materials. Gum arabic has been applied in synthesizing hydrogels and nanogels for pollutant adsorption. For instance, gum arabic-grafted poly(acrylamide) nanohydrogels have been reported for dye removal, including effective adsorption of the cationic dye Crystal Violet from water. In one study, a gum arabic-clay hybrid hydrogel was able to remove 90% of Crystal Violet (Sharma et al., 2018). Other researchers prepared oxidized gum arabic crosslinked with other biopolymers (like chitosan and pectin) to adsorb antibiotics and dyes, illustrating gum arabic's utility as a cross linkable, multi-functional polymer backbone. The appeal of gum arabic lies in its benign nature and multiple functional groups (carboxylates), which allow easy conjugation of functional moieties or nanoparticles to enhance adsorption performance. Although not as extensively studied as guar or xanthan in the context of hydrogels, gum

arabic-based hydrogels represent a promising green adsorbent technology, especially for organic pollutants (Wu et al., 2018).

2.3.5 Other Candidates: Other natural gums and polymers such as pectin, carrageenan, alginate, psyllium, karaya, and tragacanth gums have likewise been explored in hydrogel form for pollutant removal. Each brings its unique structure: e.g., carrageenan (from seaweed) yields sulfate-rich gels good for binding basic dyes, and alginate (from algae) crosslinks with calcium to form sturdy beads. A unifying theme is that natural gum-based hydrogels are renewable, non-toxic, and can be engineered to have high affinity for dyes and heavy metals, often through simple chemical modifications. The use of these materials addresses the need for adsorbents that do not themselves become new environmental hazards. By leveraging natural gums in nanocomposite hydrogels, researchers aim to achieve a sustainable approach to pollutant cleanup – where the adsorbent is as green as the goal of the remediation (Anderson et al., 2015; Abdi et al., 2024; Drapalova et al., 2023).

2.4 Pollution by Dyes: Environmental and Forensic Perspectives

The pollution caused by synthetic dyes is a significant environmental problem and also a matter of regulatory and forensic concern. Textile dyes in particular are produced and used in enormous quantities. It is estimated that globally around 800,000 tons of dyes are manufactured annually, and roughly 10–15% of these dyes are lost into the environment during manufacturing and usage (Periyasamy et al., 2024).

With over 10,000 distinct synthetic dyes in commercial use (about 70% of which are azo dyes), dye-containing effluents are both chemically diverse and challenging to treat. During textile dyeing processes, a substantial fraction of the dye does not bind to fibers conventional dyeing may see 1–15% of dye unfixed, ending up in wastewater (Kant et al., 2012). As a result, textile industry wastewater is often intensely colored and laden with toxic substances, making the textile sector a major polluter of fresh water resources. In fact, the World Bank has estimated that textile dyeing and finishing contributes up to 17–20% of industrial water pollution globally (Kant et al., 2012). The presence of dyes in water bodies has several deleterious effects. Visibly, even a small amount of dye can impart strong color to water, reducing light penetration. This inhibits

photosynthesis in aquatic ecosystems by blocking sunlight to algae and submerged plants. Dyes and associated additives can also consume dissolved oxygen or create surface foams and scums, disrupting the normal oxygen transfer at the air-water interface. Many synthetic dyes are recalcitrant and resist biodegradation, leading to persistent contamination. Additionally, dyes can break down into or carry along with them hazardous chemicals: for example, azo dyes can cleave into aromatic amines, some of which are known carcinogens. There are documented cases of dyes causing acute and chronic toxicity in aquatic life – certain dyes are lethal to fish at relatively low concentrations and can inhibit the growth of microorganisms needed for biodegradation. Some dyes (and mordant chemicals used with them) contain heavy metals like chromium, adding to their toxicity. The result of uncontrolled dye discharge is often rivers and streams turned vividly colored and biologically dead over stretches downstream of textile hubs. For example, in parts of South Asia, bright green or blue rivers (tinted by textile dyes) have become infamous environmental catastrophes. Such pollution not only affects ecology but can infiltrate drinking water sources, posing risks of mutagenic and carcinogenic effects in humans over the long term (Kant et al., 2012).

While textiles contribute the bulk of dye pollutants, food dyes present another aspect, the illegal or unsafe use of industrial dyes in consumables. Synthetic dyes are used in foods and beverages, but regulators strictly control which dyes are permitted because some industrial dyes are harmful if ingested. Unfortunately, there have been numerous instances of illegal dyes being added to foods to enhance appearance. A notorious example is the Sudan dye scandal: Sudan I, II, III, and IV are red-orange azo dyes meant for coloring oils, waxes, or shoe polish and not foods. However, starting around 2003, Sudan I was discovered as an adulterant in chili powder and curry products, leading to a massive international recall in 2005 (over 570 food products were recalled in the UK). Sudan I is classified as a Category 3 carcinogen, and its presence in food was a result of fraudulent attempts to make spices appear more vibrant. This incident raised global awareness of illegal food dyes. Similarly, Malachite Green, a vibrant green triphenylmethane dye used in aquaculture as an antifungal agent, has been found illicitly in fish destined for human consumption (Hidayah et al., 2013). Malachite Green

is both carcinogenic and mutagenic, and is banned for use in food animals in many countries (Cooksey et al., 2016; Hoogenboom et al., 2016).

Its persistent residue in fish prompted strict monitoring after it was detected in farmed fish and seafood. Other examples of harmful dye usage include Rhodamine B (a fluorescent dye used illegally to color sweets and sauces) and Orange II or Metanil Yellow (used to color turmeric or chili powders). These dyes can cause health issues ranging from allergic reactions to organ toxicity or cancer with chronic exposure. The environmental and health implications of such dyes extend to the forensic realm. Environmental forensics is a discipline where analytical science is used to trace pollutants to their source and to provide evidence of environmental violations. Dyes, by virtue of their vivid signature and chemical specificity, can be crucial markers. For instance, if a river is found contaminated with a particular dye that a nearby textile mill uses, forensic analysis can link the pollution to that mill, supporting legal action. Likewise, finding a banned dye in a food item (via lab tests) can serve as evidence against a manufacturer for food fraud. In one case, after the Sudan I scandal, regulators developed screening methods to detect a range of 19 illegal dyes in spices and foods to enforce food safety (Gray et al., 2016). Advanced chromatographic methods (like HPLC with UV-Vis or mass spectrometric detection) were implemented to routinely check products for traces of these dyes. From a forensic standpoint, the mere presence of a forbidden dye in a product or environmental sample is a red flag indicating a violation of law (Gray et al., 2016).

Finally, dyes can also be forensic trace evidence in criminal investigations unrelated to pollution per se. For example, forensic fiber analysis often involves identifying dye compounds extracted from fibers to match a fiber to a particular garment or source (Śmigiel-Kamińska et al., 2019). Paint chips, inks, and stains at crime scenes may also be analyzed for their dye content to establish links between objects or people. In such cases, analytical techniques must identify tiny amounts of dyes in complex matrices, which is challenging but feasible with modern instruments. As a 2021 review points out, detecting and characterizing dyes in complex mixtures is important to determine events like "possible match with evidence" or attempts to clean up a stain (Teran et al.,

2021). This indicates the broad forensic interest in dyes, not only to implicate polluters and food adulterators, but also to connect evidentiary dots in various criminal scenarios.

In environmental forensics, the identification of dye pollutants in soil or water samples can help pinpoint the source of contamination. Dyes often have unique compositions (for instance, specific combinations of chromophores or isotopic signatures) that can be matched to a manufacturer or industrial process. Investigators may compare the dye profile in environmental samples with reference dyes used by suspect facilities. A match could place responsibility on a particular factory for a river pollution incident. In one forensic case study, analysis of dye mixtures in wastewater allowed authorities to identify which textile plant (among several in the region) had released the pollutants, by matching the dye composition to the dye formulations known to be used by each plant. This kind of chemical matching requires sensitive and specific analytical techniques, but when successful, it turns a pollutant into a piece of evidence.

Modern forensic detection of dyes relies on techniques like chromatography (TLC, HPLC) and mass spectrometry (MS), often in tandem. A recent review emphasizes that a variety of chromatographic-MS approaches exist to detect disperse, acid, basic, and reactive dyes and their degradation products with high specificity. For forensic labs, it is important not only to detect the parent dye, but also any metabolites or evidence of intentional removal attempts (e.g., bleach by-products). The detection of multiple related dye compounds in a scene can indicate a deliberate cleanup (for example, finding both a dye and its oxidized form suggests someone tried to bleach away a stain). As Teran et al. (2021) note, "detection and characterization of dyes in complex matrices is important to determine the possible events leading to their deposition (natural degradation, attempts of removal, possible match with evidence, among others)". In practice, this means forensic scientists can tell if a dye stain was left by environmental contamination or by human activity, and whether someone tried to eradicate the evidence (Teran et al., 2021).

Another key forensic application is in fiber and textile evidence. In crimes involving physical contact, bits of fabric or fibers are often transferred between individuals or objects. Comparing the dye composition of a fiber from a suspect's clothing to fibers

found at a crime scene can substantiate a connection. Because many textiles are dyed with complex mixes of dyes, the chance of two different garments sharing an identical dye profile is low. Hence, a match of dye profiles becomes strong evidence. "Dye analysis is a common aspect of forensic investigations involving crime scene evidence such as textile fibers, hairs, plastics, and inks," and it greatly improves the evidential value of fiber matches (Smigiel-Kamińska et al., 2019).

2.5 Advantages of Utilizing Green Nanocomposite Hydrogels

The use of green nanocomposite hydrogels for dye adsorption marries the goals of pollution mitigation with forensic science. These hydrogels can act as versatile dye sponges, selectively soaking up dye molecules from contaminated media. Traditionally, to analyze dye pollutants or evidence, forensic scientists would collect water or soil samples and then concentrate the dyes via solvent extraction or adsorption on resins. Now, imagine deploying a biodegradable hydrogel pad or bead directly into a polluted stream or onto a suspect material: the hydrogel would rapidly absorb the dye pollutants, owing to its high swelling capacity and tailored binding sites, and effectively sequester the dyes within its network. This approach offers several novel advantages:

2.5.1 Concentration and Preservation of Evidence: By absorbing dilute dyes from large volumes, hydrogels concentrate the dye into a smaller mass, making it easier to detect and analyze. For environmental forensics, this means even if a dye is present at trace levels in a river, a hydrogel sampler left in the water for some time could accumulate enough dye to permit laboratory identification. The hydrogel essentially acts as a passive sampler, analogous to how activated charcoal traps air pollutants. What's more, once the dye is absorbed, it is retained in the hydrogel matrix, protected from further dilution or degradation. This is useful for preserving the chemical integrity of the dye evidence during transport to the lab. For instance, a green hydrogel could be placed at a wastewater outlet suspected of illegal dye discharge; after retrieval, the dyeladen gel can be analyzed to reveal the pollutants present, thereby linking them to the source.

2.5.2 Selective Adsorption and Cleanup: Nanocomposite hydrogels can be engineered to preferentially bind certain dye classes. Through functionalization (adding

ionic groups, molecular recognition sites, etc.), a hydrogel can exhibit selectivity, for example, a hydrogel with sulfonate and carboxyl groups might selectively grab basic (cationic) dyes like methylene blue or malachite green, which are common toxins in textile effluent (Shi et al., 2022). In a forensic scenario, this selectivity could be tuned to target the most suspicious dye in a mixture. Moreover, because the hydrogels are self-contained cleanup agents, they serve a dual role: they mitigate the spread of the pollutant by pulling it out of the environment, while also gathering it for analysis. This is particularly helpful in scenarios like a dye spill or an illegal dumping event – deploying hydrogels can help remediate the site and simultaneously collect evidence of the spillage (the type and quantity of dye).

2.5.3 Integration with Detection Methods: Researchers are exploring hydrogels that not only adsorb but also respond optically to the presence of specific dyes. Such integrations (e.g., a hydrogel loaded with a reagent that fluoresces when a dye is absorbed) could allow on-site indication that a certain dye has been captured (Inobeme et al., 2024). For forensic fieldwork, a hydrogel that changes color upon picking up a banned dye would be invaluable as a quick screening tool. Although in early stages, studies on stimuli-responsive hydrogels show this is feasible. Hydrogels have been made that change color with pH or emit fluorescence under UV when binding heavy metals or organics (Rando et al., 2024). Translating this to dye detection, one could design a hydrogel that, say, turns a visible color when it has absorbed a threshold amount of an illegal food dye, providing an immediate visual cue to investigators.

From a case perspective, consider forensic investigators examining a warehouse suspected of being used to dye counterfeit textiles with banned azo dyes. Traditional approach would involve swabbing surfaces or collecting wastewater and sending to a lab. With hydrogel adsorbents, investigators could press a small hydrogel patch against drains, sinks, or even the surface of vats. The hydrogel would mop up any residual dye molecules clinging to those surfaces. Later lab analysis of the hydrogel (by desorbing the dye and running HPLC-MS, for example) could confirm the presence of specific illegal dyes, strengthening the evidence. This approach reduces the need to transport liquid samples (which can be bulky or hazardous) and can improve the recovery of trace residues (Hou et al., 2018)

An interesting extension is using hydrogels as testbeds for simulating dye behavior. Since hydrogels can mimic biological tissues (due to high water content), forensic researchers might use them to study how dyes transfer or persist. For example, to test how a particular dye might transfer from dyed fabric to skin (important in cases of contact poisoning or staining), a hydrogel slab can serve as a skin surrogate. It would absorb dye from fabric similarly to real skin, allowing controlled experiments.

Green nanocomposite hydrogels represent a novel approach to forensic dye investigation by serving as both cleanup agents and evidence collectors. They align well with the ethos of environmental forensics: minimally invasive, environmentally benign methods that nonetheless capture clear evidence of contamination. As this field progresses, we anticipate seeing hydrogel kits for forensic teams, perhaps containing different polymer-nanocomposite formulations optimized for various dye classes. By deploying these at suspected sites (be it a crime scene, an effluent pipe, or a food processing facility), investigators can "trap" the molecular culprits and later unmask them via analytical techniques. This synergy between material science and forensic chemistry could significantly enhance our ability to monitor and enforce against the pollution of water resources by toxic dyes, all while using materials that do not contribute to the problem themselves.

CHAPTER 3 RESEARCH OBJECTIVES & HYPOTHESES

RESEARCH OBJECTIVES

- 1. To explore various routes of synthesis of hydrogel and compare them to find out the best among them.
- 2. To synthesize novel natural and synthetic hydrogel nanocomposites by microwave irradiation.
- 3. Characterization of synthesized hydrogels using instrumentation techniques.
- 4. Application of novel nanocomposite hydrogel in investigating toxic dyes as environment pollutants

HYPOTHESES

Hypothesis 1: Comparative analysis of different routes (Microwave irradiation, thermal polymerization and chemical initiation) of synthesis of hydrogels to obtain superior physicochemical properties such as enhanced swelling ratio, uniform crosslinking, and improved mechanical strength.

Hypothesis 2: Microwave irradiation facilitates efficient synthesis of novel natural and synthetic hydrogel nanocomposites with improved network homogeneity, faster gelation, and better nanoparticle incorporation.

Hypothesis 3: The synthesized hydrogels and nanocomposites will exhibit distinguishable structural, thermal, morphological, and chemical features, as confirmed by FTIR, FE-SEM, XRD, TGA analyses, validating their successful formation and stability.

Hypothesis 4: Nanocomposite hydrogel synthesized via optimized microwave routes will demonstrate high adsorption capacity and selectivity toward toxic textile dyes, due to their increased surface area, porosity, and functional group interactions, making them effective agents for environmental pollutant remediation.

CHAPTER 4 MATERIALS AND METHODOLOGY

4.1 MATERIALS

Butea monosperma (kamarkas) was purchased from local market in Jalandhar. Ammonium persulphate and N, N-methylene bis-acrylamide were purchased from Sigma Aldrich. Acrylic acid, sodium hydroxide, zinc acetate dihydrate, polyethylene glycol, ferrous sulfate, amaranth and methyl orange were supplied by Loba Chemie Pvt. Ltd. (table 4.1).

Table 4.1: Materials used for the preparation of hydrogels and nanocomposites

S.No.	Material/	Molecular Structure	Designation
	Chemicals		
2.	Butea monosperma gum (BM)	OH	Template
3.	APS- Ammonium persulphate		Initiator
4.	AA- acrylic acid,	H T	Monomer
5.	dH ₂ O -Distilled water	HOH	solvent

6.	MBA- N, N-methylene bisacrylamide	H H H H H	Cross-linker
7.	PEG- Polyethylene glycol	C2Nh4N+2On+1	Template
8.	Ferrous sulfate	O O'-S=O Fe ²⁺ O'	Initiator
9.	Amaranth	Na ⁺ O-Na ⁺ H H H O-Na H H Na H H Na H H Na H Na H Na H Na	Azo dye
10.	Methyl Orange		Azo dye

4.2 METHODOLOGY

4.2.1 Natural Hydrogel Synthesis Via Various Routes

4.2.1.1 Extraction of Butea monosperma

100 g of BM gum purchased from the market was added to 200 ml of ethanol and kept for 15minutes. The mixture was then transferred onto blotting paper to absorb the ethanol, while maintaining sterile conditions. The gum was subsequently placed in a glass petri plate and dehydrated in a hot air oven at 60°C for 1 hour. After drying, the gum was stored in a sterile glass bottle for future use (Mankotia et al., 2020).

4.2.1.2 Microwave Irradiation

Hydrogel based on *Butea monosperma* gum (BM) is synthesized using microwave radiation with distilled water as a solvent, AA as a monomer, APS as initiator, and MBA as a cross linker. In the experiment a 2000 mg of BM was weighed and added to 10mL of dH₂O. Accordingly to this a known concentration of APS followed by AA and MBA is added and the whole solution is stirred continuously in a clockwise direction. The various reaction parameters i.e., concentration of initiator, monomer, cross-linker, reaction time, and amount of solvent were varied to get the hydrogel with maximum percentage swelling. The mixture is then subjected to microwave irradiation to undergo sol-to-gel transition. A single washing is given to the synthesized hydrogel by immersing it in 10mL dH₂O for about 10 minutes and then it is dried at 60°C in hot air oven (Kumar et al., 2023) (figure 4.1).

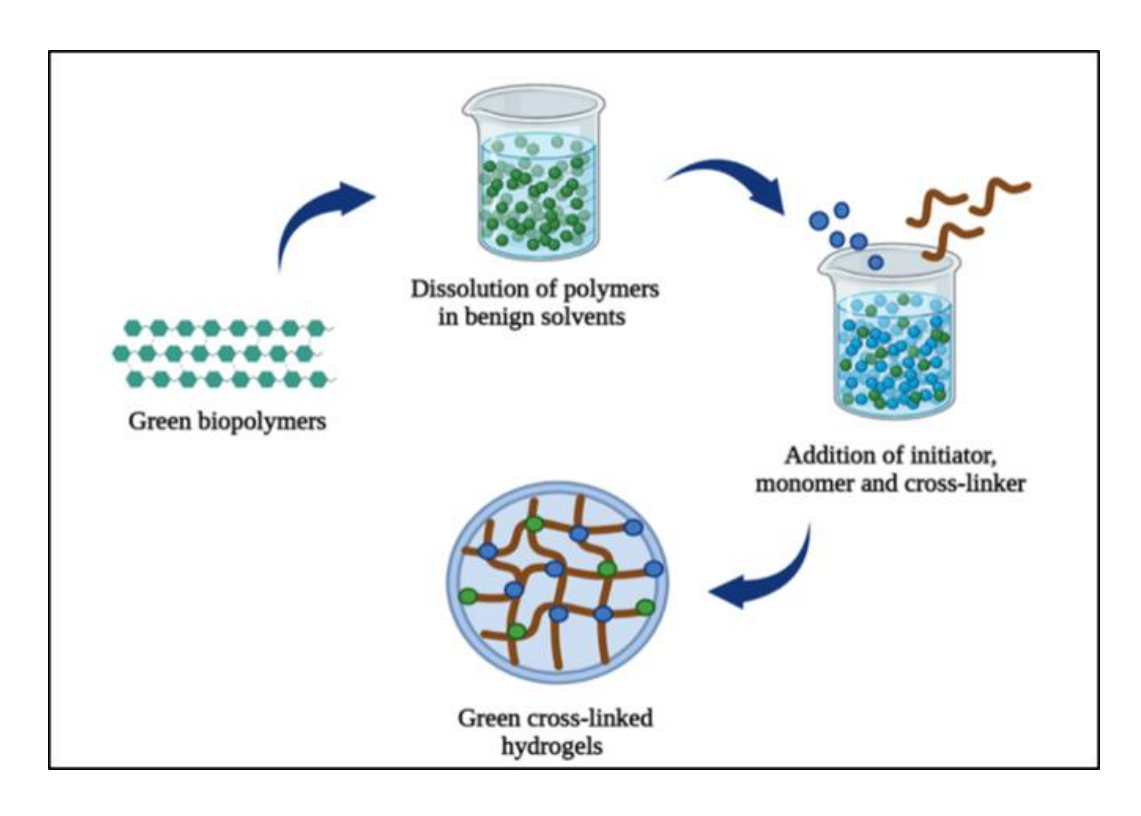


Figure 4.1: A schematic for hydrogel preparation

4.2.1.3 Thermal Polymerization

Hydrogel based on *Butea monosperma* gum (BM) was synthesized via conventional thermal polymerization utilized by Zhao et al., 2021 and Li et al., 2022. In this method, 2000 mg of BM was accurately weighed and dispersed in 10 mL of distilled water (dH₂O) under continuous magnetic stirring to ensure uniform dissolution. Once the BM was completely hydrated, a known concentration of ammonium persulfate (APS) was added as a thermal initiator, followed by the gradual addition of acrylic acid (AA) as the monomer and N,N'-methylene bisacrylamide (MBA) as the cross-linking agent. The entire reaction mixture was stirred in a clockwise direction at room temperature for 30 minutes to ensure homogeneity. Subsequently, the solution was transferred to a sealed glass container and subjected to thermal polymerization in a water bath maintained at 60–70°C for a period of 5 hours to facilitate the free radical grafting reaction and gel formation. After polymerization, the formed hydrogel was cooled to room temperature and washed once with 10 mL of distilled water to remove unreacted monomers and soluble impurities. The hydrogel was then dried in a hot air oven at 60°C until a constant weight was achieved (Zhao et al., 2021; Li et al., 2022).

4.2.1.4 Chemical Initiation

Hydrogel based on *Butea monosperma* gum (BM) was synthesized using a redox chemical initiation method. Initially, 2000 mg of BM was accurately weighed and dispersed in 10 mL of distilled water (dH₂O) under continuous stirring to form a uniform viscous solution. A redox pair consisting of ammonium persulfate (APS) and ferrous sulfate (FeSO₄) was employed as the initiator system. The required concentration of APS was first added to the hydrated BM solution, followed by the addition of a freshly prepared FeSO₄ solution to generate sulfate and hydroxyl radicals at ambient temperature. Acrylic acid (AA), serving as the monomer, and N,N'-methylene bisacrylamide (MBA) as the cross-linker, were then added sequentially with continuous stirring to promote graft copolymerization. The reaction mixture was maintained at room temperature for 6 hours to allow sufficient time for polymer network formation via radical propagation. After completion of gelation, the hydrogel was washed with 10 mL distilled water to remove unreacted species and low-molecular-weight fractions. The synthesized hydrogel was then dried in a hot air oven at 60°C until constant weight was obtained (Elsayed, M. M. 2019).

After successful synthesis of hydrogel via these three routes, best route was fixed for further hydrogel and nanocomposite preparations.

4.2.2 Synthetic hydrogel Synthesis

Polyethylene glycol (PEG) is synthesized using microwave radiation with AA as a monomer, APS as initiator, distilled water as a solvent and MBA as a cross linker. In the experiment a known amount of PEG was weighed and added to a known amount of dH₂O. Accordingly to this a known concentration of APS followed by AA and MBA is be added and the whole solution is stirred continuously in a clockwise direction and then the mixture was subjected to microwave irradiation. A single washing was be given to the synthesized hydrogel by immersing it in 10ml distilled water for about 10 minutes and then it was dried in a hot air oven at 60°C. The various reaction parameters i.e., concentration of initiator, cross-linker, monomer, reaction time, and amount of solvent was varied to get the hydrogel with maximum percentage swelling (Shi et al., 2021).

4.2.3 Hydrogel nanocomposite synthesis

4.2.3.1 Synthesis of ZnO nanoparticles

ZnO nanoparticles are created utilizing sol-gel method (Sukri et al., 2019), reactants being zinc acetate dihydrate and sodium hydroxide. A known amount of zinc acetate dihydrate is added to double distilled water and stirred continuously until the solution becomes clear. In a separate container, specific amount of sodium hydroxide is dissolved in double dH₂O. Both the solutions are then mixed together in one container and with continuous stirring. Absolute ethanol is added dropwise at 25°C. The sample is then dried at 80°C overnight for calcification. White ZnO nanoparticles are obtained, that are then utilized for nanocomposite synthesis and characterization.

4.2.3.2 Synthesis of ZnO-BM-g-poly (AA) hydrogel nanocomposite

Hydrogel based on *Butea monosperma* gum (BM) is synthesized with distilled water as a solvent, AA as a monomer, APS as initiator, and MBA as a cross linker applying microwave irradiation technique. In the experiment a 200 mg BM is weighed and added to 10 mL of dH₂O. Accordingly to this a known concentration (100 mg) of APS followed by AA and MBA is added and the whole solution is stirred continuously in a clockwise direction. After that prepared ZnO nanoparticles (200 mg) are added in the solution and then the mixture is subjected to microwave irradiation. The synthesised hydrogel nanocomposite receives a single washing by being submerged in 10mL distilled water for about 10 minutes, followed by drying in a hot air oven at 60°C. Schematic of hydrogel nanocomposite is shown in figure 4.2. The various reaction parameters i.e., concentration of monomer, initiator, cross-linker, reaction time, and amount of solvent are varied to get the hydrogel nanocomposite with supreme percentage swelling (Yu et al., 2023).

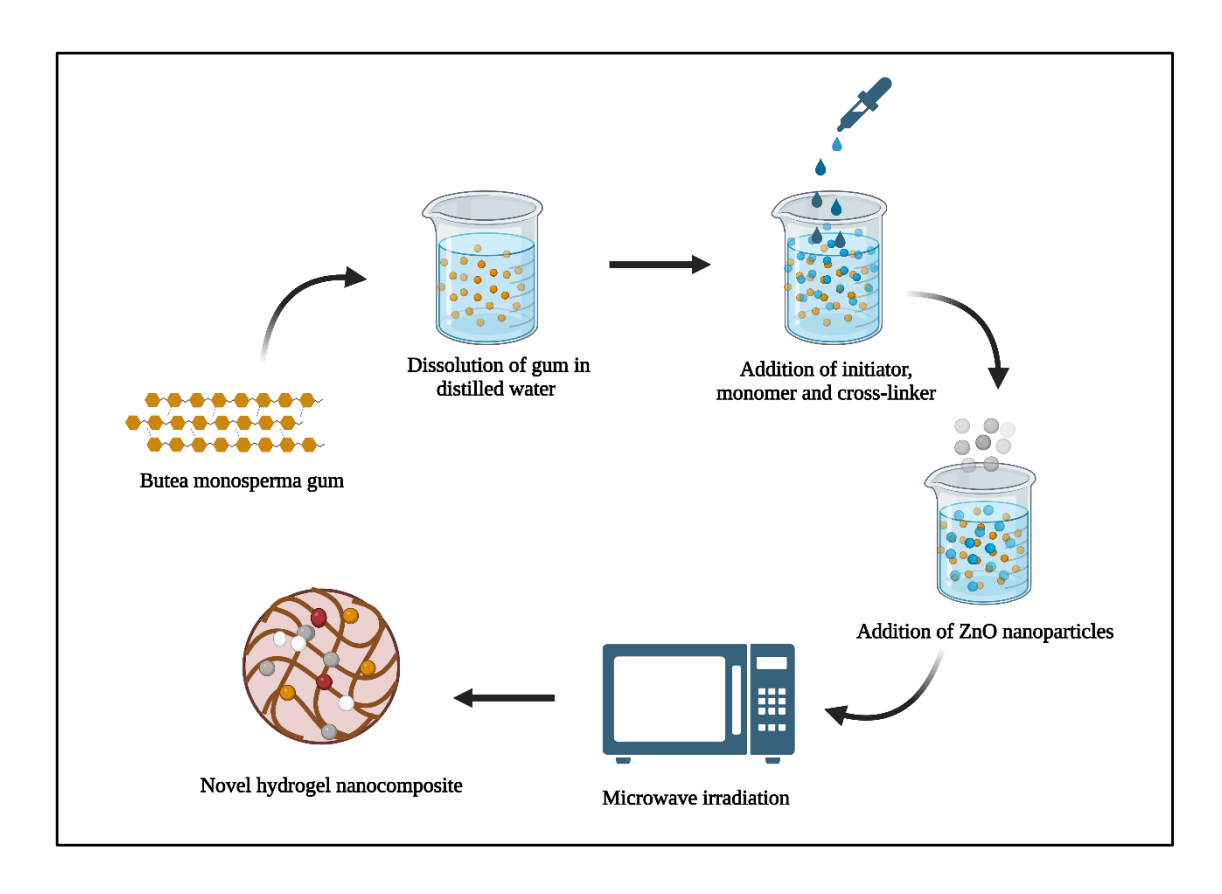


Figure 4.2: Schematic of hydrogel nanocomposite formation

4.2.3.3 Synthesis of ZnO-PEG-g-poly(AA) Hydrogel Nanocomposite

The ZnO-PEG-g-poly(acrylic acid) (AA) hydrogel nanocomposite was prepared via free radical polymerization facilitated by microwave irradiation (Hussain et al., 2024). In a typical synthesis, a precisely weighed amount (2000mg) of polyethylene glycol (PEG), serving as the polymeric backbone, was initially dissolved in an accurately measured volume of distilled water with continuous stirring at ambient conditions until a clear solution was obtained. To this PEG solution, ammonium persulfate (APS), acting as a radical initiator, was added at a predetermined concentration. Subsequently, acrylic acid (AA), functioning as the monomer, and N,N'-methylene bisacrylamide (MBA), used as the cross-linker, were sequentially incorporated into the reaction mixture with constant stirring to ensure homogeneous dispersion. After thorough mixing, a known quantity of pre-synthesized zinc oxide (ZnO) nanoparticles was carefully introduced into the reaction solution under vigorous stirring to uniformly disperse the nanoparticles within the polymeric matrix. The resulting mixture was then subjected to microwave irradiation to induce rapid polymerization and cross-linking,

leading to hydrogel network formation. Following polymerization, the synthesized hydrogel nanocomposite was subjected to a washing step by immersing it in distilled water for approximately 10 minutes to remove residual reactants and impurities. Finally, the purified hydrogel nanocomposite was dried to constant weight at 60 °C in a hot air oven. To achieve optimal hydrogel characteristics, critical synthesis parameters including monomer concentration, initiator and cross-linker ratios, irradiation time, and solvent volume were systematically optimized to enhance the swelling capacity and structural integrity of the final ZnO-PEG-g-poly(AA) hydrogel nanocomposite.

4.3 SWELLING STUDIES OF SYNTHESISED HYDROGELS AND HYDROGEL NANOCOMPOSITES

The swelling behavior studies were conducted to evaluate the percentage swelling (PS) of synthesized hydrogels and hydrogel nanocomposites (Hocine et al., 2023). Approximately 0.5 g of the dried hydrogel or hydrogel nanocomposite sample was accurately weighed and immersed into 20 mL of distilled water at room temperature. The samples were periodically withdrawn at intervals of 30 minutes, gently blotted with filter paper to remove excess surface water, and immediately weighed using an analytical balance. This process was repeated until a constant equilibrium weight of the swollen hydrogels or hydrogel nanocomposites was achieved. The percentage swelling (PS) was quantitatively calculated using the following equation:

$$P_{S} = \left(\frac{W_2 - W_1}{W_1}\right) \times 100$$

 W_1 = Initial hydrogel or hydrogel nanocomposite weight, W_2 = equilibrium swollen weight.

The hydrogel or hydrogel nanocomposite sample demonstrating the highest swelling capacity was subsequently selected for further characterization and adsorption studies.

4.4 INSTRUMENTATION AND CHARACTERIZATION

4.4.1 Microwave oven

Microwave irradiation was carried out using an IFB 17PM-MEC1 domestic microwave oven operating at a frequency of 2450 MHz, with an input power of 1200 W and a

power supply of 230 V at 50 Hz. The use of microwave energy in hydrogel synthesis offers several benefits, including rapid and uniform heating, reduced reaction time, and minimal formation of hazardous by-products (Neas, 1998). This approach is recognized as a safe, energy-efficient, and environmentally friendly method for fabricating hydrogels.

4.4.2 FTIR- Fourier transform infrared spectroscopy

The FTIR spectra of the synthesized hydrogel and hydrogel nanocomposite samples were recorded using a Perkin Elmer Spectrum 2 (Version 10.6.1) FTIR spectrophotometer equipped with an Attenuated Total Reflectance (ATR) accessory featuring a diamond crystal and a potassium bromide (KBr) focusing element. Spectral acquisition was conducted in the mid-infrared region using Spectrum 10 software. FTIR operates on the principle of absorption spectroscopy, wherein a polychromatic infrared source emits radiation that passes through an interferometer. This interferometer comprises a beam splitter that directs part of the radiation toward a stationary mirror and the rest toward a moving mirror. The reflected beams are recombined at the beam splitter, producing an interference pattern either constructive or destructive depending on the path difference. This pattern is then converted into an electrical signal by the detector, which is subsequently processed to generate the infrared spectrum. FTIR is a non-destructive, cost-effective analytical technique that requires minimal sample preparation and provides valuable information about the functional groups present in the material (Bacsik et al., 2004).

4.4.3 XRD-X-ray Diffraction

X-ray diffraction (XRD) analysis was performed using a Bruker D8 Advance diffractometer equipped with copper $K\alpha$ radiation (Cu-K α). The diffraction patterns were collected over a 2 θ range of 10° to 80° at a scanning rate of 1° per minute. XRD is a widely employed technique for investigating the crystalline structure and interatomic spacing within materials. It functions based on the principle of constructive interference generated when a crystalline substance is irradiated with monochromatic X-rays. These X-rays, emitted from a cathode ray source, interact with the sample, and only the lattice planes that satisfy Bragg's Law ($n\lambda = 2d \sin \theta$) contribute to the

diffraction pattern through constructive interference, allowing for precise structural analysis. (Epp. J 2016).

Determination of percentage crystallinity

The degree of crystallinity can be determined by differentiating the diffraction intensities associated with the crystalline and amorphous regions. It is quantified as the ratio of the crystalline peak area to the total area under the diffraction curve.

$$X_{\rm C}\% = \frac{A_{\rm C}}{A_{\rm a} + A_{\rm C}} \times 100\%$$

where X_C = percentage of crystallinity, A_a = amorphous phase area, and A_C = crystalline phase area.

4.4.4 TGA-Thermogravimetric analysis

Thermogravimetric analysis (TGA) was employed to evaluate the thermal behavior and stability of the synthesized hydrogel samples. This technique involves continuous monitoring of the sample's mass as a function of temperature under a controlled heating program. Changes in mass, such as those due to moisture evaporation, thermal degradation, or decomposition of polymeric components, are recorded over time. The analysis provides insight into the thermal stability and decomposition profile of the material. A TGA instrument from PerkinElmer (TGA4000) was utilized for this purpose. (Saadatkhah et al., 2020).

4.4.5 FESEM-Field Emission Scanning Electron microscopy

The JEOL FESEM (JSM-7610F Plus EDS: OXFORD EDS X-MaxN), equipped with a Schottky Field Emission Gun and semi-in-lens objective, offers ultrahigh-resolution imaging down to 1.0 nm at 15 kV and 1.3 nm at 1 kV. Operating at accelerating voltages from 0.1 to 30 kV with magnifications up to 1,000,000×, it ensures stable probe currents and high electron collection efficiency. The Gentle Beam (GB) mode enhances surface detail at low voltages, making it ideal for analyzing delicate, non-conductive materials. Integrated secondary and backscattered electron detectors provide both morphological and compositional insights (Prabhu et al., 2021). The hydrogel and nanocomposites were analyzed for their surface morphology.

4.4.6 UV-Visible Spectroscopy

UV-Visible absorption spectra were recorded using a double-beam UV-Visible spectrophotometer over a wavelength range of 200–800 nm for checking the adsorption capacity of hydrogel and nanocomposites. The instrument operates based on the Beer-Lambert law, measuring the absorbance of light by a sample at specific wavelengths to determine electronic transitions within molecules. Quartz cuvettes with a 1 cm path length were used, and distilled water served as the reference blank. This technique is widely employed for analyzing optical properties, bandgap estimations, and concentration of chromophore compounds (Upstone et al., 2012).

4.5 ADSORPTION KINETICS

Noor and Yusoff (2020) performed the adsorption studies on their synthesized hydrogel. Their method demonstrated that any dye solution should be prepared first. Efficiency of hydrogel and its nanocomposite with regard to adsorption kinetic, pH, adsorbent dosage, and dye concentration were be studied. The dye removal capacity (R) and adsorption efficiency (q) should be noted by the following equations:

$$R\% = \frac{C_0 - C_T}{C_0} \times 100$$

$$q = \frac{(C_0 - C_T)V}{W} \times 100$$

where C_0 and C_T = dye concentrations at time 0 and t, V= dye solution volume

4.5.1 Preparation of standard curve

The standard curve of dye adsorption of dyes (Amaranth (AR) and Methyl Orange (MO)) were prepared. For the preparation the dyes were dissolved in the distilled water at various concentrations and the absorption capacity was noted by UV-Visible Spectrophotometer.

A standard curve is a tool that allows us to estimate the dye concentration of unknown samples by comparing them to standards with known dye concentrations. By standard curve the R2 value was noted.

4.5.2 Adsorption experiments

Adsorption experiments were carried out on two different dyes Amaranth (AR) and Methyl orange (MO) via synthesized Bm-g-poly (AA) hydrogel and ZnO-BM-g-poly (AA) hydrogel nanocomposite.

Steps of adsorption were as follows:

- The dried hydrogel and hydrogel nanocomposite was weighed 2.5 g each.
- The concentration of AR and MO was varied in the range of 2-10 ppm.
- The dye solution was prepared via dissolving known amount of dye in distilled water to get ppm solution.
- The weighed amount of hydrogel was put in flask bottles containing various dye solutions.
- The U.V spectra of dye solution at 0 hr with hydrogel was noted.
- After interval of 30 mins, the absorption of dye on hydrogel was recorded with the help of U.V. spectrophotometer.

4.6 DESORPTION EXPERIMENTS

Adsorption–desorption studies were carried out to assess the regeneration and reusability of ZnO-BM-g-poly(AA) hydrogel nanocomposite for the removal of Amaranth (AR) and Methyl orange (MO) (Aljeboree et al., 2024).

The experimental procedure was as follows:

- After completion of the adsorption experiment and attainment of equilibrium, the
 dye-loaded hydrogel nanocomposite was separated from the remaining dye solution
 by filtration/decantation. The recovered adsorbents were gently rinsed with a small
 volume of distilled water to remove loosely adhering dye molecules and blotted on
 filter paper to remove excess surface moisture.
- For desorption, a known mass (2.5 g) of the dye-loaded ZnO-BM-g-poly(AA)
 nanocomposite was transferred to conical flasks containing a fixed volume of
 desorbing medium.

- To identify suitable regenerating media, desorption was performed using aqueous solutions of NaOH, HCl, and HNO₃ in the concentration range 0.01–0.10 N, as well as acetone, ethanol and distilled water.
- The flasks were kept on an orbital shaker at room temperature to facilitate release of AR and MO from the nanocomposite matrix into the desorbing solutions. At selected time intervals, aliquots of the supernatant were withdrawn and their absorbance was recorded at the respective λmax of AR and MO using a UV–Vis spectrophotometer.
- The concentration of dye desorbed at each interval was obtained from the corresponding calibration curve, and the amount of dye released per gram of adsorbent was calculated. Desorption efficiency (%) was determined as the ratio of the total amount of dye desorbed to the amount initially adsorbed, multiplied by 100.
- After desorption, ZnO-BM-g-poly(AA) nanocomposite were thoroughly rinsed with deionized water until neutral pH, followed by drying at 65 °C for 12 h in a hotair oven.
- The regenerated adsorbents were then reused for fresh AR and MO solutions under the same conditions as the initial adsorption run, and adsorption—desorption cycles were repeated to evaluate the operational stability and reusability of the materials.

Amount desorbed per gram:

q.des =
$$\frac{(C_d V_d)}{m}$$
 (mg/g)

Desorption (%):
$$=\frac{qt.Desorption}{qt.adsorption} \times 100$$

Where, Desorbed dye concentration in solution: $C_d(\text{mg/L})$, Volume of desorbing solution: $V_d(L)$ and Mass of dye-loaded adsorbent used: m(g)

CHAPTER 5 RESULTS AND DISCUSSION

5.1 NATURAL HYDROGEL SYNTHESIS VIA VARIOUS ROUTES

5.1.1 Microwave Irradiation

The purified extracted Butea monosperma gum is utilized for the synthesis of hydrogel. Poly(AA) grafted *Butea monosperma* gum (BM) is synthesized using microwave irradiation method. APS and MBA are utilized being an initiator and a cross-linking representative correspondingly. The main steps of radical polymerization of AA with BM are chain initiation, propagation and termination. The reaction propagates by the generation of free radicals on both BM and monomer due to the microwave radiation. APS is a thermal initiator which gets decomposed and resulted in the formation of sulphate ion radicals under microwave irradiation. Subsequently, the water molecules absorb the energy from microwave and pass it to the AA molecules leading to dielectric heating that consequently led to double bonds breakage and also in the production of another set of free radicals. A number of radicals are produced on the hydroxyl group of backbone (BM) (Sharma et al., 2014).



Figure 5.1: Synthesized BM-g-poly(AA) hydrogel

The chain initiation starts with the molecules of monomer that are present nearby to the reaction sites, turn into BM radical acceptor and later itself turn into donor of free radicals to the surrounding molecules. The next step of propagation led to the reaction of polymer chains with cross-linker end groups. This way the cross-linked structure of the copolymer was formed. Synthesized BM-g-poly (AA) hydrogel is displayed in figure 5.1. Figure 5.2 highlights the chemical reactions taking place during the process and 5.3 the schematic of bond formation during radical polymerization.

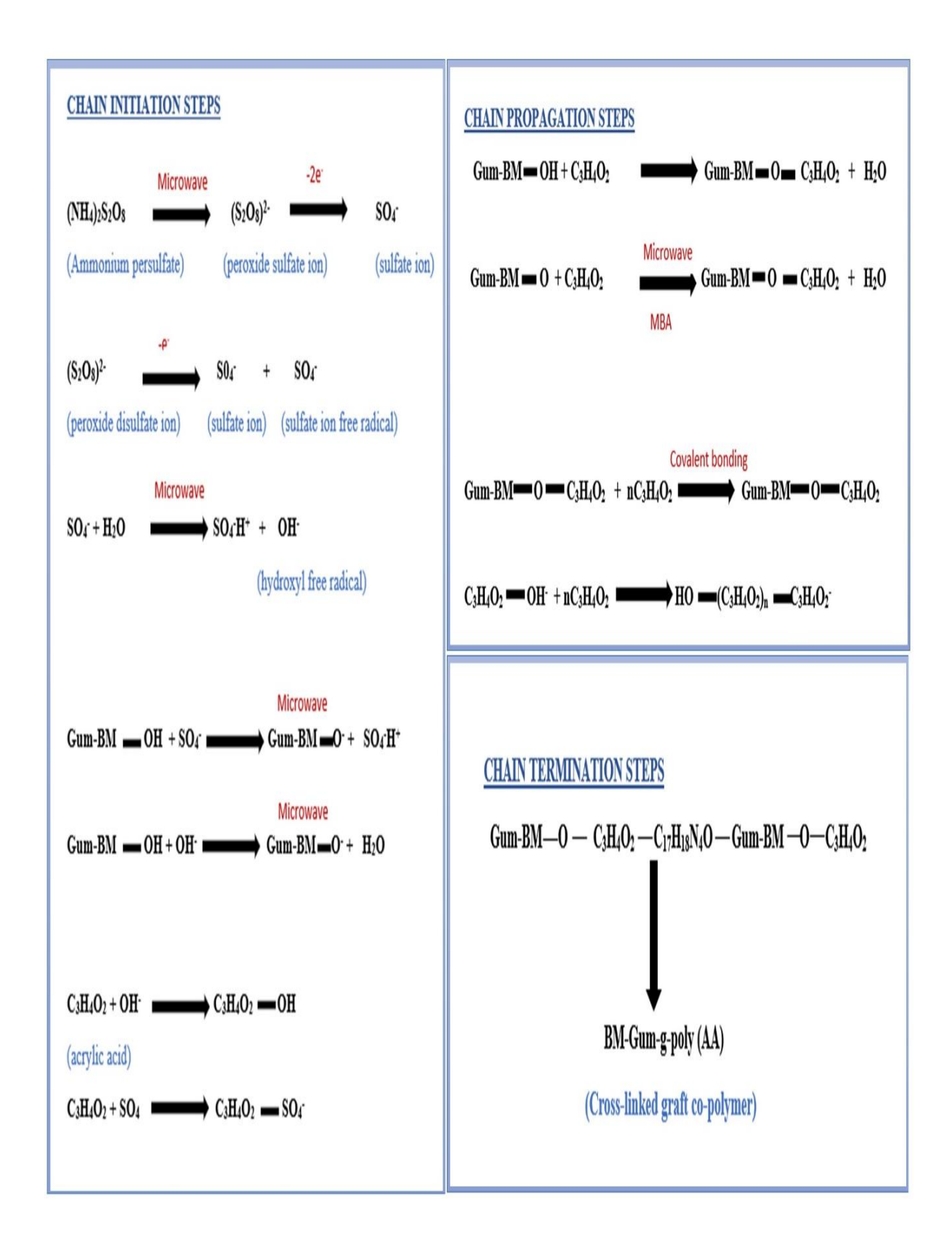


Figure 5.2: Process of chain initiation, propagation and termination during formation of hydrogel

Figure 5.3: Bond Formation during Radical polymerization

5.1.2 Thermal Polymerization

Poly(AA)-grafted *Butea monosperma* gum (BM) was synthesized via conventional thermal polymerization using APS as a thermal initiator and MBA as the cross-linking agent. Upon heating the reaction mixture at 60–70°C, APS thermally decomposed, producing sulfate ion radicals which initiated the radical polymerization process. These radicals abstracted hydrogen atoms from the hydroxyl groups present on the BM backbone, generating active BM macroradicals. Simultaneously, acrylic acid (AA) underwent thermal activation, leading to the formation of vinyl radicals. The initiation step involved radical attack by BM or sulfate radicals on the double bond of AA, resulting in the start of chain growth. During the propagation phase, growing poly(AA) chains continued to add AA monomers, forming a graft copolymer structure on the BM backbone. MBA served as a cross-linker by reacting with the growing polymer chains,

thereby forming a three-dimensional hydrogel network (figure 5.4). Although the reaction proceeded successfully, the process was relatively slower, required prolonged heating, and exhibited less uniform grafting efficiency compared to microwave irradiation (Li et al., 2022; Bakshi et al., 2024).



Figure 5.4: Hydrogel formed via Thermal polymerization

5.1.3 Chemical Initiation

Poly(AA)-grafted BM hydrogel was also synthesized through a redox-initiated polymerization route using APS and Fe²⁺ ions (from FeSO₄) as the redox initiator system, with MBA as the cross-linking agent. The redox pair initiated the generation of sulfate and hydroxyl radicals at ambient temperature via electron transfer reactions. These radicals activated the hydroxyl functionalities on the BM backbone, forming BM macroradicals. Acrylic acid (AA) underwent radical initiation and began chain propagation by successive monomer addition to the radical chain ends. The initiation predominantly occurred at the sites where radical species from APS and Fe²⁺ interacted with BM or AA. The chain propagation step continued until termination by radical recombination or disproportionation. Cross-linking with MBA occurred concurrently, leading to a covalently bonded three-dimensional network structure (figure 5.5). While redox initiation allowed polymerization under mild temperature conditions, the reaction was relatively slower than microwave-assisted synthesis and often showed lower grafting efficiency due to the diffusional limitations and uneven radical distribution (He et al., 2024; Khanam et al., 2025).

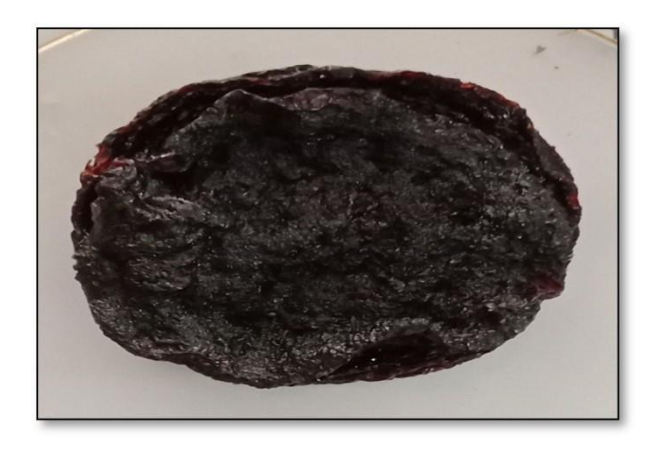


Figure 5.5: Hydrogel formed via Chemical (redox) initiation

5.1.4 Synthetic hydrogel Synthesis (PEG-g-poly (AA) hydrogel)

PEG-grafted-poly(acrylic acid) hydrogel (PEG-g-poly(AA)) is synthesized via microwave irradiation-assisted radical polymerization. Ammonium persulfate (APS) acts as the initiator, and N,N'-methylene-bis-acrylamide (MBA) serves as the cross-linking agent. The fundamental steps involved in the radical polymerization include chain initiation, propagation, and termination (Wang et al., 2023).

The polymerization reaction initiates upon exposure to microwave irradiation, whereby APS, functioning as a thermal initiator, decomposes thermally, generating sulfate radical anions (SO₄⁻). Concurrently, microwave energy absorption by water molecules results in dielectric heating, transferring the thermal energy to acrylic acid (AA) monomers. Consequently, AA monomer molecules undergo double bond cleavage, producing reactive free radicals. Parallelly, hydroxyl end-groups of PEG are activated by microwave radiation, forming radical active sites along the PEG backbone. These PEG radicals initiate the grafting reaction by reacting with nearby AA monomer radicals. Initially, AA radicals function as radical acceptors when interacting with the PEG backbone, and subsequently transform into radical donors, extending polymerization by further reacting with additional AA monomers. The propagation step continues as the growing polymer chains interact with MBA, which serves to cross-link polymer chains through bifunctional vinyl groups. This interaction results in the formation of a three-dimensional, cross-linked hydrogel network structure.

Ultimately, chain termination occurs through radical-radical recombination or disproportionation reactions, stabilizing the hydrogel network and producing the synthetic hydrogel, PEG-g-poly(AA) as shown in figure 5.6.



Figure 5.6: Synthesized PEG-g-poly(AA) hydrogel

5.2 HYDROGEL NANOCOMPOSITE FORMATION MECHANISM

5.2.1 ZnO nanoparticle formation

ZnO nanoparticles are prepared utilizing sol-gel method as explained in the methodology. The prepared ZnO nanoparticles are white in colour and oval in shape confirmed by instrumentation discussed under instrumentational analysis (figure 5.7) (Sukri et al., 2019).



Figure 5.7: Prepared ZnO nanoparticles

5.2.2 Synthesis of ZnO-BM-g-poly (AA) hydrogel nanocomposite

The ZnO-BM-g-poly(AA) hydrogel nanocomposite is synthesized via a microwave-assisted radical polymerization method involving poly(acrylic acid) (AA), *Butea monosperma* gum (BM), and zinc oxide nanoparticles (ZnO). Ammonium persulfate (APS) acts as a thermal radical initiator, and N,N'-methylene-bis-acrylamide (MBA) is employed as a cross-linking agent. The fundamental polymerization involves the initiation, propagation, and termination steps, which are influenced significantly by microwave radiation.

- Radical Generation (Initiation Step): Under microwave irradiation, APS thermally decomposes, producing reactive sulfate ion radicals (SO₄⁻). Concurrently, water molecules absorb microwave energy, resulting in dielectric heating. This heat facilitates the homolytic cleavage of the double bonds present in AA monomers, forming AA radicals (CH₂–CH–COOH). Simultaneously, microwave irradiation promotes radical formation at the hydroxyl-rich sites of the BM gum backbone (–OH), generating macroradicals on BM chains.
- Chain Propagation (Grafting and Cross-linking): The radical species generated on BM and AA monomers initiate polymerization by interacting with each other through radical addition reactions. Initially, the AA radicals act as radical acceptors, bonding covalently to reactive sites on the BM gum backbone. Upon binding, these grafted radicals further act as radical donors, initiating polymerization with adjacent AA monomer radicals. This chain-growth reaction continues, forming polymer chains grafted onto the BM backbone. MBA molecules, having two vinyl groups, actively participate in cross-linking reactions. These cross-linkers connect polymer chains by reacting with radical ends of growing polymer chains, forming stable covalent bonds and producing a three-dimensional polymeric network structure with BM as the backbone (Choudhary et al., 2022).
- Incorporation of ZnO Nanoparticles (Nanocomposite Formation): The optimized BM-g-poly(AA) hydrogel network incorporates ZnO nanoparticles through physical and chemical interactions. When ZnO nanoparticles are introduced into the reaction medium and exposed again to microwave irradiation, surface functional groups (–OH) on ZnO interact strongly via

hydrogen bonding and electrostatic attractions with carboxyl (–COOH) groups from poly(acrylic acid) chains. Surface hydroxyl groups (Zn–OH) present on ZnO nanoparticles form strong intermolecular hydrogen bonds with carboxyl groups (–COOH) on poly(AA). Such hydrogen bonding significantly enhances interfacial interactions and ensures strong anchoring of ZnO nanoparticles within the hydrogel matrix. The carboxylate ions (–COO⁻), produced by partial ionization of poly(acrylic acid) in aqueous conditions, strongly interact electrostatically with positively charged zinc centers (Zn²⁺ ions) on the ZnO nanoparticle surfaces. Additionally, these carboxylate groups may coordinate directly to Zn²⁺ ions on the ZnO surface, forming stable coordination bonds, further embedding nanoparticles into the hydrogel network structure.

- Chain Termination (Stabilization of Network): The reaction ultimately terminates by radical–radical recombination or disproportionation, stabilizing the hydrogel's three-dimensional polymeric network. Consequently, a cross-linked network structure containing uniformly dispersed ZnO nanoparticles forms, leading to the creation of the final ZnO-BM-g-poly(AA) hydrogel nanocomposite (figure 5.8).
- **Finalization and Drying:** Upon completion of microwave treatment, the nanocomposite hydrogel is allowed to cool to room temperature and subsequently dried at approximately 60°C overnight. This drying step removes excess solvent (water) and locks the polymeric chains and nanoparticles into a stable, well-defined structure (Sharma et al., 2014).



Figure 5.8: ZnO-BM-g-poly (AA) hydrogel nanocomposite

5.2.3 Synthesis of ZnO-PEG-g-poly(AA) Hydrogel Nanocomposite

ZnO-PEG-g-poly(acrylic acid) hydrogel nanocomposite is synthesized via microwave-assisted radical polymerization, utilizing poly(ethylene glycol) (PEG), acrylic acid (AA), zinc oxide nanoparticles (ZnO), APS (initiator), and MBA (cross-linker). The synthesis involves three primary stages: radical initiation, propagation, and termination. Initially, microwave irradiation induces thermal decomposition of APS, generating sulfate radical anions (SO₄⁻). Simultaneously, absorbed microwave energy leads to dielectric heating of water molecules, promoting homolytic cleavage of the acrylic acid double bonds and resulting in AA radicals formation. Concurrently, microwave radiation activates hydroxyl groups (–OH) at PEG chain ends, creating reactive PEG-based radicals. During propagation, PEG radicals graft onto AA monomer radicals, producing grafted polymer chains (PEG-g-poly(AA)). MBA cross-links these polymer chains via covalent bonding, establishing a stable three-dimensional network.

Subsequently, ZnO nanoparticles are incorporated into the PEG-g-poly(AA) hydrogel. Under further microwave exposure, ZnO nanoparticles chemically interact with the hydrogel network through strong hydrogen bonding and coordination interactions between nanoparticle surface hydroxyl groups and carboxylate groups (-COO⁻) of poly(acrylic acid). Finally, the synthesized ZnO-PEG-g-poly(AA) nanocomposite hydrogel (figure 5.9) is cooled and dried overnight at 60°C, yielding a robust polymeric nanocomposite with uniformly dispersed ZnO nanoparticles embedded within its polymer matrix (Wang et al., 2023).



Figure 5.9: ZnO-PEG-g-poly(AA) hydrogel nanocomposites

5.3 SWELLING AND OPTIMIZATION STUDIES

5.3.1 BM-g-poly (AA) hydrogel

5.3.1.1 Microwave Irradiation

Optimized reaction conditions

The optimization of various factors namely, initiator concentration, reaction time, solvent concentration, monomer concentration and crosslinker concentration is done. These factors highly influence the degree of swelling of hydrogels (Jeong et al., 2010; Virk et al., 2022; Makhado et al., 2022). Various reaction conditions influencing percentage swelling (P_s) are discussed below:

Effect of initiator concentration on Ps

The initiator concentration is ranged from 0.0219-0.0394 mol/L to learn about its outcome on swelling percentage (figure 5.10A) (table 5.1). The P_s increased with growing the initiator concentration initially and later decreased with increasing the concentration. The highest P_s is achieved at initiator concentration 0.03067 mol/L that is $310 \pm 0.6\%$. At lesser concentrations the upsurge in P_s is ascribed to the rise in number of free radicals generated on BM that corresponds to rapid graft polymerization. However, premature end of the reaction occurred at higher initiator concentration which did not permit grafting reactions to take place. Consequently, at high initiator concentrations lesser P_s was observed (Sharma et al., 2014).

Table 5.1: Initiator optimization of natural hydrogel

S.No	Back-	Solvent	Initiator	Monomer	time	Cross-	
	bone	(ml)	(g)	(ml)	(sec)	linker	Mean
	(g)					(g)	

							(%Ps) ±
							S.D
1.	0.2	10	0.05	2	40	0.05	302 ± 0.4
2.	0.2	10	0.06	2	40	0.05	300 ± 0.5
3.	0.2	10	0.07	2	40	0.05	310 ± 0.6
4.	0.2	10	0.08	2	40	0.05	304 ± 0.3
5.	0.2	10	0.09	2	40	0.05	294 ± 0.5

Effect of amount of solvent on Ps

Solvent concentration and its outcomes on the P_s are displayed in the figure 5.10 B and table 5.2. The rise in P_s is detected until 6 mL of the concentration and then decreased. For achieving a maximum Ps of $328 \pm 0.4\%$, it was determined that 6 mL of solvent was the optimal quantity. This may be due to the generation of hydroxyl radical ions at the optimal solvent concentration, which generates more active sites for polymerization and thus increases Ps (Nath et al., 2023). There was no hydrogel formation below 6 mL of solvent.

Table 5.2 : Solvent optimization of natural hydrogel

S.No	Back- bone (g)	Solvent (ml)	Initiato r (g)	Monomer (ml)	time (sec)	Cross- linker (g)	Mean (%Ps) ± S.D
1.	0.2	6	0.07	2	40	0.05	328 ± 0.4
2.	0.2	7	0.07	2	40	0.05	290 ± 0.5

3.	0.2	8	0.07	2	40	0.05	280 ± 0.4
4.	0.2	9	0.07	2	40	0.05	288 ± 0.5
5.	0.2	10	0.07	2	40	0.05	266 ± 0.3

Effect of monomer concentration on Ps

By changing the monomer content, the variations in swelling % are investigated. The P_s increased with rise in concentration of monomer achieving maximum P_s at 3mL concentration of AA giving 452 \pm 0.6% swelling degree (Figure 5.10C) (table 5.3). Further this concentration no hydrogel formation occurred.

This behaviour stems from the fact that the hydrophilic monomer AA is initially readily accessible for cross-linking with the BM backbone, boosting the affinity of water absorption and ultimately to high Ps. However, at the optimal AA concentration, the Ps emerged attributable to the increased viscosity of the solution, thus restricted free radicals and monomer molecules from migrating around, as well as because homo polymerization prevailed over graft copolymerization (Vakili et al., 2021; Thakur et al., 2022).

Table 5.3: Monomer Optimization of natural hydrogel

S.No	Back-	Solvent	Initiator	Monomer	time	Cross-	
	bone	(ml)	(g)	(ml)	(sec)	linker	Mean
	(g)					(g)	(%P _s) ±
							S.D
1.	0.2	6	0.07	1	40	0.05	212 ± 0.5
2.	0.2	6	0.07	1.5	40	0.05	262 ± 0.3

3.	0.2	6	0.07	2	40	0.05	308 ± 0.7
4.	0.2	6	0.07	2.5	40	0.05	312 ± 1.0
5.	0.2	6	0.07	3	40	0.05	452 ± 0.6
6.	0.2	6	0.07	3.5	40	0.05	Didn't form

Effect of Cross-linker on Ps

The concentration of cross-linker is investigated in range from 0.0432-0.0864 mol/L to study its effect on P_s (figure 5.10D) (table 5.4). Crosslinker is required because it completely dissolves the hydrophilic polymer chains into an aqueous solution, rendering the hydrogel insoluble in water. The P_s increased by the rise in concentration of MBA till 0.0648 mol/L where maximum P_s of $420 \pm 1.0\%$ is achieved. According to Flory's network theory, the cross-linking density and fluid absorbency of hydrogels are governed by the concentration of the cross-linking chains. Consequently, when cross-linker concentration grew, the number of network chains also increased, improving the cross-linking density. The swelling capacity of the grafted polymer reduced when cross-linker concentration increased above 0.0648 mol/L. It is owing to the fact that with increased cross-linker concentration there may be generation of many chains in the polymeric network resulting in highly compact and rigid structure. Due to its inability to successfully absorb a high volume of water, the recommended construction would result in minimal swelling (Nath et al., 2023).

Table 5.4: Cross-linker optimization of natural hydrogel

S.No	Back-	Solvent	Initiator	Monomer	time	Cross-	
	bone	(ml)	(g)	(ml)	(sec)	linker	Mean
	(g)					(g)	$(\%P_s) \pm$
							S.D

1.	0.2	6	0.07	3	40	0.04	246 ± 0.5
2.	0.2	6	0.07	3	40	0.05	300 ± 0.4
3.	0.2	6	0.07	3	40	0.06	420 ± 1.0
4.	0.2	6	0.07	3	40	0.07	224 ± 0.5
5.	0.2	6	0.07	3	40	0.08	200 ± 0.7

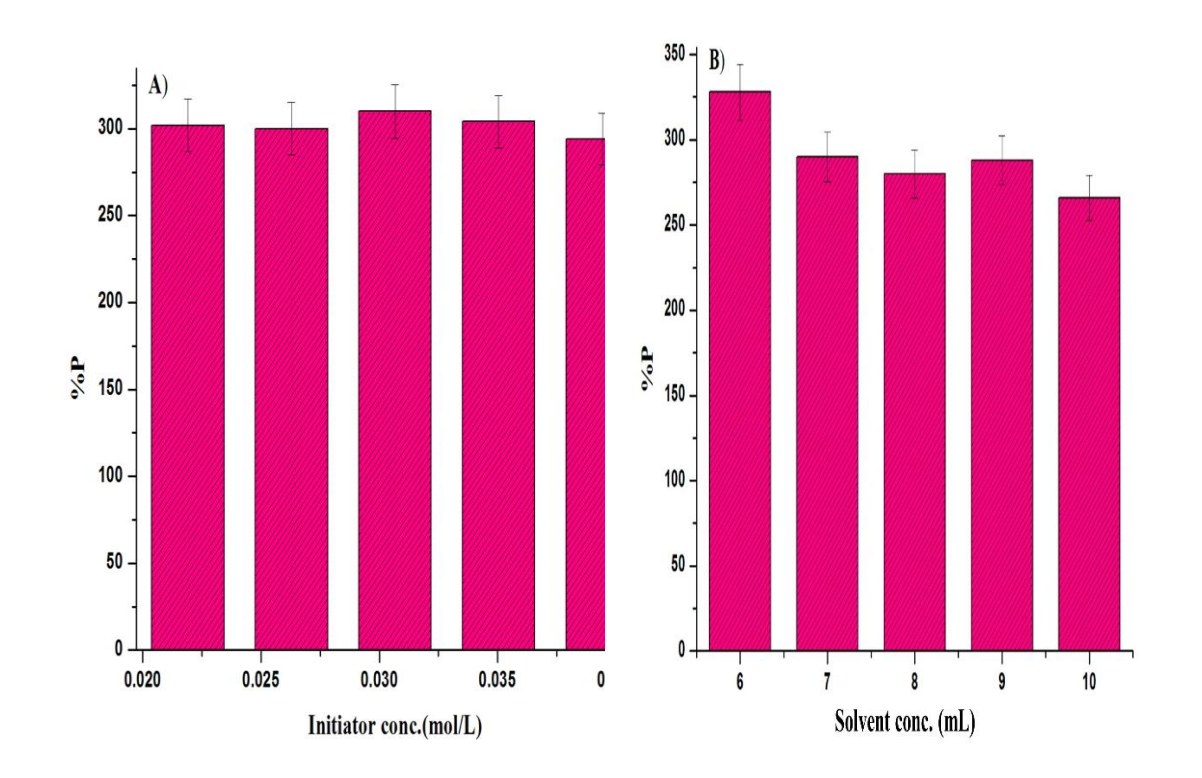
Effect of reaction time on Ps

The changes in P_s are examined with respect to reaction time to obtain a hydrogel with higher water absorbency. To achieve maximum P_s , the reaction time is varied from 30-44 seconds. It can be observed from the figure 5.10E that the P_s increased up to 40s and then gradually decreased. The maximum P_s is achieved at a reaction time of 40s that is $448 \pm 1.0\%$. At higher reaction time there is a decrease in P_s due to minor availability of consuming reactants and also by lessening of active free sites for grafting with increased reaction time (table 5.5).

Table 5.5: Time of reaction optimization of natural hydrogel

S.No	Back-	Solvent	Initiator	Monomer	time	Cross-	
	bone	(ml)	(g)	(ml)	(sec)	linker	Mean
	(g)					(g)	(%Ps) ±
							S.D
1.	0.2	6	0.07	3	30	0.06	180 ± 0.5
2.	0.2	6	0.07	3	32	0.06	194 ± 0.4
3.	0.2	6	0.07	3	34	0.06	214 ± 0.6
4.	0.2	6	0.07	3	36	0.06	236 ± 0.5
5.	0.2	6	0.07	3	38	0.06	340 ± 0.9

6.	0.2	6	0.07	3	40	0.06	448 ± 1.0
7.	0.2	6	0.07	3	42	0.06	400 ± 0.7
8.	0.2	6	0.07	3	44	0.06	260 ± 0.6



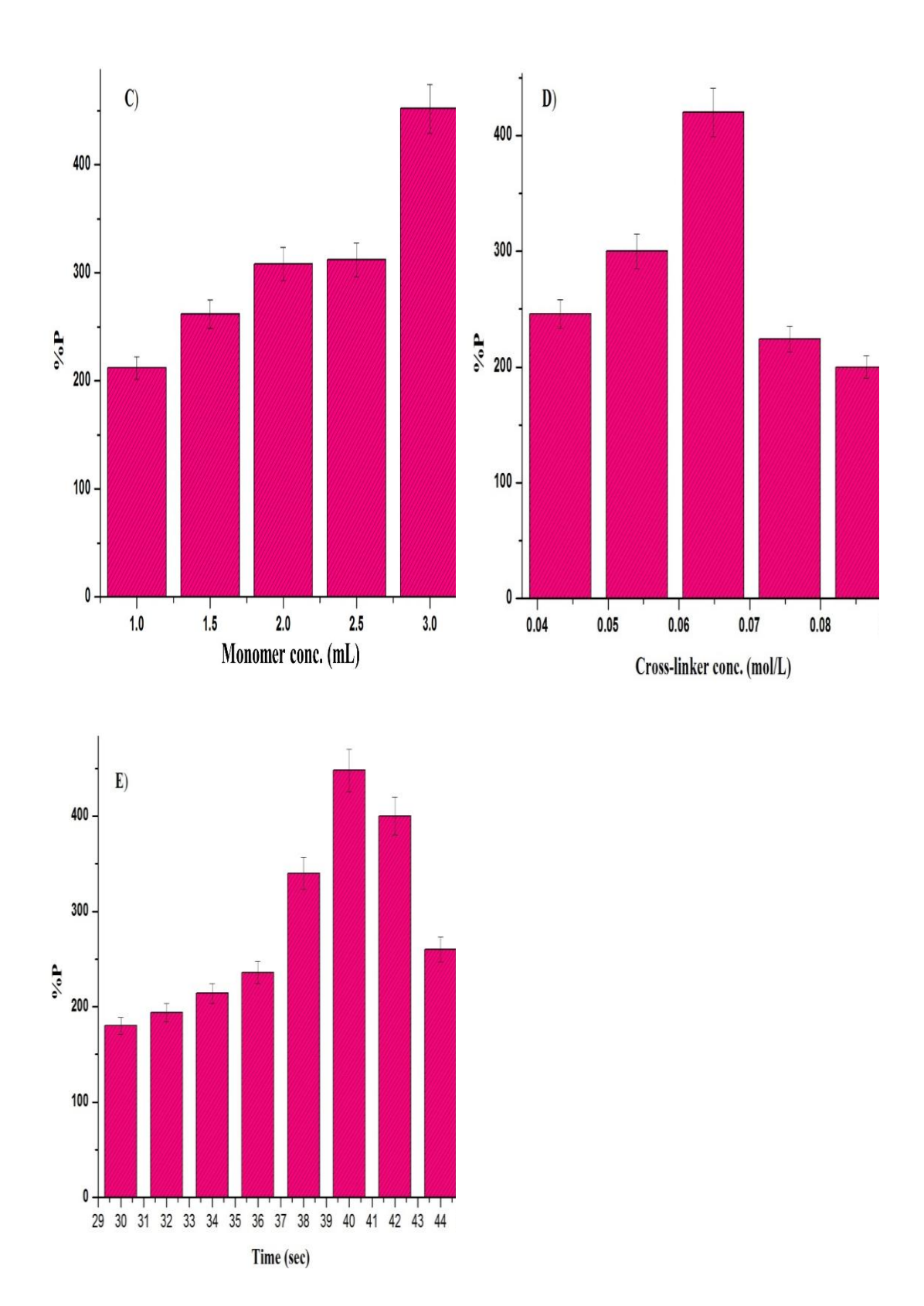


Figure 5.10: Variation in swelling percentage (%P) with respect to (A) Initiator concentration, (B) Solvent, (C) Monomer, (D) Cross-linker and (E) Time of BM-g-poly (AA) hydrogel

5.3.1.2 Thermal Polymerization

The hydrogel synthesized via thermal polymerization exhibited a maximum swelling percentage of $312 \pm 0.9\%$, significantly lower than that achieved through microwave-assisted synthesis. Using 0.2 g of *Butea monosperma* (BM) gum in 10 mL of distilled water, with 0.07 g of APS as the thermal initiator, 3 mL of acrylic acid (AA) as monomer, and 0.06 g of MBA as the cross-linker, the reaction was carried out at elevated temperatures for 5 hours. The lower swelling behavior observed in the thermally synthesized hydrogel may be attributed to slower and less uniform heat distribution during polymerization, which likely led to lower grafting efficiency and a denser, more rigid cross-linked structure. This reduced the hydrogel's capacity to absorb water effectively compared to the rapid and volumetrically uniform heating provided by microwave irradiation (Zhao et al., 2021).

5.3.1.3 Chemical Initiation

In the case of chemical initiation via redox polymerization, the maximum swelling percentage recorded was $278 \pm 1.2\%$. The synthesis was performed using 0.2 g of BM in 10 mL of distilled water, initiated with a redox pair of 0.07 g APS and 0.01 g FeSO₄, combined with 3 mL of AA and 0.06 g of MBA. The reaction proceeded over a period of 6 hours at ambient conditions. The comparatively lower swelling percentage is likely due to slower radical generation and less efficient grafting under redox conditions, which may result in less porous and tightly cross-linked hydrogel networks. Additionally, the extended reaction time and possible oxidative degradation of functional groups may also contribute to the diminished water uptake capacity relative to the microwave-assisted route (Khanam et al., 2025).

Microwave irradiation synthesis was finalized and further utilized for synthesis as it shows best swelling percentage (table 5.6).

Table 5.6: Optimized swelling of Natural Hydrogel Synthesized via different routes

Hydrogel	Route	BM	Solvent	Initiator	Monomer	Cross-	Reaction	Mean
		(g)	(mL)	(APS, g)	(AA, mL)	linker (MBA, g)	time	(%Ps) ± S.D
BM-g- poly(AA)	Microwave Irradiation	0.2	6	0.07	3	0.06	40 s	448 ± 1.0
BM-g- poly(AA)	Thermal Polymerization	0.2	10	0.07	3	0.06	5 hr	312 ± 0.9
BM-g- poly(AA)	Chemical Initiation	0.2	10	0.07/ FeSO4= 0.01	3	0.06	6 hr	278 ± 1.2

5.3.2 ZnO-BM-g-poly (AA) hydrogel nanocomposite

For the synthesis of ZnO-BM-g-poly(AA) hydrogel nanocomposites, the previously optimized conditions for BM-g-poly(AA) hydrogel (backbone: 0.2 g, solvent: 6 mL, initiator: 0.07 g, monomer: 3 mL, cross-linker: 0.06 g, reaction time: 40 s) were employed while varying ZnO nanoparticle concentration (0.05–0.25 g) to evaluate their influence on percentage swelling (Ps). The incorporation of ZnO nanoparticles significantly enhanced the swelling properties, as observed in Table 4.1. Initially, the swelling increased consistently from 268% at 0.05 g ZnO to a maximum of 515% at an optimal concentration of 0.2 g ZnO. The improved swelling at optimal ZnO concentration is attributed to enhanced hydrophilicity and increased interaction between ZnO nanoparticles and polymeric networks via hydrogen bonding and electrostatic interactions. However, further increase in ZnO concentration (0.25 g) led to a reduction in swelling (370%) due to possible nanoparticle aggregation, causing

rigidity within the hydrogel structure and restricting its water absorption capacity. Thus, 0.2 g ZnO nanoparticles were established as the optimum concentration for achieving maximum swelling ($515 \pm 0.8\%$) in ZnO-BM-g-poly(AA) hydrogel nanocomposites as displayed in figure 5.11 and table 5.7. Figure 5.12 displays the various concentrations of nanocomposites places in swelling studies.

Table 5.7: Optimized reaction conditions for ZnO-BM-g-poly-(AA hydrogel nanocomposite

S.No	Back-	Solven	Initiator	Monomer	time	Cross-	ZnO (g)	
	bone	t	(g)	(ml)	(sec)	linker		Mean
	(g)	(ml)				(g)		(%P _s) ±
								S.D
1.	0.2	6	0.07	3	40	0.06	0.05	268 ± 0.6
2.	0.2	6	0.07	3	40	0.06	0.1	354 ± 0.7
3.	0.2	6	0.07	3	40	0.06	0.15	425 ± 1.0
4.	0.2	6	0.07	3	40	0.06	0.2	515 ± 0.8
5.	0.2	6	0.07	3	40	0.06	0.25	370 ± 0.5

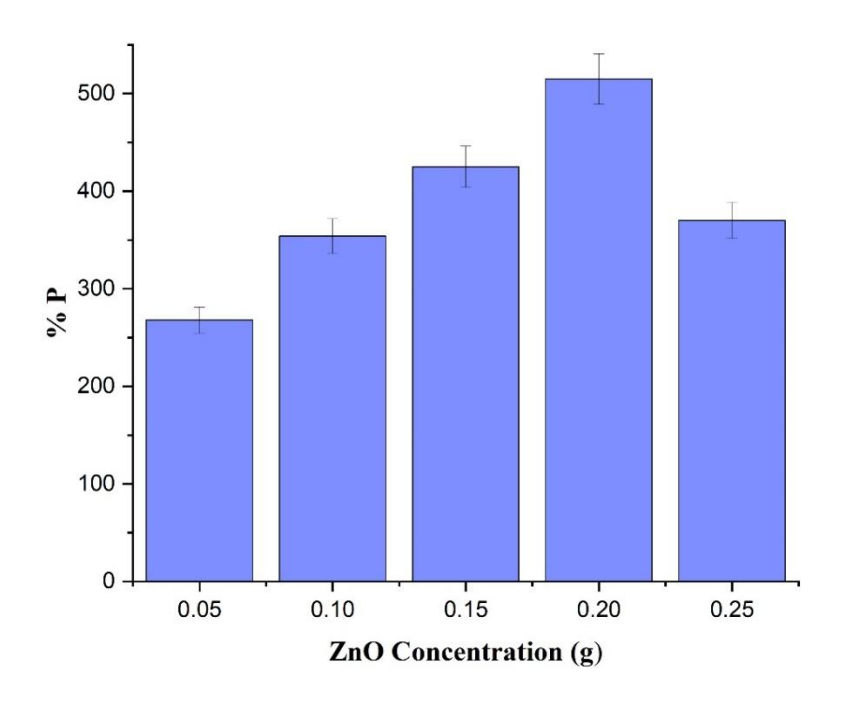


Figure 5.11: Optimized reaction conditions with maximum %P for ZnO-BM-g-poly-(AA) hydrogel nanocomposite



Figure 5.12: Swelling studies for hydrogel nanocomposite.

5.3.3 PEG-g-poly(AA) hydrogel

Optimized reaction conditions

The optimization of various factors namely, initiator concentration, reaction time, solvent concentration, monomer concentration and crosslinker concentration is done for synthesis of hydrogel from synthetic backbone. Various reaction conditions influencing percentage swelling (P_s) are discussed below:

Effect of initiator concentration on Ps

The influence of initiator concentration (ammonium persulfate, APS) on the swelling behavior of PEG-g-poly(AA) hydrogel was evaluated by varying its amount from 0.05 to 0.09 g, with all other parameters held constant. As shown in Table 5.8 and figure 5.13A, the swelling percentage (%Ps) increased significantly with rising APS concentration, from $110 \pm 0.4\%$ at 0.05 g to a maximum of $215 \pm 1.0\%$ at 0.08 g. This enhancement is attributed to the increased generation of free radicals with higher initiator content, which promotes effective grafting of acrylic acid onto the PEG backbone and leads to a more hydrophilic network structure. However, further increase to 0.09 g resulted in a reduced %Ps of $190 \pm 0.5\%$, likely due to excessive radical concentration causing premature termination reactions and self-polymerization, which interfere with graft copolymerization (Saidi et al., 2020). Therefore, 0.08 g of APS was identified as the optimal initiator concentration for achieving maximum swelling in the PEG-g-poly(AA) hydrogel system.

Table 5.8: Initiator optimization of synthetic hydrogel

S.No	Synthet ic Back- bone (g)	Solvent (ml)	Initiator (g)	Monomer (ml)	time (sec)	Cross- linker (g)	Mean (%P _s) ± S.D
1.	0.2	10	0.05	2	120	0.05	110 ± 0.4
2.	0.2	10	0.06	2	120	0.05	150 ± 0.7

3.	0.2	10	0.07	2	120	0.05	205 ± 0.6
4.	0.2	10	0.08	2	120	0.05	215 ± 1.0
5.	0.2	10	0.09	2	120	0.05	190 ± 0.5

Effect of amount of solvent on Ps

The effect of solvent volume (distilled water) on the swelling behavior of synthetic hydrogel was assessed by varying the solvent from 8 to 12 mL while keeping other synthesis parameters constant. As presented in Table 5.9 and figure 5.13B, the swelling percentage (%Ps) increased with solvent volume, reaching a maximum of $220 \pm 1.0\%$ at 10 mL. This increase can be attributed to improved solvation and dispersion of reactants, which facilitates uniform radical generation and efficient grafting of acrylic acid onto the PEG backbone. However, a further rise in solvent volume beyond 10 mL led to a slight decline in swelling, with %Ps decreasing to $215 \pm 0.6\%$ at 11 mL and $205 \pm 0.5\%$ at 12 mL. The reduction in swelling at higher solvent volumes may be due to dilution of reactants, which lowers the probability of effective collisions between active species and reduces network density (Saidi et al., 2020; Khan et al., 2024). Thus, 10 mL of distilled water was identified as the optimal solvent volume for achieving maximum swelling in the PEG-g-poly(AA) hydrogel system.

Table 5.9: Solvent optimization of synthetic hydrogel

S.No	Back- bone (g)	Solvent (ml)	Initiator (g)	Monomer (ml)	time (sec)	Cross- linker (g)	Mean (%Ps) ± S.D
1.	0.2	8	0.08	2	120	0.05	175 ± 0.5
2.	0.2	9	0.08	2	120	0.05	185 ± 0.7

3.	0.2	10	0.08	2	120	0.05	220 ± 1.0
4.	0.2	11	0.08	2	120	0.05	215 ± 0.6
5.	0.2	12	0.08	2	120	0.05	205 ± 0.5

Effect of monomer concentration on Ps

The impact of monomer (acrylic acid) concentration on the swelling behavior of hydrogel was studied by varying its volume from 1.0 to 3.5 mL, while maintaining all other synthesis parameters constant. As shown in Table 5.10 and figure 5.13C, the swelling percentage (%Ps) increased progressively from $180 \pm 0.6\%$ at 1.0 mL to a maximum of $240 \pm 0.5\%$ at 2.5 mL. This enhancement is attributed to the greater availability of hydrophilic carboxylic groups from acrylic acid, which increases the hydrogel's affinity for water and promotes effective grafting onto the PEG backbone. However, a further increase in monomer concentration beyond 2.5 mL led to a noticeable decline in swelling, with %Ps decreasing to $208 \pm 0.5\%$ at 3.0 mL and $190 \pm 0.4\%$ at 3.5 mL. The decline is likely due to increased solution viscosity and the onset of homopolymerization, which restricts effective grafting and diffusion of monomer chains, leading to a denser network with lower water uptake (Khan et al., 2024; Hwang et al., 2024). Therefore, 2.5 mL was identified as the optimal acrylic acid concentration for maximizing the swelling capacity of PEG-g-poly(AA) hydrogel.

Table 5.10: Monomer Optimization of synthetic hydrogel

S.No	Back-	Solvent	Initiator	Monomer	time	Cross-	
	bone	(ml)	(g)	(ml)	(sec)	linker	Mean
	(g)					(g)	$(\%P_s) \pm$
							S.D
1.	0.2	10	0.08	1	120	0.05	180 ± 0.6

2.	0.2	10	0.08	1.5	120	0.05	195 ± 0.8
3.	0.2	10	0.08	2	120	0.05	222 ± 1.0
4.	0.2	10	0.08	2.5	120	0.05	240 ± 0.5
5.	0.2	10	0.08	3	120	0.05	208 ± 0.5
6.	0.2	10	0.08	3.5	120	0.05	190± 0.4

Effect of crosslinker concentration on Ps

The effect of cross-linker (MBA) concentration on the swelling behavior of synthetic hydrogel was investigated by varying its amount from 0.05 to 0.09 g while keeping other synthesis parameters constant. As observed in Table 5.11 and figure 5.13D, the swelling percentage (%Ps) increased initially, reaching a maximum value of $245 \pm 1.0\%$ at 0.06 g MBA. This enhancement is attributed to the formation of an optimal cross-linked network that effectively traps water molecules while maintaining structural flexibility. However, further increases in cross-linker concentration beyond this point resulted in a marked decline in swelling capacity, with %Ps decreasing to $200 \pm 0.6\%$ at 0.07 g and continuing to drop to $182 \pm 0.5\%$ at 0.09 g. The decline is likely due to the formation of a highly dense and rigid network structure, which limits the hydrogel's ability to absorb water (Hwang et al., 2024). Thus, 0.06 g MBA was identified as the optimum cross-linker concentration for achieving maximum swelling in the PEG-g-poly(AA) hydrogel system.

Table 5.11: Cross-linker optimization of synthetic hydrogel

S.No	Back-	Solvent	Initiator	Monomer	time	Cross-	
	bone	(ml)	(g)	(ml)	(sec)	linker	Mean
	(g)					(g)	

							$(\%P_s) \pm$
							S.D
1.	0.2	10	0.08	2.5	120	0.05	235 ± 0.5
2.	0.2	10	0.08	2.5	120	0.06	245 ± 1.0
3.	0.2	10	0.08	2.5	120	0.07	200 ± 0.6
4.	0.2	10	0.08	2.5	120	0.08	185 ± 0.4
5.	0.2	10	0.08	2.5	120	0.09	182 ± 0.5

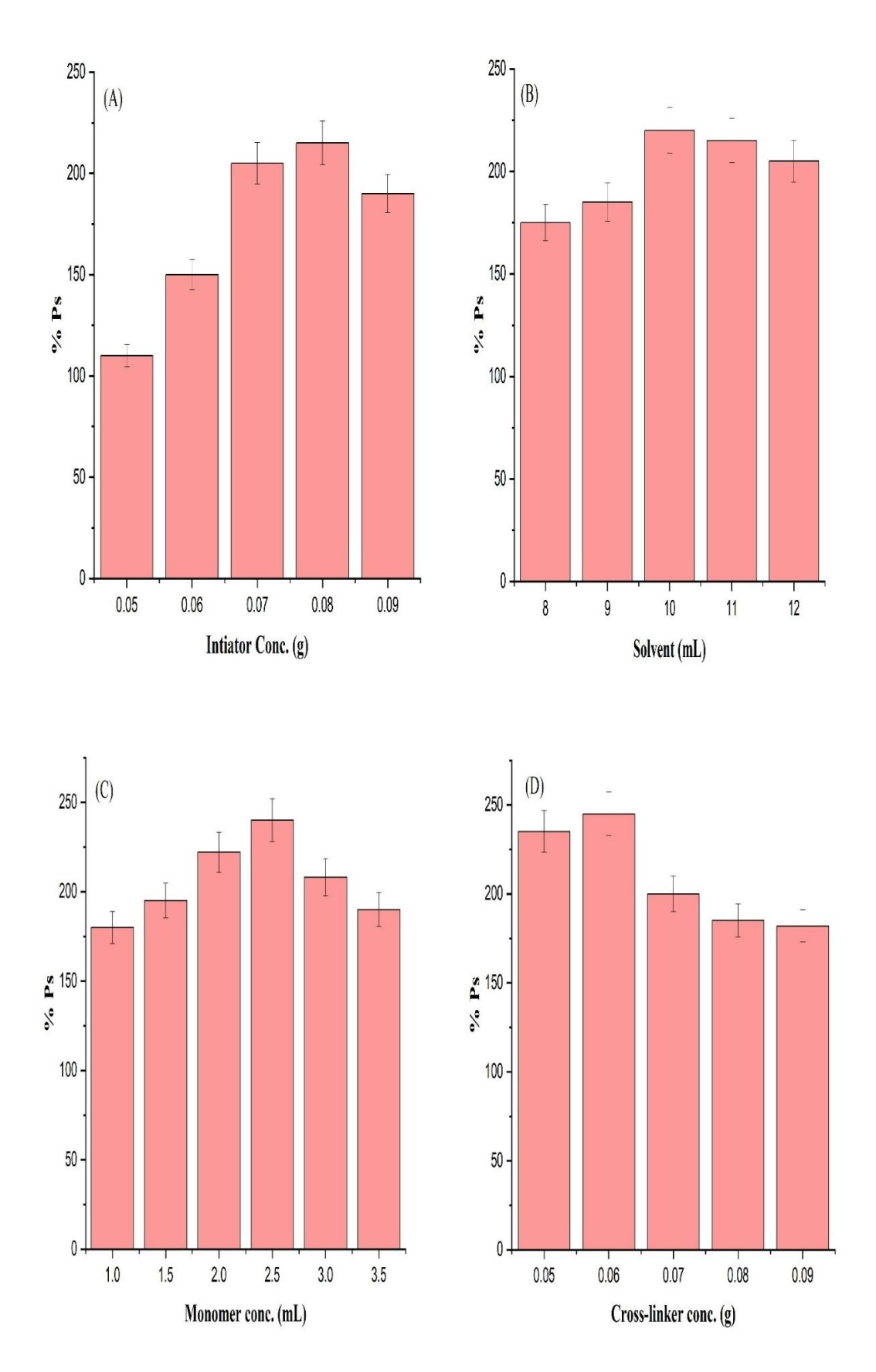
Effect of reaction time on Ps

The influence of reaction time on the percentage swelling (%Ps) of hydrogel was evaluated to determine the optimal polymerization duration for maximum water absorbency. As shown in Table 5.12 and figure 5.13E, the reaction time was varied from 110 to 135 seconds while keeping other parameters constant. It was observed that the swelling percentage increased steadily from $176 \pm 0.5\%$ at 110 seconds to a peak value of $246 \pm 1.0\%$ at 120 seconds. This increase can be attributed to sufficient availability of free radicals and active monomer units during this period, promoting effective grafting and network formation. However, a further increase in reaction time beyond 120 seconds led to a gradual decline in %Ps, with values dropping to $225 \pm 0.6\%$ at 125 seconds and $212 \pm 0.4\%$ at 135 seconds. The decline is likely due to the depletion of active sites on the PEG backbone and excessive cross-linking, which results in a denser network structure with reduced swelling capability (Hwang et al., 2024). Therefore, the optimal reaction time for maximum swelling in the PEG-g-poly(AA) hydrogel system was determined to be 120 seconds.

Table 5.12: Time of reaction optimization of synthetic hydrogel

S.No	Back-	Solvent	Initiator	Monomer	time	Cross-	
	bone	(ml)	(g)	(ml)	(sec)	linker	Mean
	(g)					(g)	(%P _s) ±
							S.D
1.	0.2	10	0.08	2.5	110	0.06	176 ± 0.5
2.	0.2	10	0.08	2.5	115	0.06	198 ± 0.8
3.	0.2	10	0.08	2.5	120	0.06	246 ± 1.0
4.	0.2	10	0.08	2.5	125	0.06	225 ± 0.6
5.	0.2	10	0.08	2.5	130	0.06	220 ± 0.5
6.	0.2	10	0.08	25.	135	0.06	212 ± 0.4

The optimized synthesis conditions for PEG-g-poly(AA) hydrogel were determined based on the maximum swelling percentage observed under varying experimental parameters. The hydrogel exhibited the highest swelling capacity of $246 \pm 1.0\%$ when synthesized using 0.2 g of synthetic backbone, 10 mL of distilled water as solvent, 0.08 g of ammonium persulfate (APS) as the initiator, 2.5 mL of acrylic acid as the monomer, and 0.06 g of N,N'-methylene bisacrylamide (MBA) as the cross-linker, with a reaction time of 120 seconds. These conditions provided an optimal balance between free radical availability, effective grafting, and network flexibility, enabling maximum water absorption while maintaining the structural integrity of the hydrogel.



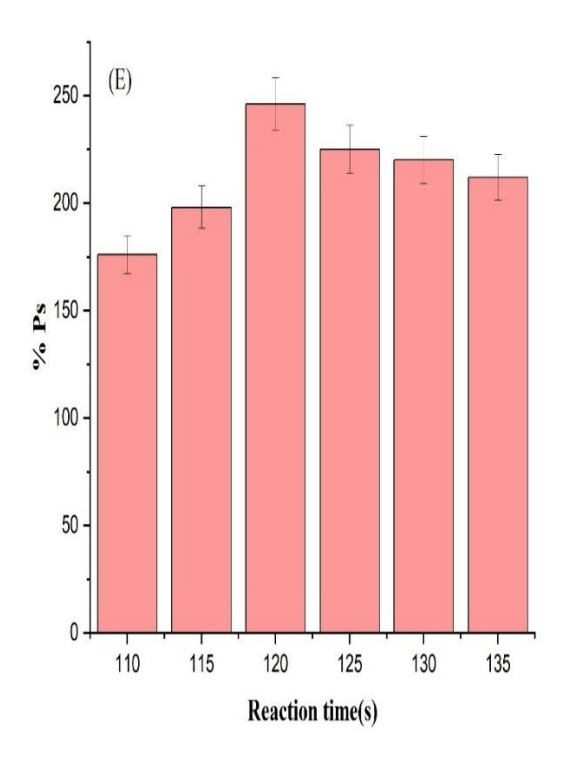


Figure 5.13: Variation in swelling percentage (%P) with respect to (A) Initiator concentration, (B) Solvent, (C) Monomer, (D) Cross-linker and (E) Time of PEGg-poly (AA) hydrogel

5.3.4 ZnO-PEG-g-poly(AA) Hydrogel Nanocomposite

The optimization of synthetic hydrogel nanocomposite was carried out by varying the concentration of ZnO nanoparticles from 0.05 to 0.25 g while keeping all other synthesis parameters constant. The swelling percentage (%Ps) increased progressively from $215 \pm 0.5\%$ at 0.05 g ZnO to a maximum of $280 \pm 0.8\%$ at 0.20 g ZnO. This enhancement in swelling is attributed to the high surface area and hydrophilic nature of ZnO nanoparticles, which promote effective interaction with the polymer network and enhance water uptake through hydrogen bonding and improved pore structure. However, a further increase in ZnO concentration to 0.25 g resulted in a slight reduction in swelling to $275 \pm 0.6\%$, likely due to nanoparticle agglomeration and excessive physical cross-linking, which reduce the hydrogel's elasticity and water absorption capacity (Hussain et al., 2024). Based on these findings, the optimal concentration of

ZnO for achieving maximum swelling in the PEG-g-poly(AA) hydrogel nanocomposite was determined to be 0.20 g (table 5.13 and figure 5.14).

Table 5.13: Optimized reaction conditions for ZnO-PEG-poly (AA) hydrogel nanocomposite

S.No	Back-	Solvent	Initiator	Monomer	time	Cross-	ZnO (g)	
	bone	(ml)	(g)	(ml)	(sec)	linker		Mean
	(g)					(g)		(%Ps) ±
								S.D
1.	0.2	10	0.08	2.5	120	0.06	0.05	215 ± 0.5
2.	0.2	10	0.08	2.5	120	0.06	0.1	224 ± 0.7
3.	0.2	10	0.08	2.5	120	0.06	0.15	255 ± 1.0
4.	0.2	10	0.08	2.5	120	0.06	0.2	280 ± 0.8
5.	0.2	10	0.08	2.5	120	0.06	0.25	275 ± 0.6

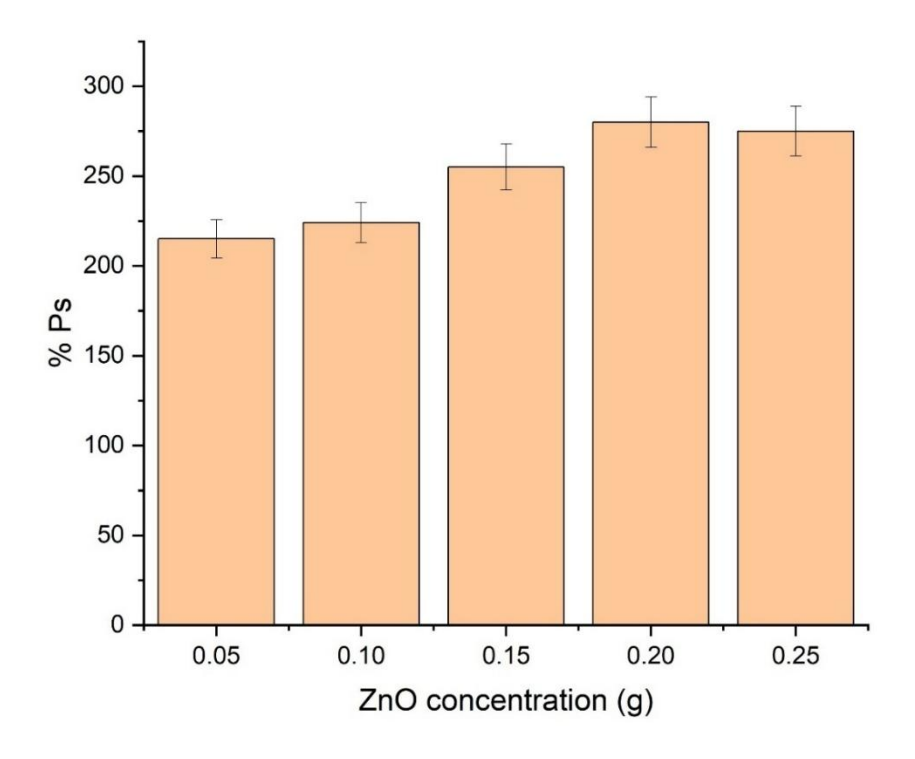


Figure 5.14: Optimized reaction conditions with maximum %P for ZnO-PEG based hydrogel nanocomposite

Based on the experimental data for all four hydrogel systems, the maximum percentage swelling observed under their respective optimized reaction conditions is as follows:

- The BM-g-poly(AA) hydrogel exhibited a maximum swelling of 448 ± 1.0%, achieved at 0.2 g BM, 6 mL distilled water, 0.07 g APS, 3 mL acrylic acid, 0.06 g MBA, and a reaction time of 40 seconds.
- The ZnO-BM-g-poly(AA) hydrogel nanocomposite showed a maximum swelling of $515 \pm 0.8\%$, optimized at the same hydrogel conditions with an additional 0.2 g ZnO nanoparticles.
- The PEG-g-poly(AA) hydrogel reached a maximum swelling of $246 \pm 1.0\%$, using 0.2 g PEG, 10 mL water, 0.08 g APS, 2.5 mL acrylic acid, 0.06 g MBA, and a reaction time of 120 seconds.
- The ZnO-PEG-g-poly(AA) hydrogel nanocomposite displayed its highest swelling of $280 \pm 0.8\%$ under identical conditions to its base hydrogel with the incorporation of 0.2 g ZnO.

Only these hydrogels and nanocomposites were carried forward for instrumentational analysis due to their successful formation.

5.4 INSTRUMENTATIONAL ANALYSIS

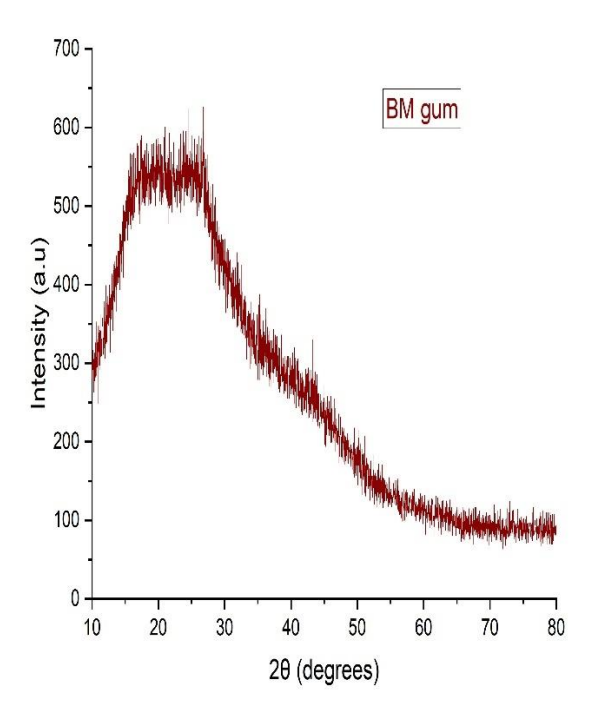
5.4.1 XRD Analysis

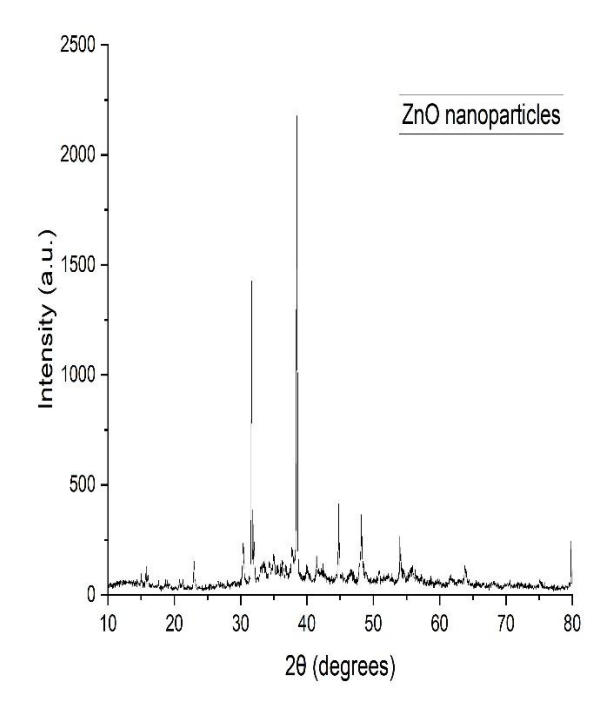
X-ray diffraction (XRD) analysis was employed to investigate the crystallinity and structural changes in BM gum, ZnO nanoparticles, BM-g-poly(AA) hydrogel, ZnO-BM-g-poly(AA) hydrogel nanocomposite, PEG-g-poly(AA) hydrogel, and ZnO-PEG-g-poly(AA) nanocomposite (Figure 5.15). The native BM gum displayed a broad and diffused peak around $2\theta \approx 20^\circ$, indicative of its amorphous nature, consistent with its polysaccharide backbone and lack of long-range order. Upon grafting with acrylic acid, the BM-g-poly(AA) hydrogel exhibited a broader hump in the same region, confirming reduced crystallinity and enhanced cross-linking, resulting from the random orientation of grafted polymer chains within the matrix. ZnO diffractogram displayed two sharp peaks at $2\theta = 34.4$ and 39.9 confirming the crystalline nature of nanoparticles. The miller indices values of (100), (001), (002), (110), (101), (102) confirmed the oval shape (Archana et al., 2022).

The incorporation of ZnO nanoparticles into the BM-g-poly(AA) matrix led to the appearance of sharp diffraction peaks at 2θ values of approximately 31.7°, 34.4°, 36.2°, 47.5°, 56.6°, 62.8°, and 67.9°, corresponding to the (100), (002), (101), (102), (110), (103), and (112) planes of oval wurtzite ZnO structure (JCPDS Card No. 36-1451). These peaks confirmed the successful incorporation of crystalline ZnO nanoparticles into the hydrogel network.

Similarly, the PEG-g-poly(AA) hydrogel showed a largely amorphous pattern with a broad peak near $2\theta \approx 19$ – 21° , indicating the dominant amorphous nature of PEG and the cross-linked polyacrylic acid chains. This lack of sharp crystalline peaks suggests that the grafting and crosslinking disrupted the regular packing of PEG chains, leading to an irregular, flexible polymeric network ideal for swelling and diffusion-based applications.

In the ZnO-PEG-g-poly(AA) nanocomposite, characteristic peaks corresponding to ZnO nanoparticles were again observed at $2\theta \approx 31.7^{\circ}$, 34.4° , and 36.2° , confirming the crystalline nature of ZnO within the amorphous hydrogel matrix. The intensity of these peaks, although lower than in pure ZnO, confirmed successful dispersion of ZnO nanoparticles within the PEG-g-poly(AA) framework. The coexistence of broad amorphous halos and sharp crystalline ZnO peaks illustrates the formation of a semi-crystalline nanocomposite structure, suitable for enhanced mechanical stability, surface functionality, and potential application in adsorption and environmental remediation (Priyadarshi et al., 2020).





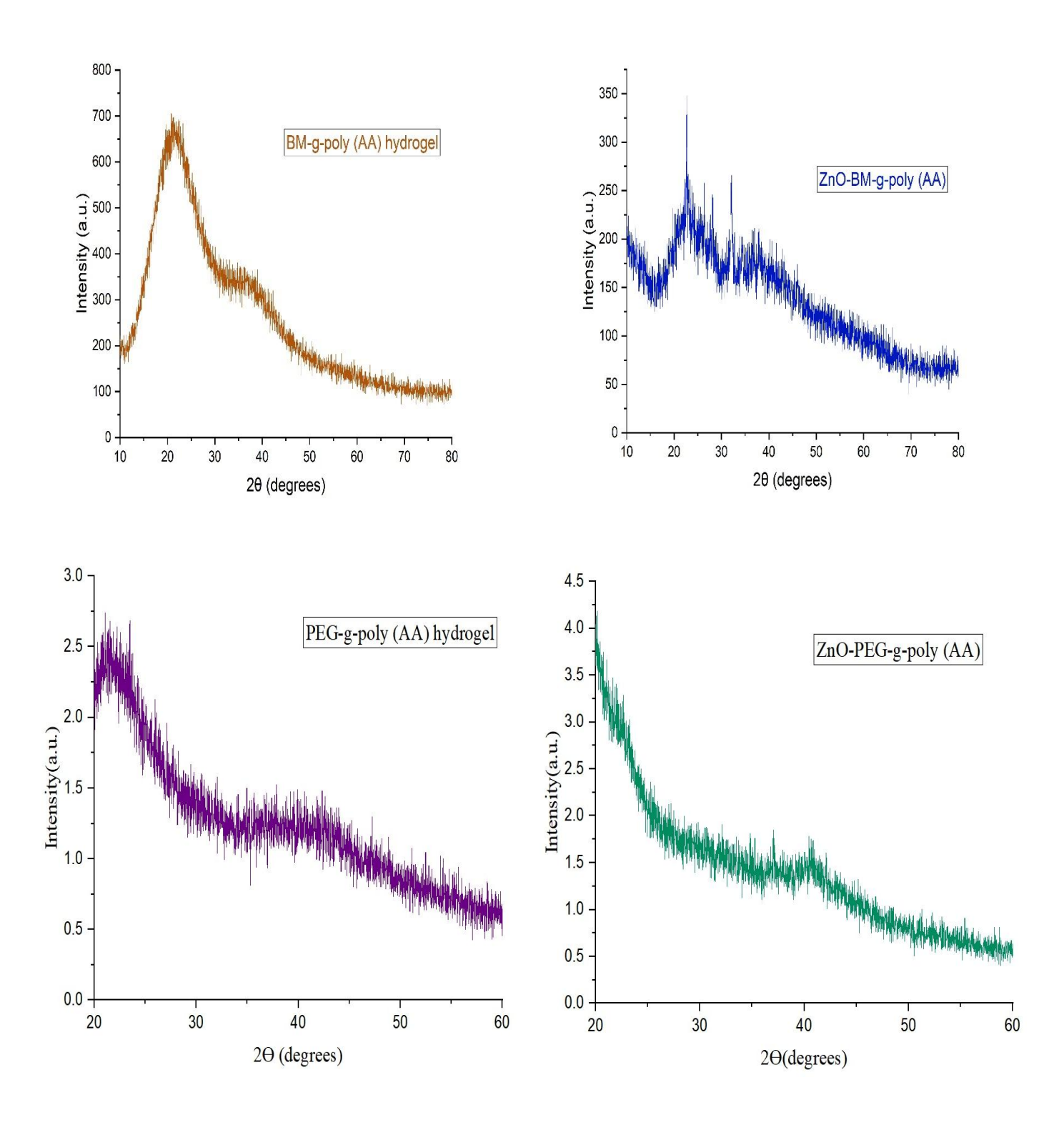


Figure 5.15: X-ray diffraction pattern of BM gum, ZnO nanoparticles, BM-g-poly (AA) hydrogel, ZnO-BM-g-poly (AA) hydrogel nanocomposite, PEG-g-poly (AA) hydrogel and ZnO-PEG-g-poly(AA) hydrogel nanocomposite

5.4.2 FTIR Analysis

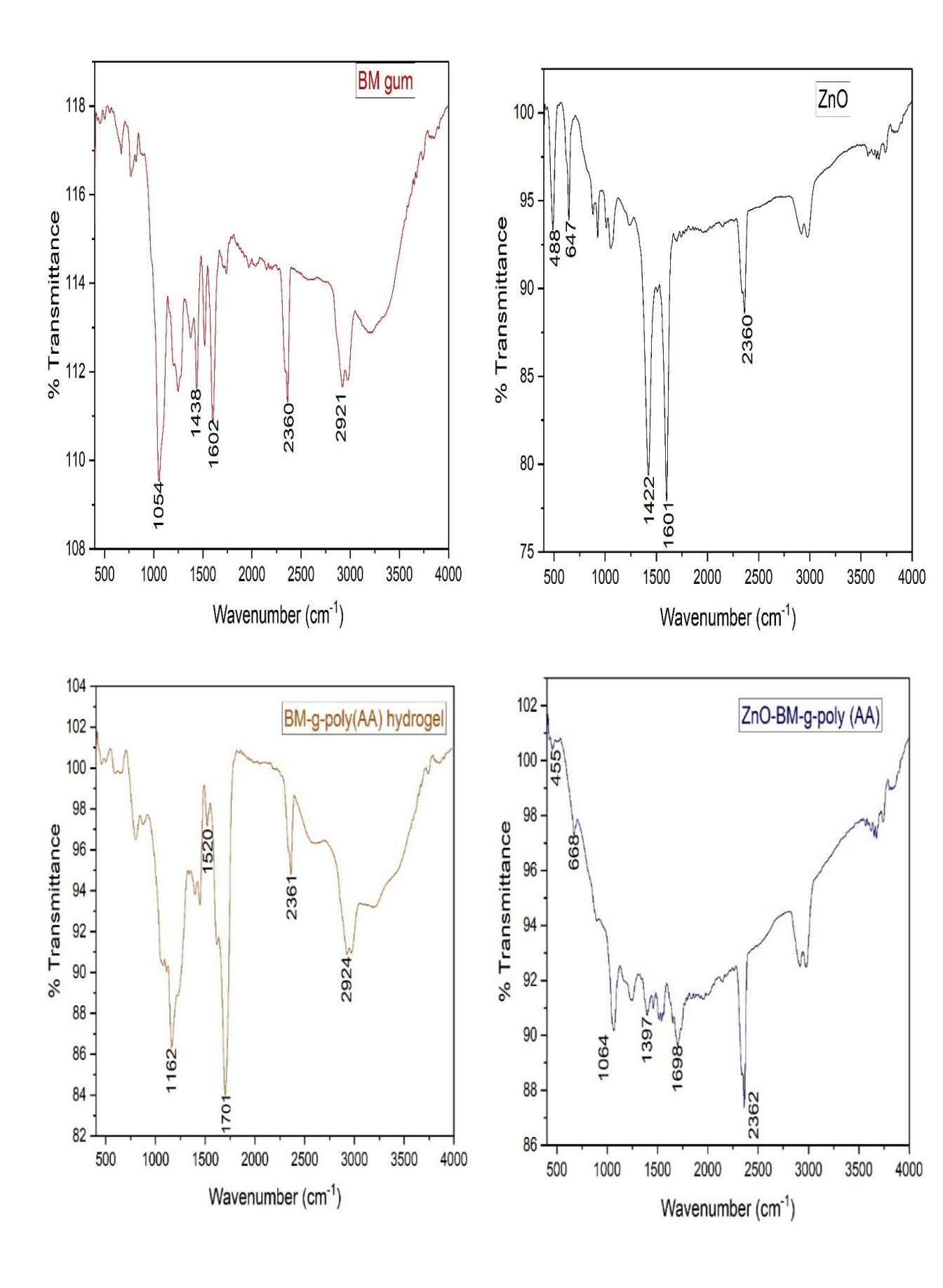
FTIR Spectra of BM gum showed various peaks. CH₂ and -CH asymmetric stretching resulted a characteristic peak at 2921 cm⁻¹. Characteristic peaks at 1438 and 1054 cm⁻¹ were due to -CH bending and C-N stretching respectively. These peaks confirmed the polysaccharide nature of BM gum (Virk et al., 2022).

The characteristic peaks at 1701 and 1520 cm⁻¹ in BM-g-poly (AA) hydrogel were due to C=O stretch in -COOH group and C-N stretching of amide bond respectively. Vibrational peaks at 2924 and 2361 cm⁻¹ were due to -CH stretch in acrylic acid which confirmed the grafting and formation of cross-linked structure. The peaks ranging in 1000-1300 cm⁻¹ were due to C-O stretching of alcohols (Priyadarshi et al., 2020). In the nanocomposite, absorption bands at 1457 and 1397 cm⁻¹ were due to asymmetric stretching of -COO- groups and symmetrical deformations of CH₂ attached to carboxyl groups. There were absorption bans in region 400-600 cm⁻¹ due to Zn-O vibrations confirming the formation of nanocomposite in ZnO-BM-g-poly (AA) nanocomposite (Thakur et al., 2020). In ZnO nanoparticles, a characteristic band at 647 cm⁻¹ is due to presence of hydroxyl group in Zn (OH)₂. The band at 488 cm⁻¹ in ZnO is attributed to Zn-O stretching mode of ZnO lattice. Other bands ranging from 3000-3200 cm⁻¹ are due to water absorbed from air and represent hydroxyl group (Soleymani et al., 2021; Shao et al., 2022) (figure 5.16).

The FTIR spectrum of PEG-g-poly(AA) hydrogel confirms the successful grafting and crosslinking of poly(acrylic acid) onto the PEG backbone. A broad absorption band at 3452 cm⁻¹ corresponds to the O–H stretching vibrations of hydroxyl groups, indicating the presence of both PEG and acrylic acid units. The peak at 2877 cm⁻¹ is assigned to C–H stretching vibrations from the aliphatic chains. A strong band observed at 1727 cm⁻¹ corresponds to the C=O stretching of carboxylic acid groups from acrylic acid, confirming successful polymer grafting (Shi et al., 2021). The absorption peaks at 1453 cm⁻¹ and 1349 cm⁻¹ are attributed to –CH₂ bending and symmetric deformation. The

bands at 1249 cm⁻¹, 1161 cm⁻¹, and 1085 cm⁻¹ are due to C–O–C stretching and C–O vibrations from ether linkages of PEG. The peaks around 947–839 cm⁻¹ may be associated with C–C and out-of-plane bending vibrations. Importantly, the bands at 582 cm⁻¹ likely reflect skeletal vibrations of the polymer network. Collectively, these spectral features confirm the formation of PEG-g-poly(AA) hydrogel with an interpenetrated and functionalized polymeric structure (Hussain et al., 2024) (figure 5.16).

The FTIR spectrum of the ZnO-PEG-g-poly(AA) nanocomposite confirms the successful incorporation of ZnO nanoparticles into the PEG-g-poly(acrylic acid) hydrogel matrix. A broad band observed at 3292 cm⁻¹ corresponds to O–H stretching vibrations, indicating the presence of hydroxyl groups from both the hydrogel network and surface-adsorbed water. The band at 2910 cm⁻¹ is attributed to C-H stretching vibrations from aliphatic chains of PEG. A strong peak at 1714 cm⁻¹ corresponds to the C=O stretching vibration of carboxylic acid groups, confirming the presence of acrylic acid moieties. Peaks at 1416 cm⁻¹ and 1237 cm⁻¹ represent CH₂ bending and C-O-C stretching, respectively, while the bands at 1142 cm⁻¹ and 1089 cm⁻¹ further confirm ether linkages and the polysaccharide backbone. Notably, absorption bands at 587 cm⁻¹ and 475 cm⁻¹ are characteristic of Zn–O vibrations, confirming the successful loading of ZnO nanoparticles within the hydrogel structure. The peak at 843 cm⁻¹ may also contribute to metal-oxygen bending vibrations. These spectral features collectively support the formation of a ZnO-integrated nanocomposite with a functionalized polymer matrix suitable for advanced environmental or biomedical applications (Wang et al., 2023; Saidi et al., 2020).



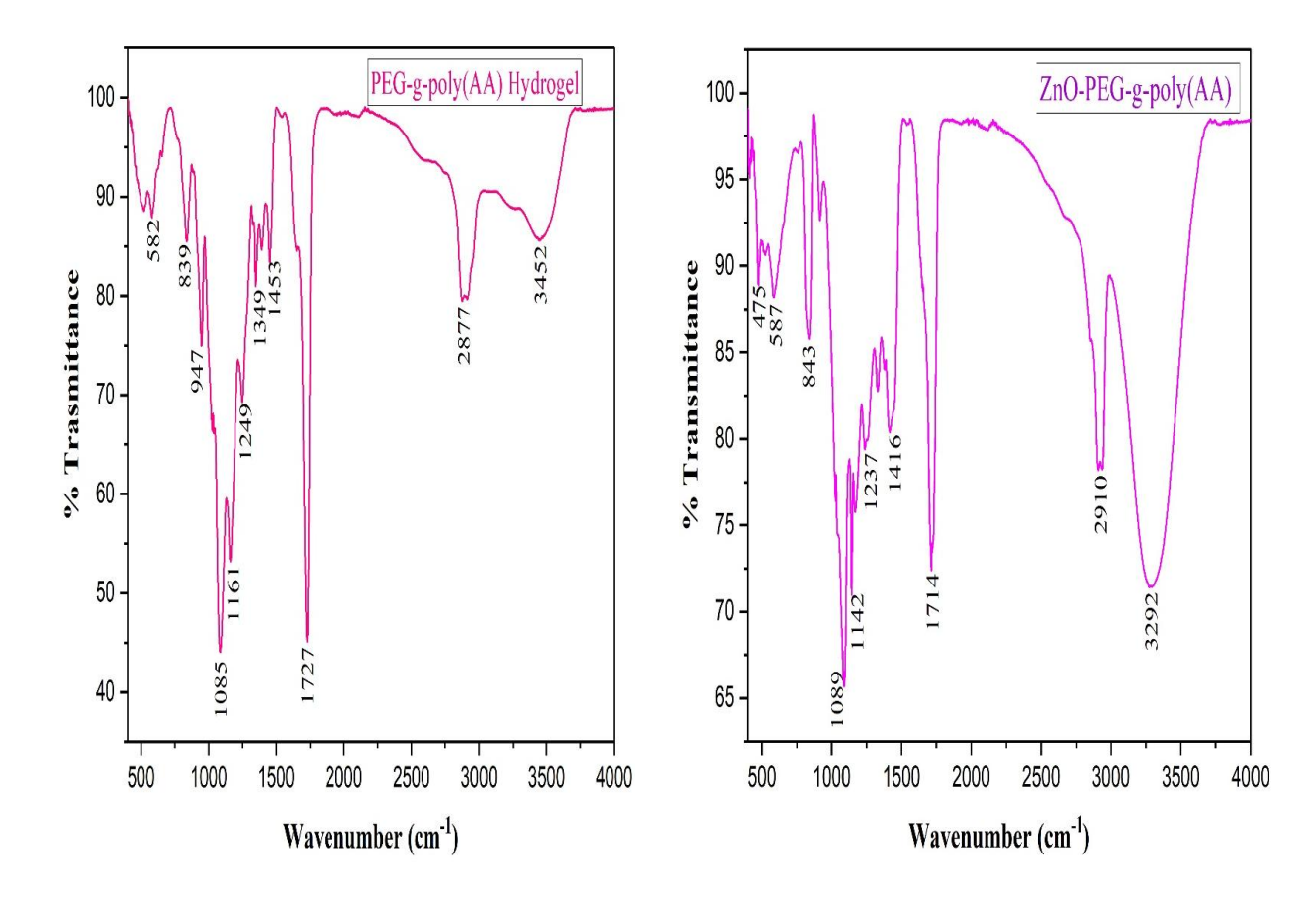


Figure 5.16: FTIR-spectra of BM gum, ZnO nanoparticles, BM-g-poly (AA) hydrogel, ZnO-BM-g-poly (AA) hydrogel nanocomposite, PEG-g-poly (AA) hydrogel and ZnO-PEG-g-poly(AA) hydrogel nanocomposite

5.4.3 Thermogravimetric analysis

TGA analysis was carried out to examine the thermal behaviour of the polysaccharide gum *Butea monosperma* (BM), BM-g-poly (AA) hydrogel, and ZnO-BM-g-poly (AA) hydrogel nanocomposite (figure 5.17). There were various degradation stages in all cases as shown in figure. In the first stage there is frequent weight loss in polysaccharide gum and cross-linked structures of both hydrogel and nanocomposite. In second stage there is sudden weight loss in higher amounts due to decomposition of backbone and loss of hydroxyl groups in both hydrogel and nanocomposite. The hydrogel and nanocomposite displayed very good thermal stability as initially only 20-25% weight loss is there in first stage of decomposition due to free water and unreacted reactants. In next stage also 25-60% weight loss is there arising because of thermal destruction of carboxylic groups, splitting of backbone, covalent bond breakage and cross-linking

disruption (Virk et al., 2022). In nanocomposite the thermal stability is improved as there is less degradation at second stage due to ZnO nanoparticles as ZnO nanoparticles have higher thermal stability. This TGA signifies that the hydrogel nanocomposite is more stable than hydrogel (Pereira et al., 2020).

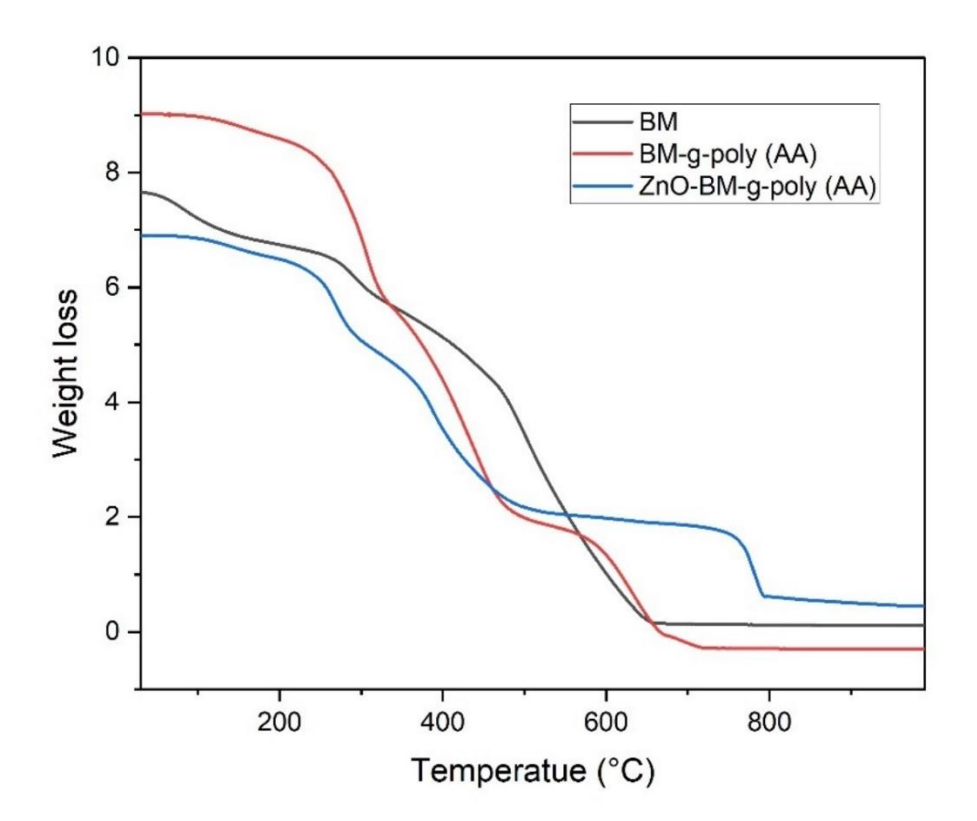
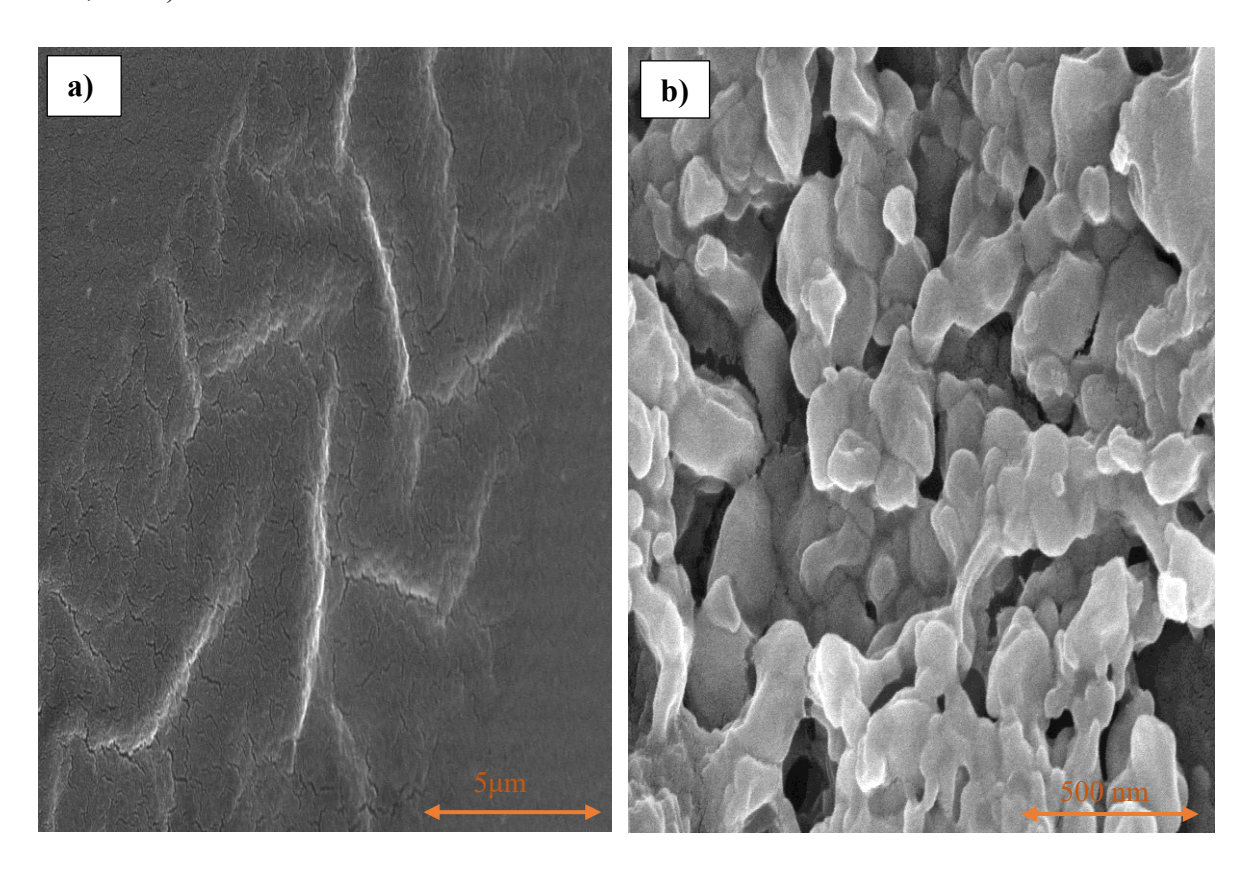


Figure 5.17: Thermogravimetric analysis

5.4.4 FE-SEM Analysis

Field emission scanning electron microscopy (FE-SEM) images of BM gum, BM-g-poly(AA) hydrogel, ZnO-BM-g-poly(AA) hydrogel nanocomposite, PEG-g-poly(AA) hydrogel, ZnO-PEG-g-poly(AA) nanocomposite and ZnO nanoparticles were recorded to evaluate their surface morphology and structural integrity (Figure 5.18a–f). The BM gum exhibited a relatively smooth and non-uniform surface with occasional cracks, characteristic of its amorphous nature, consistent with previous XRD results (Figure 5.18a). In contrast, the BM-g-poly(AA) hydrogel (Figure 5.18b) and ZnO-BM-g-poly(AA) hydrogel nanocomposite (Figure 5.18c) revealed a porous, interconnected, and globular morphology with cage-like geometric networks, confirming the successful

grafting and cross-linked polymerization of acrylic acid onto the BM matrix. This morphological transformation reflects the formation of a robust 3D hydrogel framework. The ZnO nanoparticles (Figure 5.18f) demonstrated well-defined oval shapes with a tendency to aggregate into assemblies, indicating their crystalline nature and high surface energy. Notably, the PEG-g-poly(AA) hydrogel (figure 5.18d) and ZnO-PEG-g-poly(AA) nanocomposite (Figure 5.18e) exhibited a denser, more compact morphology with embedded ZnO nanoparticles homogeneously dispersed within the polymeric matrix. The presence of spherical domains and smooth-textured regions suggested effective interaction between PEG chains, poly(acrylic acid), and ZnO nanoparticles, further supporting successful nanocomposite synthesis with potential application in dye adsorption and environmental remediation (Pereira et al., 2020; Rose et al., 2021).



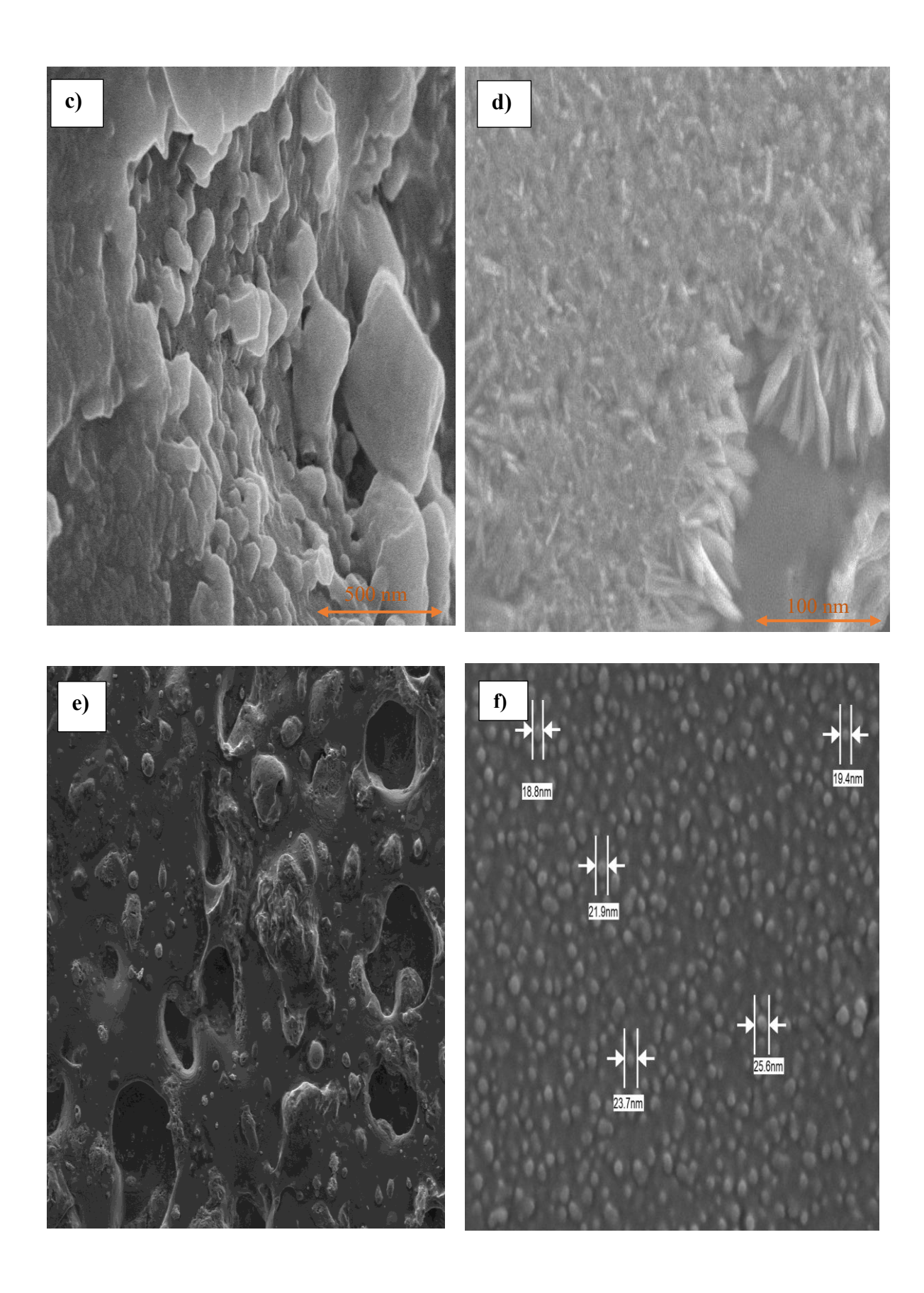


Figure 5.18: FE-SEM micrographs of a) BM gum, b) BM-g-poly (AA) hydrogel, c) ZnO-BM-g-poly (AA) hydrogel nanocomposite, d) PEG-g-poly (AA) hydrogel, e) ZnO-PEG-g-poly (AA) nanocomposite and f) ZnO nanoparticles.

5.5 ADSORPTION KINETICS

Amaranth and methyl orange dyes were selected for adsorption kinetic studies using BM-g-poly(AA) hydrogel and its ZnO-BM-g-poly (AA) nanocomposite due to the superior swelling capacities exhibited by these materials. The high degree of swelling facilitates enhanced diffusion of dye molecules into the hydrogel matrix, thereby increasing the availability of active binding sites for adsorption. The hydrophilic nature of the hydrogel network, combined with its porous structure, promotes efficient dye uptake from aqueous solutions. Additionally, the presence of functional groups such as —COOH in the grafted poly(acrylic acid) chains contributes to electrostatic interactions with the anionic dye molecules, further improving adsorption efficiency. These properties make the selected hydrogels ideal candidates for evaluating the kinetics of dye removal.

5.5.1 STANDARDIZATION AND VALIDATION

5.5.1.1 Standard for Amaranth (AR) (Yang et al., 2024)

Stock solution (1000 ppm)= 100 mg of dye in 100 ml distilled water

Working solutions are displayed in table 5.14 and standard curve obtained is shown in figure 5.19.

Table 5.14: Standard working solutions for AR

Sr.No.	AR (µL)	dH ₂ O (mL)	Concentration	Absorbance
			(ppm)	(a.u.)
1.	0	10	0	0
2.	20	10	2	0.07
3.	40	10	4	0.147

4.	60	10	6	0.232
5.	80	10	8	0.303
	100	10	10	0.382

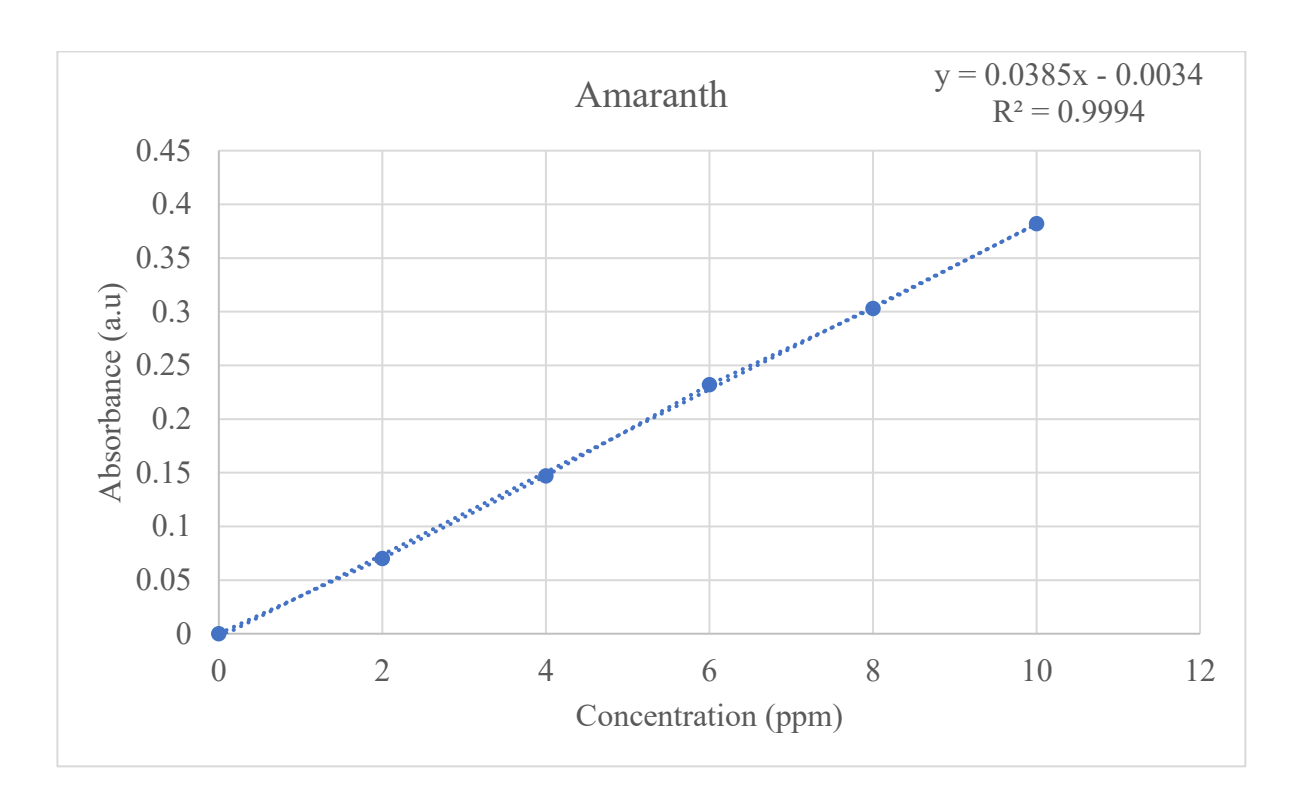


Figure 5.19: Standard curve of Amaranth absorption in U.V spectrophotometer

5.5.1.2 Standard for Methyl Orange (MO) (Yang et al., 2024)

Stock solution (1000 ppm)= 100 mg of dye in 100 ml distilled water

Working solutions are shown in table 5.15 and standard curve obtained is shown in figure 5.20.

Table 5.15: Standard working solutions for MO

Sr.No.	MO (µL)	dH ₂ O (mL)	Concentration	Absorbance
			(ppm)	(a.u.)

1.	0	10	0	0
2.	20	10	2	0.142
3.	40	10	4	0.285
4.	60	10	6	0.449
5.	80	10	8	0.561
6.	100	10	10	0.662

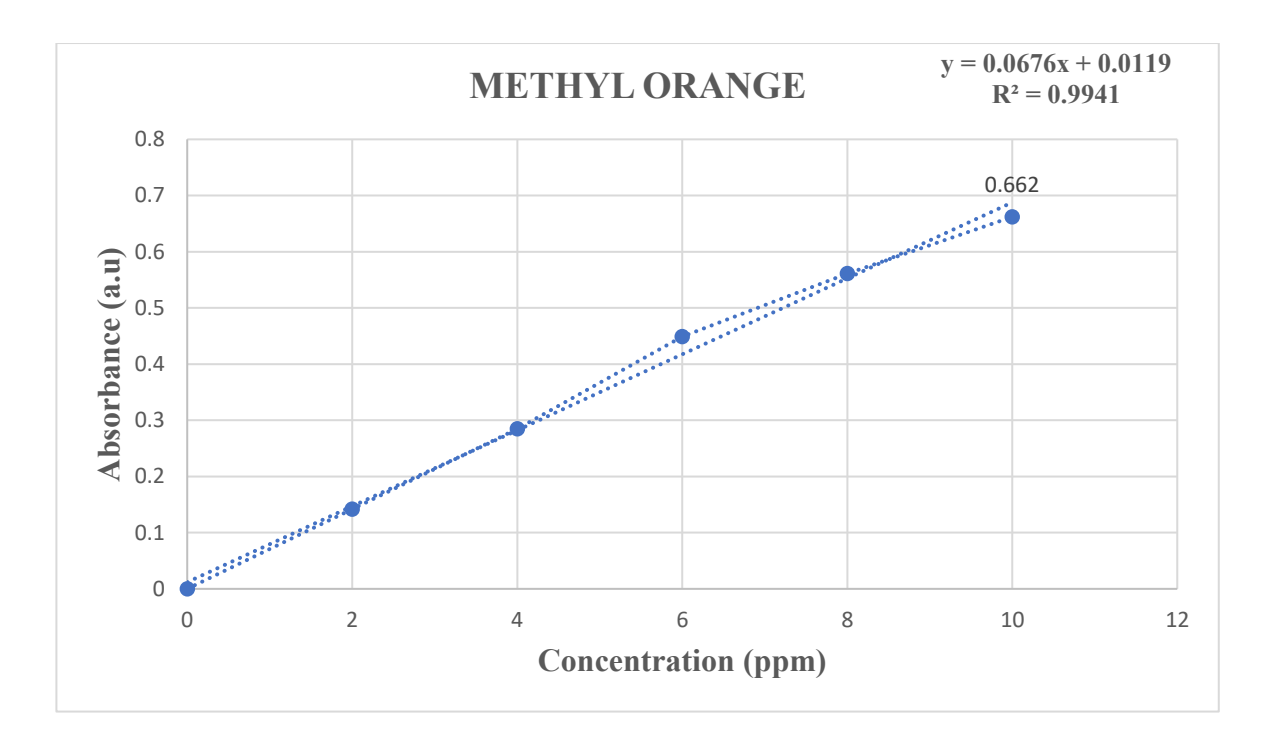


Figure 5.20: Standard curve of Methyl orange absorption in U.V spectrophotometer

5.5.2 AMARANTH DYE REMOVAL VIA HYDROGEL AND NANOCOMPOSITE

The dye removal capacity (R) and adsorption efficiency (q) should be noted by the following equations (Xue et al., 2023):

$$R\% = \frac{c_0 - c_T}{c_0} \times 100 \tag{1}$$

$$q = \frac{(C_0 - C_T)V}{W} \times 100 \tag{2}$$

where C_0 and C_T = dye concentrations at time 0 and t, V= dye solution volume

5.5.2.1 Time Reaction

The influence of reaction time on amaranth dye removal reveals distinct differences in adsorption behavior between the BM-g-poly(AA) hydrogel and its ZnO-based nanocomposite. In the case of the hydrogel, a gradual increase in dye removal was observed, reaching $74.5 \pm 0.32\%$ at 6 hours, indicating slower diffusion and gradual saturation of available functional groups. In contrast, the nanocomposite achieved significantly higher removal efficiency of $88.9 \pm 0.33\%$ within the same duration, with more rapid adsorption evident within the first 3 hours, where over 84% removal was already accomplished. This enhanced rate can be attributed to the presence of ZnO nanoparticles, which facilitate faster electron transfer and provide additional active sites through surface hydroxyl groups that interact with the sulfonic acid moieties of amaranth dye. The improved kinetics in the nanocomposite suggest that ZnO not only increases adsorption capacity but also reduces the time required to reach equilibrium, making the nanocomposite more effective for time-sensitive dye removal applications (Singh et al., 2022).

Table 5.16: Amaranth removal efficiency of hydrogel with respect to time

Time (hr)	Ci (mg/L)	Ct (mg/L)	qt (mg/g) ±	Removal ± S.D (%)
			S.D	
0.5	10	9.262	0.0184 ±	7.38 ± 0.53
			0.02	
1	10	8.846	0.028 ± 0.03	11.54 ± 0.28
1.5	10	8.327	0.0418 ±	16.73 ± 0.27
			0.02	

2	10	7.963	0.0509 ±	20.37 ± 0.27
			0.02	
2.5	10	7.314	0.067 ± 0.01	26.86 ± 0.32
3	10	6.405	0.089 ± 0.02	35.95 ± 0.23
3.5	10	5.366	0.115 ± 0.03	46.34 ± 0.58
4	10	4.327	0.142 ± 0.01	56.73 ± 0.26
4.5	10	3.028	0.174 ± 0.02	69.72 ± 0.34
5	10	2.768	0.181 ± 0.02	72.32 ± 0.25
5.5	10	2.67	0.183 ± 0.02	73.3 ± 0.28
6	10	2.55	0.186 ± 0.01	74.5 ± 0.32

Table 5.17: Amaranth removal efficiency of nanocomposite with respect to time

Time (hr)	Ci (mg/L)	Ct (mg/L)	qt (mg/g) ±	Removal ± S.D (%)
			S.D	
0.5	10	6.54	0.0865 ±	34.6 ± 0.48
			0.03	
1	10	6.12	0.097 ± 0.02	38.8 ± 0.56
1.5	10	5.2	0.12 ± 0.03	48.0 ± 0.41
2	10	4.6	0.135 ± 0.01	54.0 ± 0.30
2.5	10	3.5	0.162 ± 0.02	65.0 ± 0.47
3	10	1.56	0.211 ± 0.02	84.4 ± 0.26

3.5	10	1.22	0.219 ± 0.01	87.8 ± 0.59
4	10	1.3	0.217 ± 0.01	87.0 ± 0.39
4.5	10	1.36	0.216 ± 0.03	86.4 ± 0.28
5	10	1.22	0.219 ± 0.01	87.8 ± 0.59
5.5	10	1.21	0.219 ± 0.03	87.9 ± 0.54
6	10	1.11	0.22 ± 0.02	88.9 ± 0.33

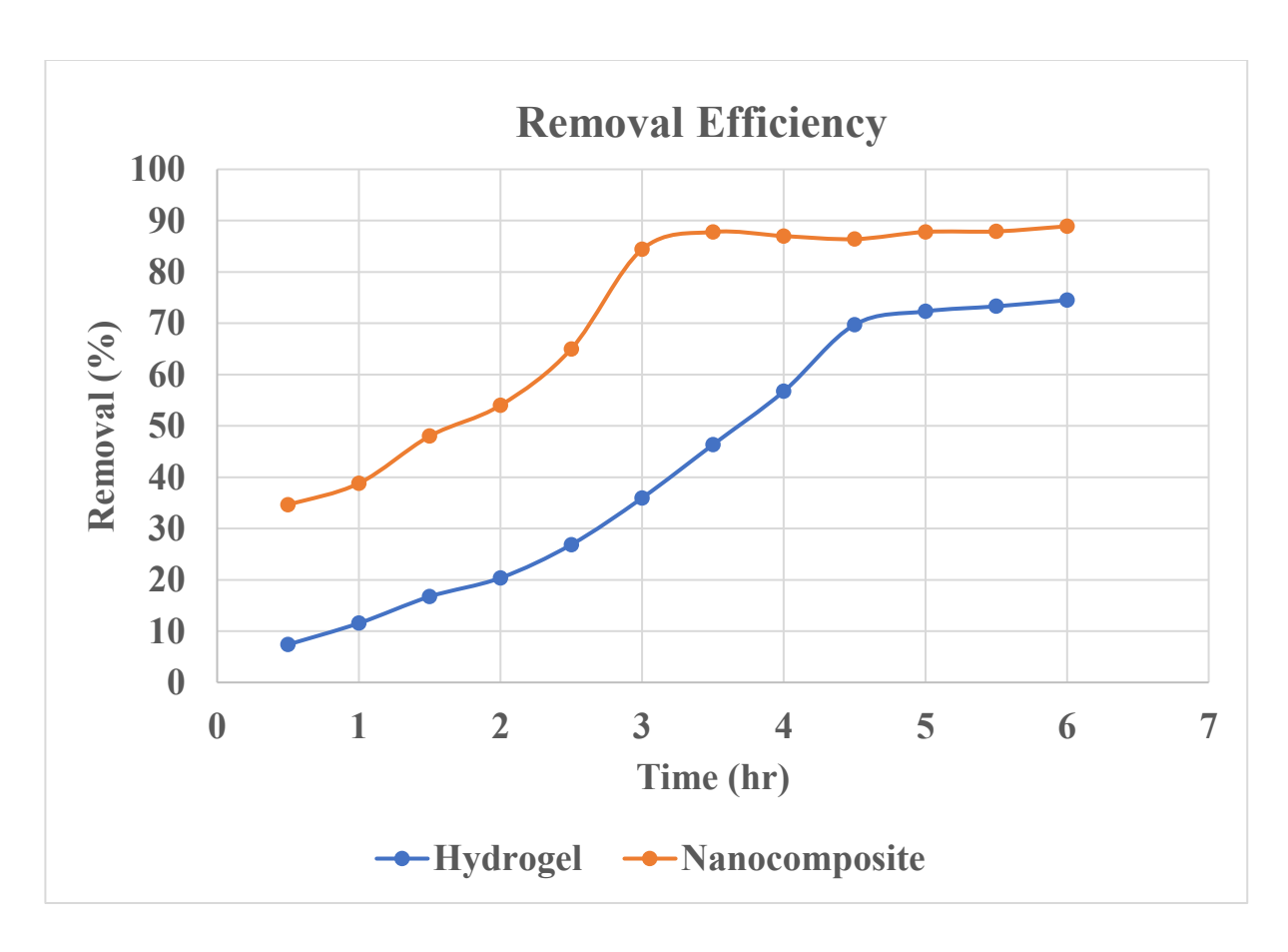


Figure 5.21: Amaranth removal efficiency of hydrogel and nanocomposite with respect to time

5.5.2.2 Adsorbent Dosage Reaction

The influence of adsorbent dosage on the removal efficiency of Amaranth dye was evaluated for both hydrogel and its ZnO-based nanocomposite over a range of 0.5–3 g under fixed conditions (Ci = 10 mg/L; V = 50 mL). For the hydrogel, an increase in dosage from 0.5 g to 2 g led to a significant rise in percentage removal, reaching a maximum of $73.5 \pm 0.30\%$ at 2 g, after which the removal efficiency slightly declined and plateaued around 72% for higher dosages. However, the corresponding adsorption capacity (qt) decreased beyond 1.5 g, indicating possible site saturation or particle aggregation limiting surface area accessibility. In contrast, the nanocomposite exhibited superior performance across all dosages, achieving a peak removal of $88.0 \pm 0.35\%$ at 2 g, with qt values consistently higher than those of the hydrogel, peaking at 1.11 ± 0.007 mg/g at 3 g. The enhanced performance of the nanocomposite can be attributed to the presence of ZnO nanoparticles, which provide additional active sites and facilitate improved dye-adsorbent interactions. Overall, the nanocomposite demonstrates greater adsorption capacity and removal efficiency, particularly at higher dosages, due to its synergistically reinforced structure (Aljeboree et al, 2024; Singh et al., 2022).

Table 5.18: Amaranth removal efficiency of hydrogel with respect to dosage

Dosage (g)	Ci	Ct (mg/L)	$qt (mg/g) \pm S.D$	Removal ± S.D
	(mg/L)			(%)
0.5	10	8.34	0.166 ± 0.004	16.6 ± 0.42
1	10	6.55	0.172 ± 0.005	34.5 ± 0.32
1.5	10	4.23	0.192 ± 0.006	57.7 ± 0.70
2	10	2.65	$0.183.7 \pm 0.005$	73.5 ± 0.30
2.5	10	2.75	0.145 ± 0.004	72.5 ± 0.61
3	10	2.8	0.12 ± 0.003	72.0 ± 0.45

Table 5.19: Amaranth removal efficiency of nanocomposite with respect to dosage

Dosage (g)	Ci (mg/L)	Ct (mg/L)	$qt \pm S.D (mg/g)$	Removal ± S.D
				(%)
0.5	10	4.5	0.137 ± 0.004	55.0 ± 0.66
1	10	3.2	0.34 ± 0.006	68.0 ± 0.31
1.5	10	2.1	0.592 ± 0.007	79.0 ± 0.68
2	10	1.2	0.88 ± 0.009	88.0 ± 0.35
2.5	10	1.4	1.07 ± 0.008	86.0 ± 0.41
3	10	2.6	1.11 ± 0.007	74.0 ± 0.53

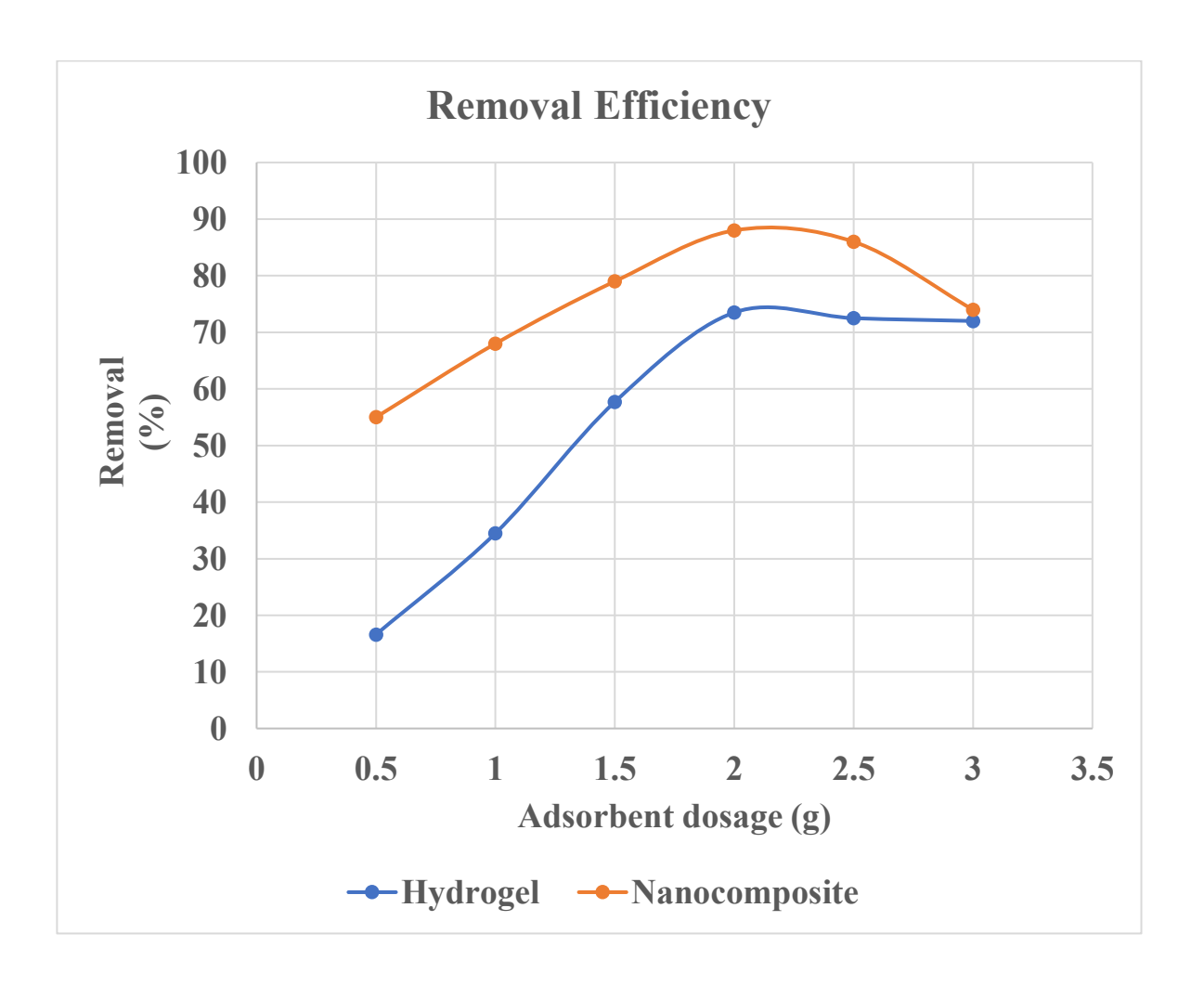


Figure 5.22: Amaranth removal efficiency of hydrogel and nanocomposite with respect to Adsorbent Dosage

5.5.2.3 pH Reaction

The effect of pH on Amaranth dye adsorption was studied using both the hydrogel and its ZnO-based nanocomposite at a fixed adsorbent dose of 2g and dye solution volume of 50 mL. For the hydrogel, the removal efficiency increased with rising pH from 5 to 7, achieving a maximum of $73.2 \pm 0.57\%$ at pH 7. This enhancement is attributed to the increasing ionization of functional groups on the hydrogel surface and the favorable electrostatic attraction between negatively charged dye molecules and deprotonated polymer sites. Beyond pH 7, the efficiency declined due to possible electrostatic repulsion and reduced interaction between dye and adsorbent. The nanocomposite demonstrated significantly better performance across all pH levels, with maximum removal of $88.0 \pm 0.38\%$ also observed at pH 7. The consistently higher qt values for the nanocomposite suggest an increased availability of active sites and improved binding affinity, owing to the incorporation of ZnO nanoparticles which enhance surface reactivity (Aljeboree et al., 2025). These results confirm that both adsorbents perform optimally under neutral conditions, but the nanocomposite exhibits superior dye removal due to its enhanced physicochemical properties.

Table 5.20: Amaranth removal efficiency of hydrogel with respect to pH

pH	Ci (mg/L)	Ct (mg/L)	qt ± S.D	Removal ±
			(mg/g)	S.D (%)
5	10	6.85	0.0787 ± 0.002	31.5 ± 0.32
6	10	4.55	0.136 ± 0.004	54.5 ± 0.42
7	10	2.68	0.183 ± 0.005	73.2 ± 0.57
8	10	4.24	0.144 ± 0.004	57.6 ± 0.42
9	10	5.58	0.111 ± 0.003	44.2 ± 0.53

Table 5.21: Amaranth removal efficiency of nanocomposite with respect to pH

pH	Ci (mg/L)	Ct (mg/L)	qt ± S.D	Removal ±
			(mg/g)	S.D (%)
5	10	2.11	0.197 ± 0.004	78.9 ± 0.36
6	10	1.88	0.203 ± 0.005	81.2 ± 0.42
7	10	1.2	0.22 ± 0.006	88.0 ± 0.38
8	10	2.3	0.192 ± 0.004	77.0 ± 0.41
9	10	2.24	0.194 ± 0.005	77.6 ± 0.33

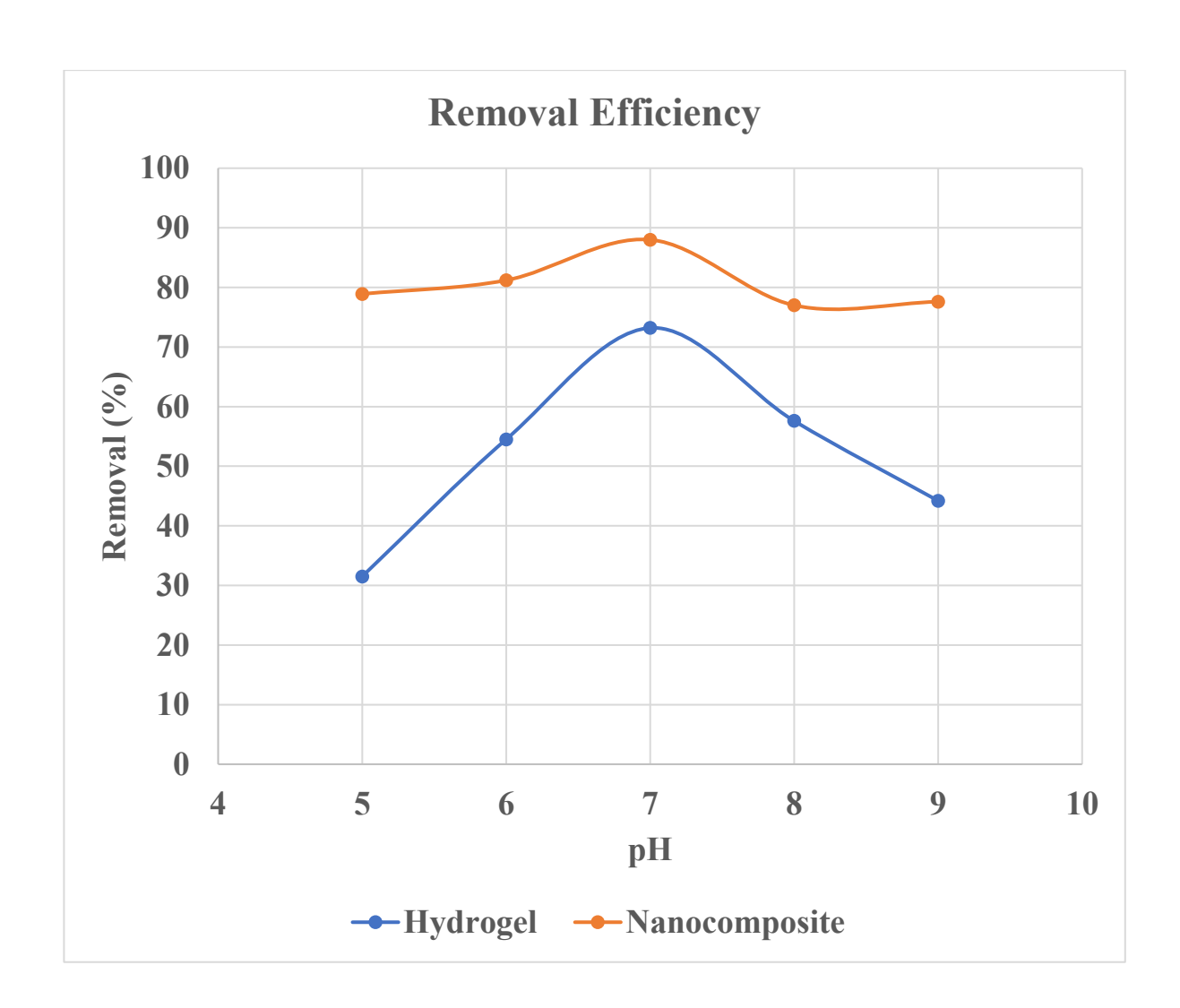


Figure 5.23 : Amaranth removal efficiency of hydrogel and nanocomposite with respect to pH

5.5.2.4 Initial concentration reaction

The influence of initial dye concentration on Amaranth adsorption was evaluated for both the hydrogel and its ZnO-based nanocomposite using a fixed adsorbent dosage of 2 g and solution volume of 50 mL. For the hydrogel, removal efficiency increased steadily from $48.16 \pm 0.42\%$ at 6 mg/L to a maximum of $77.5 \pm 0.33\%$ at 10 mg/L, after which it plateaued, indicating saturation of available active sites. Although qt values increased with concentration, a slight decline in removal percentage at higher concentrations suggests limited adsorption capacity under fixed adsorbent conditions. In contrast, the nanocomposite exhibited consistently higher removal across all concentrations, reaching $87.0 \pm 0.32\%$ at 10 mg/L and maintaining similar efficiency up to 14 mg/L. The enhanced performance and higher qt values of the nanocomposite can be attributed to the increased surface area and active binding sites provided by ZnO nanoparticles, which promote stronger dye–adsorbent interactions (Aljeboree et al., 2025; Jabir et al., 2022). These findings emphasize the nanocomposite's superior capacity for adsorbing dye molecules even at elevated concentrations, making it a more efficient and robust material for practical dye removal applications.

Table 5.22: Amaranth removal efficiency of hydrogel with respect to initial concentration

Initial conc.	Ci (mg/L)	Ct (mg/L)	qt ± S.D	Removal S.D ±
			(mg/g)	(%)
6	6	3.11	0.72 ± 0.005	48.16 ± 0.42
8	8	3.1	0.122 ± 0.004	61.25 ± 0.37
10	10	2.25	0.194 ± 0.005	77.5 ± 0.33
12	12	2.8	0.23 ± 0.006	76.66 ± 0.39

14	14	3.22	0.269 ± 0.007	77.0 ± 0.41

Table 5.23: Amaranth removal efficiency of nanocomposite with respect to initial concentration

Initial conc.	Ci (mg/L)	Ct (mg/L)	qt ± S.D	Removal ±
			(mg/g)	S.D (%)
6	6	2.23	0.094 ± 0.003	62.83 ± 0.35
8	8	1.99	0.150 ± 0.004	75.12 ± 0.41
10	10	1.3	0.217 ± 0.005	87.0 ± 0.32
12	12	1.63	0.259 ± 0.006	86.42 ± 0.36
14	14	1.9	0.303 ± 0.007	86.43 ± 0.38

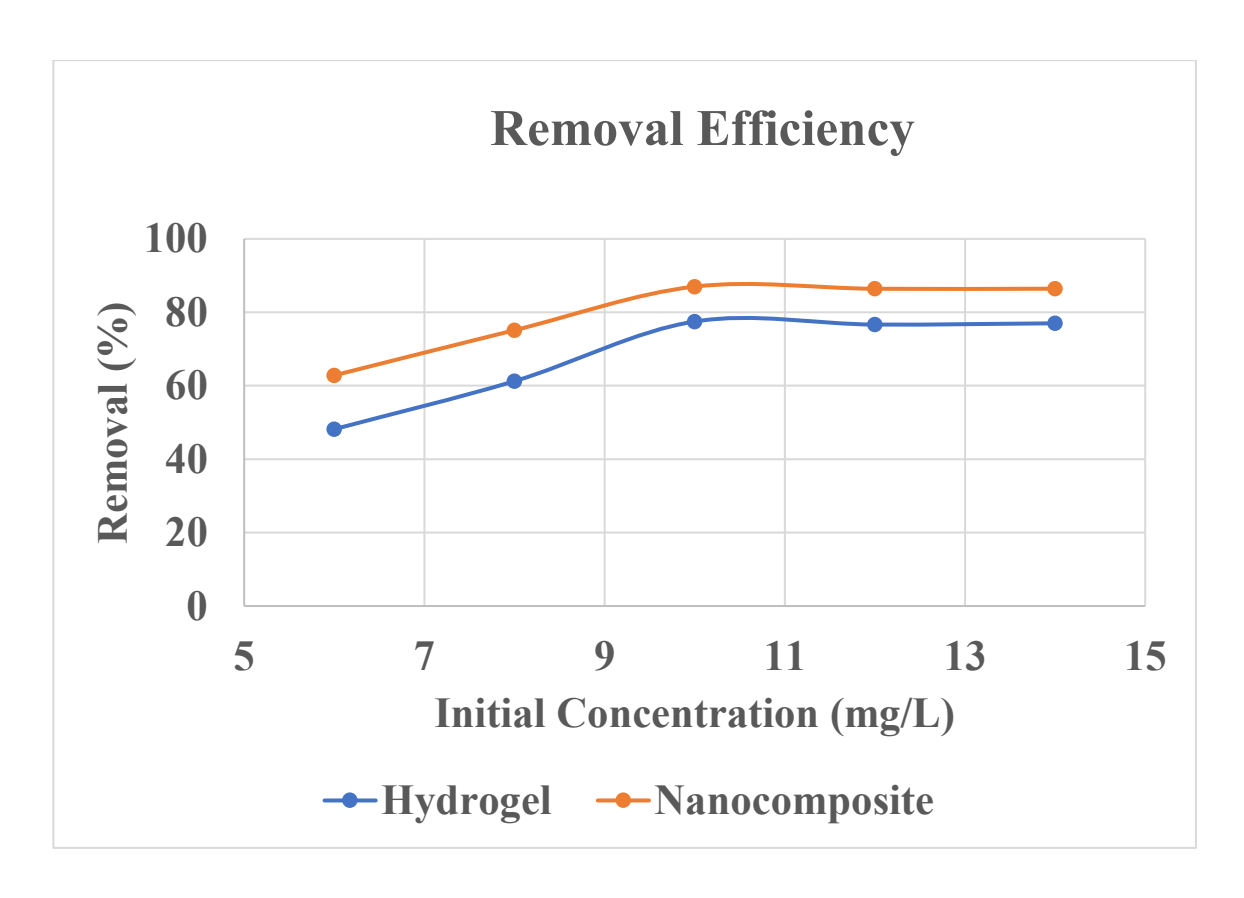


Figure 5.24: Amaranth removal efficiency of hydrogel and nanocomposite with respect to Initial concentration

5.5.3 METHYL ORANGE DYE REMOVAL VIA HYDROGEL AND NANOCOMPOSITE

5.5.3.1 Time Reaction

The effect of contact time on the removal efficiency of methyl orange dye was investigated for both the BM-g-poly (AA) hydrogel and its ZnO-based nanocomposite, using a constant adsorbent dosage of 2 g and dye solution volume of 50 mL over a reaction period of 0.5 to 5 hours. For the hydrogel, dye removal increased gradually with time, reaching $85.64 \pm 0.30\%$ at 5 hours. The qt values followed a similar trend, indicating progressive occupation of available active sites. Initial adsorption was relatively slow due to limited interaction between dye molecules and active sites; however, the rate increased beyond 2.5 hours as more surface interactions occurred, eventually plateauing due to saturation. In contrast, the nanocomposite demonstrated significantly faster and higher adsorption performance, attaining $90.10 \pm 0.29\%$ removal within the same time frame. This improvement is reflected in higher qt values throughout, with near saturation achieved by 4.5 hours. The enhanced efficiency of the nanocomposite can be attributed to the increased surface area and improved dyeadsorbent interactions imparted by ZnO nanoparticles, which facilitate faster adsorption kinetics and higher capacity (Aljeboree et al., 2025; Jabir et al., 2022). These findings confirm the nanocomposite's superiority in methyl orange removal, especially under shorter contact durations.

Table 5.24: Methyl orange removal efficiency of hydrogel with respect to time

Time (hr)	Ci (mg/L)	Ct (mg/L)	qt ± S.D(mg/g)	Removal ± S.D (%)
0.5	10	9.64645	0.008 ± 0.001	3.53 ± 0.22
1	10	8.995562	0.025 ± 0.001	10.04 ± 0.25

1.5	10	8.847633	0.028 ± 0.001	11.52 ± 0.26
2	10	8.107988	0.047 ± 0.002	18.92 ± 0.3
2.5	10	7.028107	0.074 ± 0.002	29.71 ± 0.34
3	10	5.08	0.123 ± 0.003	49.2 ± 0.28
3.5	10	3.522189	0.162 ± 0.004	64.78 ± 0.33
4	10	1.954142	0.201 ± 0.004	80.46 ± 0.29
4.5	10	1.525148	0.211 ± 0.003	84.74 ± 0.32
5	10	1.436391	0.214 ± 0.003	85.64 ± 0.30

Table 5.25: Methyl orange removal efficiency of nanocomposite with respect to time

Time (hr)	Ci (mg/L)	Ct (mg/L)	$qt \pm S.D (mg/g)$	Removal ± S.D
				(%)
0.5	10	9.12	0.022 ± 0.001	8.80 ± 0.25
1	10	8.24	0.044 ± 0.001	17.60 ± 0.28
1.5	10	7.24	0.069 ± 0.002	27.6 ± 0.31
2	10	6.02	0.0995 ± 0.002	39.8 ± 0.27
2.5	10	5.064	0.123 ± 0.003	49.36 ± 0.33
3	10	4.67	0.133 ± 0.003	53.3 ± 0.26
3.5	10	2.21	0.194 ± 0.004	77.9 ± 0.35
4	10	1.05	0.223 ± 0.003	89.5 ± 0.30

4.5	10	1	0.225 ± 0.002	90.00 ± 0.27
5	10	0.99	0.225 ± 0.002	90.10 ± 0.29

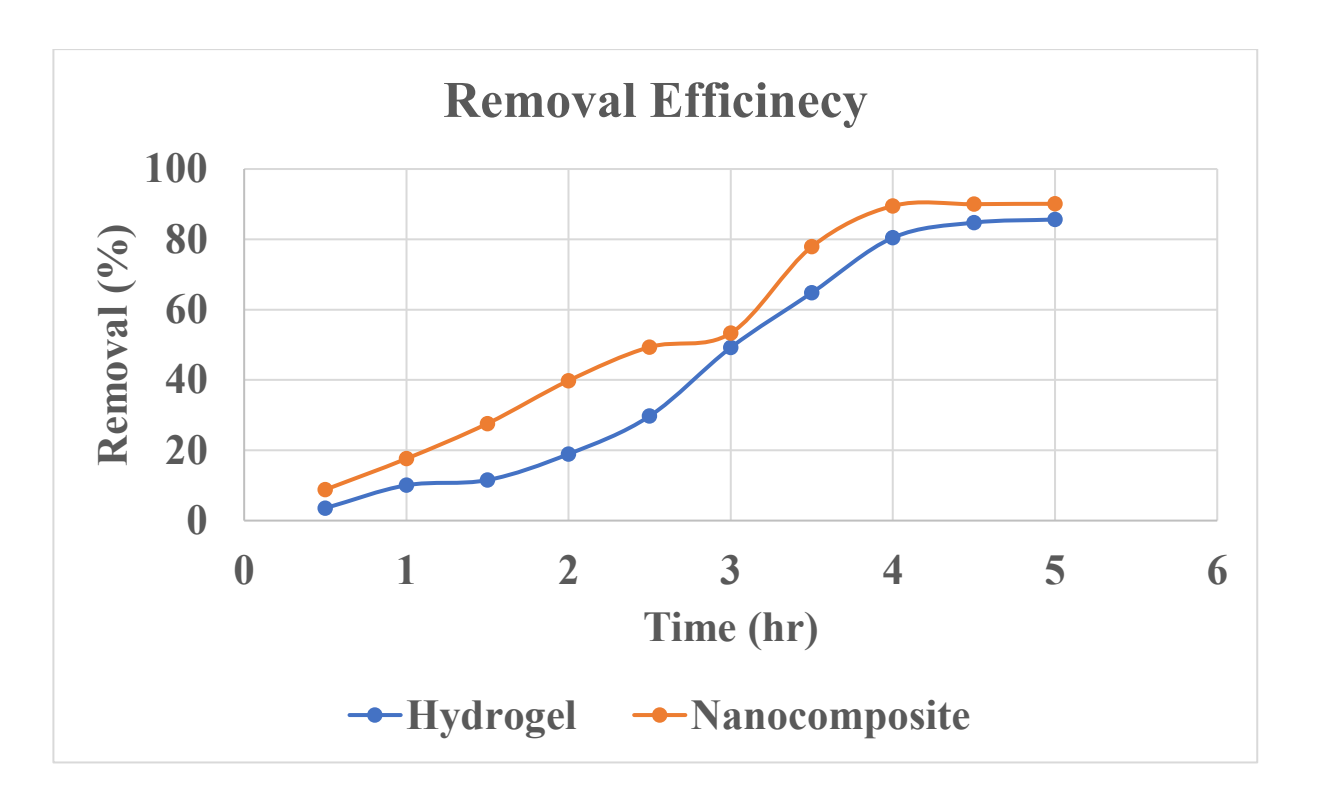


Figure 5.25: MO removal efficiency of hydrogel and nanocomposite with respect to time

5.5.3.2 pH Reaction

The impact of pH on methyl orange dye adsorption was evaluated for both the hydrogel and its ZnO-based nanocomposite at a fixed adsorbent dosage of 2 g and a dye solution volume of 50 mL. For the hydrogel, the removal efficiency increased from $49.4 \pm 0.34\%$ at pH 5 to a maximum of $84.0 \pm 0.30\%$ at pH 7, followed by a decline at higher pH levels. This pattern can be attributed to the increased ionization of functional groups on the hydrogel surface near neutral pH, enhancing electrostatic interactions with the anionic methyl orange dye. However, beyond pH 7, reduced adsorption is likely due to electrostatic repulsion and possible competition with OH $^-$ ions. The nanocomposite outperformed the hydrogel across all pH levels, reaching a peak removal of $89.8 \pm 0.31\%$ at pH 7. The higher qt values at each pH point indicate the

greater affinity and capacity of the nanocomposite for dye uptake, owing to the additional surface functionality and active sites provided by ZnO nanoparticles. These results confirm that neutral pH conditions are most favorable for adsorption and that the nanocomposite exhibits enhanced performance due to its improved structural and surface characteristics (Aljeobree et al., 2024; Benhalima et al., 2023).

Table 5.26: Methyl orange removal efficiency of hydrogel with respect to pH

pН	Ci (mg/L)	Ct (mg/L)	qt (mg/g)± S.D	Removal (%) ±
				S.D
5	10	5.06	0.123 ± 0.003	49.4 ± 0.34
6	10	4.32	0.142 ± 0.004	56.8 ± 0.38
7	10	1.6	0.21 ± 0.005	84.0 ± 0.30
8	10	3.24	0.169 ± 0.004	67.6 ± 0.42
9	10	3.9	0.152 ± 0.003	61.0 ± 0.36

Table 5.27: Methyl orange removal efficiency of nanocomposite with respect to pH

pН	Ci (mg/L)	Ct (mg/L)	$qt (mg/g) \pm S.D$	Removal (%) ±
				S.D
5	10	4.55	0.136 ± 0.004	54.5 ± 0.35
6	10	2.89	0.177 ± 0.005	71.1 ± 0.38
7	10	1.02	0.224 ± 0.006	89.8 ± 0.31
8	10	2.67	0.183 ± 0.005	73.3 ± 0.36
9	10	3.14	0.171 ± 0.004	68.6 ± 0.34

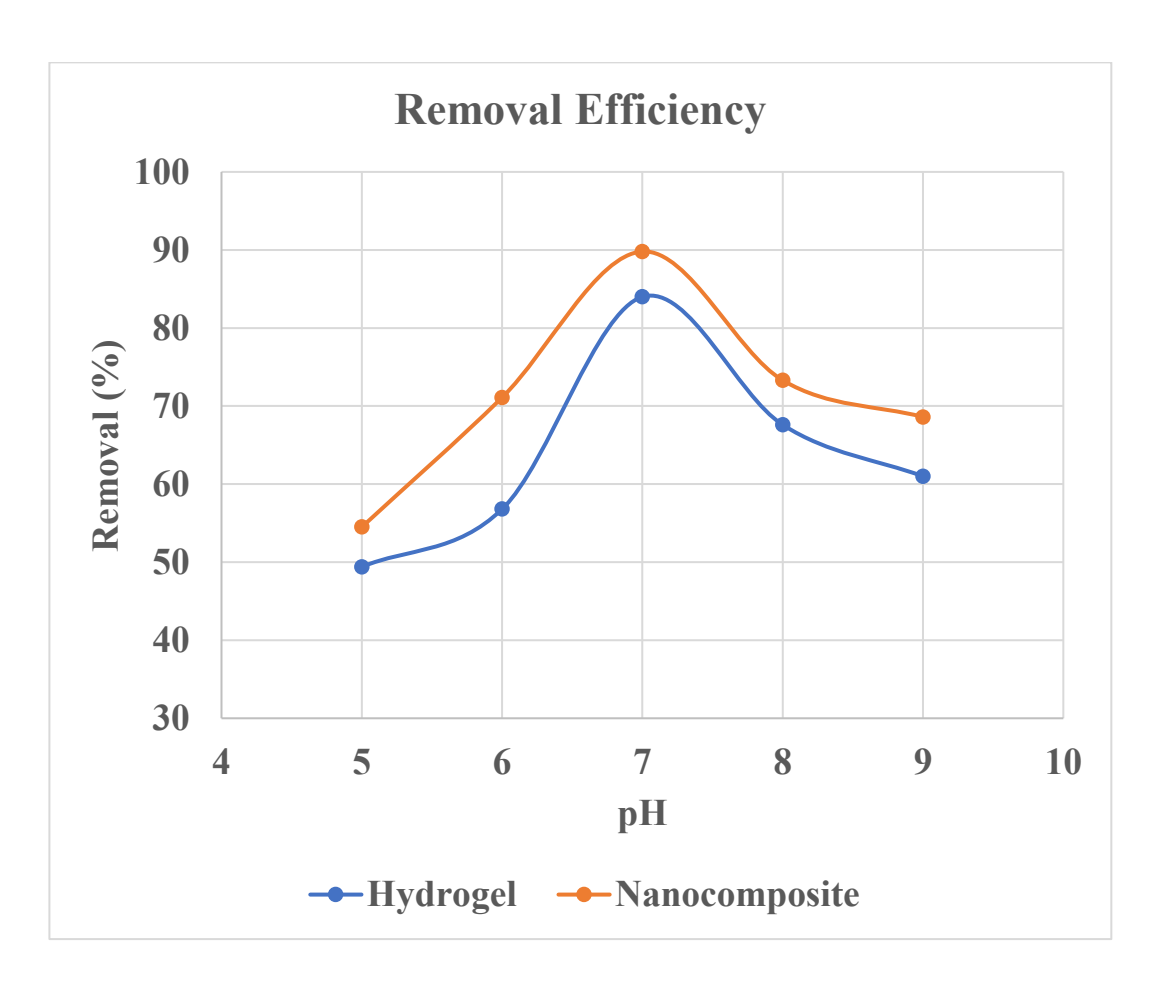


Figure 5.26: MO removal efficiency of hydrogel and nanocomposite with respect to pH

5.5.3.3 Adsorbent Dosage Reaction

The effect of adsorbent dosage on methyl orange dye removal was examined for both the hydrogel and its ZnO-based nanocomposite using dosages ranging from 0.5 to 3 g under fixed volume conditions (50 mL dye solution, Ci = $10 \, \text{mg/L}$). For the hydrogel, removal efficiency increased with dosage, reaching a maximum of $86.55 \pm 0.32\%$ at 3 g, while the adsorption capacity (qt) gradually declined from $0.468 \pm 0.012 \, \text{mg/g}$ at $0.5 \, \text{g}$ to $0.144 \pm 0.004 \, \text{mg/g}$ at 3 g. This trend reflects the saturation of available dye molecules at higher adsorbent concentrations and the relative reduction in dye uptake per gram of adsorbent. In contrast, the nanocomposite displayed superior performance, achieving the highest removal of $89.1 \pm 0.28\%$ at just 2 g dosage, beyond which a slight decline in efficiency was observed due to potential particle aggregation or site overlap.

The consistently higher qt values for the nanocomposite compared to the hydrogel indicate improved adsorption kinetics and surface accessibility, resulting from the integration of ZnO nanoparticles (Benhalima et al., 2023). These results suggest that while increasing dosage enhances dye removal, the nanocomposite achieves greater efficiency at lower dosages, highlighting its improved adsorption characteristics.

Table 5.28: Methyl orange removal efficiency of hydrogel with respect to dosage

Dosage (g)	Ci (mg/L)	Ct (mg/L)	$qt (mg/g) \pm S.D$	Removal (%) ±
				S.D
0.5	10	5.32	0.468 ± 0.012	46.8 ± 0.33
1	10	3.44	0.328 ± 0.009	65.6 ± 0.39
1.5	10	2.056	0.264 ± 0.008	79.44 ± 0.42
2	10	1.65	0.208 ± 0.007	83.5 ± 0.36
2.5	10	1.42	0.172 ± 0.005	85.8 ± 0.34
3	10	1.345	0.144 ± 0.004	86.55 ± 0.32

Table 5.29: Methyl orange removal efficiency of nanocomposite with respect to dosage

Dosage (g)	Ci (mg/L)	Ct (mg/L)	$qt (mg/g) \pm S.D$	Removal (%) ±
				S.D
0.5	10	4.2	0.58 ± 0.010	58.0 ± 0.36
1	10	2.43	0.378 ± 0.009	75.7 ± 0.40

1.5	10	1.54	0.282 ± 0.007	84.6 ± 0.34
2	10	1.09	0.222 ± 0.006	89.1 ± 0.28
2.5	10	1.13	0.177 ± 0.005	88.7 ± 0.30
2	10	1.0	0.125 + 0.004	91.0 + 0.22
3	10	1.9	0.135 ± 0.004	81.0 ± 0.33

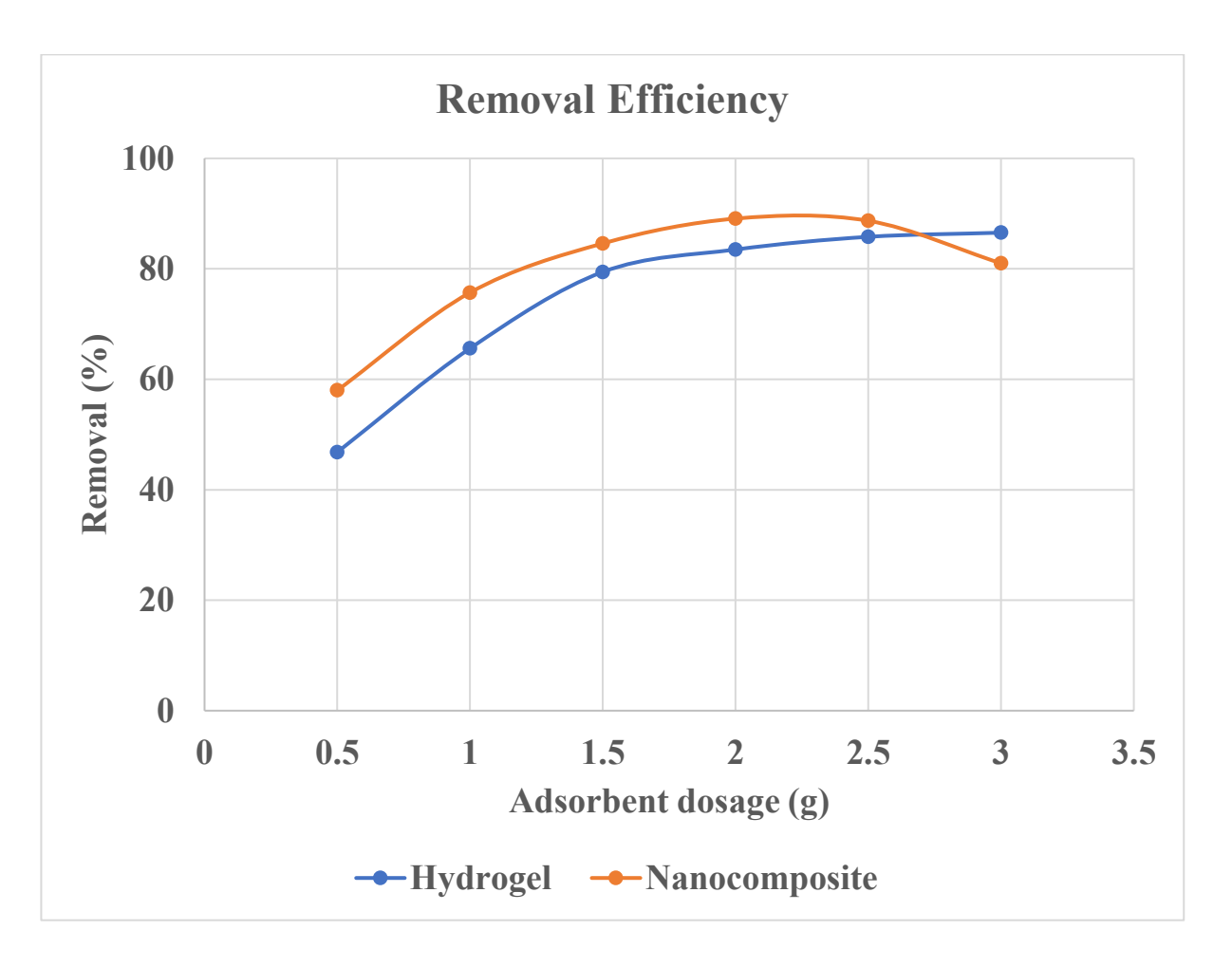


Figure 5.27: MO removal efficiency of hydrogel and nanocomposite with respect to Adsorbent dosage

5.5.3.4 Initial Concentration reaction

The effect of initial dye concentration on methyl orange adsorption was studied using both hydrogel and ZnO-based nanocomposite adsorbents, with a constant dosage of 2 g in 50 mL dye solution. For the hydrogel, the removal efficiency increased from

 $49.66 \pm 0.35\%$ at 6 mg/L to a maximum of $85.72 \pm 0.33\%$ at 14 mg/L. Similarly, the adsorption capacity (qt) showed a positive correlation with increasing initial concentration, indicating a greater driving force for mass transfer and more interaction between dye molecules and available adsorption sites (Xiong et al., 2023). However, a plateau in removal percentage beyond 10 mg/L suggests that active sites on the hydrogel surface become saturated under fixed dosage conditions. The nanocomposite exhibited consistently higher adsorption performance, achieving $88.3 \pm 0.30\%$ removal at 10 mg/L and maintaining high efficiencies at elevated concentrations. This can be attributed to the improved surface area, porosity, and active binding functionalities introduced by ZnO nanoparticles, which facilitate enhanced interaction with methyl orange molecules. The higher qt values for the nanocomposite further confirm its superior adsorption capability, making it more effective than the hydrogel for dye removal, particularly under higher pollutant loads.

Table 5.30: Methyl orange removal efficiency of hydrogel with respect to initial concentration

Initial conc.	Ci (mg/L)	Ct (mg/L)	$qt (mg/g) \pm S.D$	Removal (%) ±
				S.D
6	6	3.02	0.074 ± 0.003	49.66 ± 0.35
8	8	2.54	0.136 ± 0.005	68.25 ± 0.38
10	10	1.45	0.213 ± 0.006	85.5 ± 0.32
10	10	1.43	0.213 ± 0.000	63.3 ± 0.32
12	12	1.78	0.255 ± 0.007	85.16 ± 0.36
14	14	1.998	0.300 ± 0.008	85.72 ± 0.33

Table 5.31: Methyl orange removal efficiency of nanocomposite with respect to initial concentration

Initial conc.	Ci (mg/L)	Ct (mg/L)	$qt (mg/g) \pm S.D$	Removal (%) ±
				S.D
6	6	2.98	0.075 ± 0.003	50.33 ± 0.34
8	8	2.22	0.144 ± 0.005	72.25 ± 0.36
10	10	1.17	0.220 ± 0.006	88.3 ± 0.30
12	12	1.76	0.256 ± 0.007	85.33 ± 0.33
14	14	1.89	0.302 ± 0.008	86.5 ± 0.31

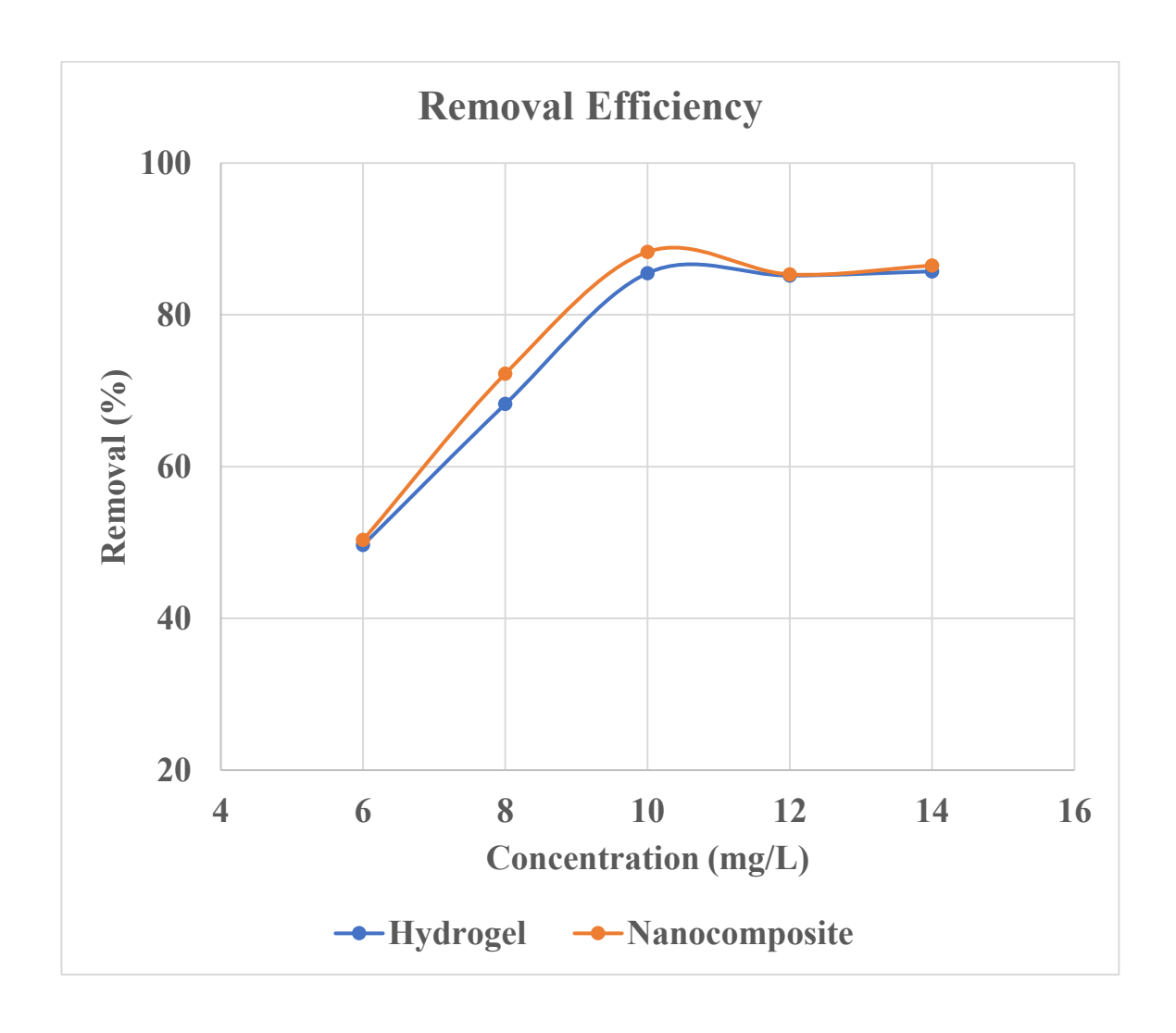


Figure 5.28: MO removal efficiency of hydrogel and nanocomposite with respect to initial concentration

5.6 DESORPTION STUDIES

5.6.1 Screening of solvents

During solvent screening, the behaviour of the acidic anionic azo dyes Amaranth (AR) and methyl orange (MO) on the ZnO-BM-g-poly(AA) adsorbent clearly indicated that alkaline conditions were the most favourable for regeneration. In alkaline media such as NaOH, the -COOH groups of the poly(acrylic acid) backbone are deprotonated to -COO-, which introduces additional negative charges into the hydrogel network. This increase in negative charge enhances electrostatic repulsion between the anionic dye species and the polymer matrix, thereby promoting the release of the dye molecules from the surface and their desorption back into the solution. In contrast, in the presence of strong acids (HCl, HNO₃), the polymer is protonated, which can increase the affinity of the matrix for the anionic dyes and, in some cases, lead to partial degradation or weakening of the hydrogel structure under repeated use. Organic solvents such as ethanol and acetone did not effectively disrupt the ionic interactions governing dye binding in this aqueous system and therefore showed comparatively low desorption efficiencies, while distilled water alone resulted in negligible dye release. Among all regenerating media evaluated (NaOH, HCl, HNO3, acetone, ethanol and distilled water), 0.05 N NaOH provided the highest desorption efficiencies for both MO and AR (~79–82 %) without any visible damage to the hydrogel matrix. On this basis, 0.05 N NaOH was selected as the optimal desorbing medium for subsequent adsorptiondesorption cycle studies (Aljeboree et al., 2024).

Table 5.32: Screening of different desorbing media for AR and MO-loaded ZnO-BM-g-poly(AA) hydrogel nanocomposite (Ci = 10 mg/L, contact time = 2 h)

Desorbing	Conc. (N)	q.des (mg/g) ±	Desorption (%)	Observation
medium		S.D	± S.D	

NaOH	0.05	0.176 ± 0.005	80.0 ± 0.6	No damage,
				good swelling
HC1	0.05	0.082 ± 0.003	37.3 ± 0.5	Slight matrix
				softening
HNO3	0.05	0.071 ± 0.003	27.5 ± 0.7	Low desorption
Ethanol	-	0.04 ± 0.002	18.2 ± 0.5	Poor desorption
Acetone	-	0.035 ± 0.002	15.5 ± 0.4	Poor desorption
Distilled water	-	0.022 ± 0.001	10.2 ± 0.3	Negligible
				desorption

5.6.2 Desorption of Amaranth from Hydrogel nanocomposite

Table 5.33: Desorption of Amaranth (AR) from ZnO–BM-g-poly(AA) hydrogel nanocomposite (Desorbing medium: 0.05 N NaOH, contact time = 2 h)

Initial conc. (Ci) (mg/L)	$(q.des) (mg/g) \pm S.D.$	Desorption (%) ± S.D.
6	0.060 ± 0.002	79.8 ± 0.6
	0.110 . 0.004	01.0 . 0.7
8	0.118 ± 0.004	81.2 ± 0.7
10	0.176 + 0.005	20.0 + 0.5
10	0.176 ± 0.005	80.0 ± 0.5
12	0.202 ± 0.006	78.9 ± 0.6
12	0.202 ± 0.000	78.9 ± 0.0
14	0.242 ± 0.007	80.1 ± 0.7
	0.2 12 = 0.007	00.1 = 0.7

Desorption (%) is calculated with respect to the amount of Amaranth initially adsorbed on the ZnO–BM-g-poly(AA) nanocomposite at the corresponding initial concentration. The results successfully demonstrated that 81% of amaranth can be recovered from hydrogel nanocomposite (fig. 5.29, table 5.33).

5.6.3 Desorption of Methyl orange from Hydrogel nanocomposite

Table 5.34: Desorption of methyl orange (MO) from ZnO-BM-g-poly(AA) hydrogel nanocomposite (Desorbing medium: 0.05 N NaOH, contact time = 2 h)

Initial conc. (Ci) (mg/L)	q.des $(mg/g) \pm S.D.$	Desorption (%) ± S.D.
6	0.065 ± 0.003	78.6 ± 0.8
8	0.124 ± 0.004	80.3 ± 0.7
10	0.186 ± 0.005	79.5 ± 0.6
12	0.214 ± 0.006	80.7 ± 0.7
14	0.255 ± 0.007	81.0 ± 0.7

For methyl orange, the ZnO–BM-g-poly(AA) hydrogel nanocomposite exhibited good regeneration behaviour (fig. 5.29, table 5.34), with desorption efficiencies in the range of ~79–81% in 0.05 N NaOH, indicating that nearly 80% of the previously adsorbed dye could be recovered without noticeable damage to the adsorbent matrix (Mohammad & Suzylawati (2020)).

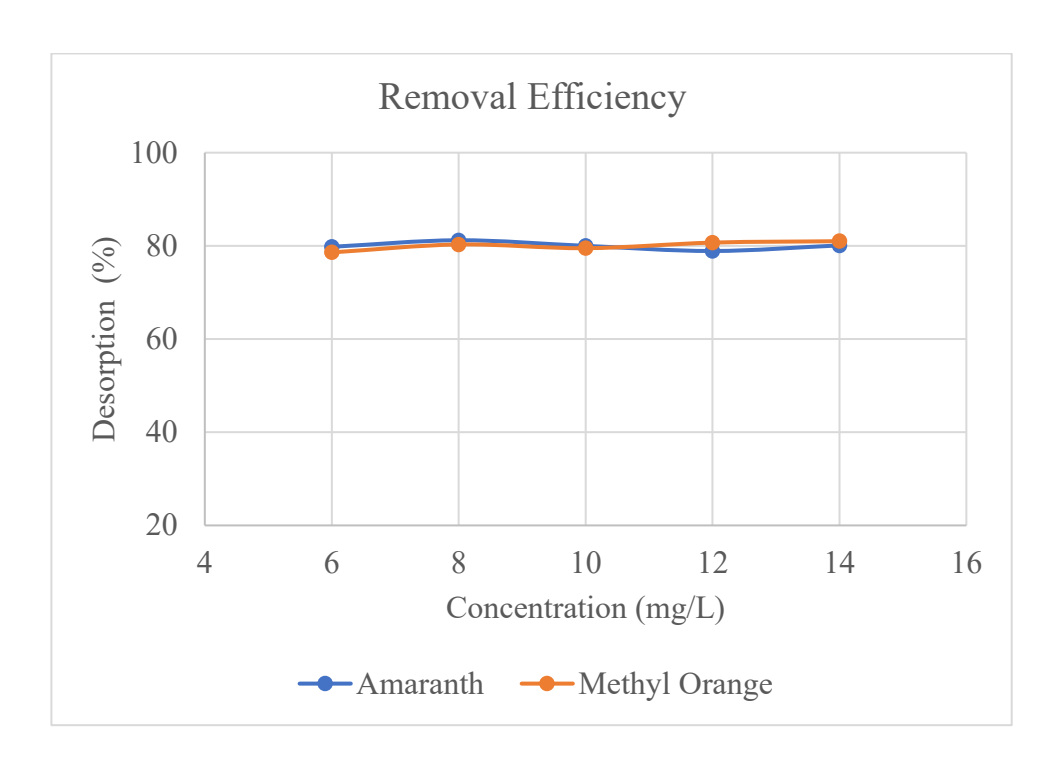


Figure 5:29: Desorption of Amaranth and Methyl orange from ZnO-BM-g-poly(AA) hydrogel nanocomposite.

CHAPTER 6 SUMMARY AND CONCLUSION

In summary, this research developed green nanocomposite hydrogels for the removal of toxic dyes from water, successfully achieving all the stated objectives. A Butea monosperma gum (BM) polysaccharide was grafted with acrylic acid to form a natural hydrogel, and a synthetic poly(ethylene glycol) (PEG)-based hydrogel was also prepared for comparison. Various polymerization routes like microwave irradiation, conventional thermal heating, and redox (chemical) initiation were explored for hydrogel synthesis. Among these, microwave-assisted synthesis proved to be the most effective route, yielding hydrogels with the highest water uptake and more uniform network structure. The BM-g-poly(AA) hydrogel synthesized under microwave irradiation exhibited a markedly higher swelling capacity (up to ~450% in optimized conditions) than the same hydrogel prepared by thermal (~312% max) and redox (~278% max) methods. The superior performance of the microwave route is attributed to rapid, volumetrically uniform heating and efficient free-radical generation, which together enhanced grafting efficiency and produced a more open, porous network. In contrast, the thermally and chemically initiated hydrogels required longer reaction times (hours versus ~40 seconds for microwave) and formed denser cross-linked structures with lower swelling due to slower or less uniform radical formation. Consequently, the microwave method was selected as the optimal synthesis route, and it was employed to fabricate all further hydrogel samples.

Using the microwave technique, the study synthesized novel hydrogel nanocomposites by incorporating zinc oxide (ZnO) nanoparticles into both natural and synthetic hydrogel matrices. The ZnO–BM-g-poly(AA) nanocomposite hydrogel and ZnO–PEG-g-poly(AA) nanocomposite hydrogel were successfully prepared, as confirmed by comprehensive characterization. Fourier-transform infrared (FTIR) spectroscopy verified the chemical structure of the grafted hydrogels and the presence of ZnO in the nanocomposites (e.g. appearance of Zn–O vibrational bands in the composite). Thermogravimetric analysis (TGA) demonstrated improved thermal stability in the ZnO-loaded hydrogels, reflecting the stabilizing effect of the inorganic nanoparticles. Field-emission scanning electron microscopy (FE-SEM) revealed the cross-linked hydrogel network morphology and indicated that ZnO particles were well-dispersed within the polymer matrix, confirming successful nanocomposite formation. These

characterization results substantiate that the microwave-assisted method effectively grafted polymer chains onto both natural and synthetic backbones and uniformly integrated ZnO nanoparticles, yielding robust nanocomposite hydrogels with the intended composition and structure.

The swelling behavior of the hydrogels was extensively evaluated and optimized, since high swelling is crucial for a toxic pollutant adsorption. The natural BM-g-poly(AA) hydrogel showed exceptional swelling capacity under optimized conditions (exceeding 400% in water), owing to the hydrophilicity of the poly(acrylic acid) chains and the porous network formed on the BM gum backbone. In contrast, the PEG-g-poly(AA) synthetic hydrogel reached a lower maximum swelling (~240% under optimum conditions), indicating that the natural gum-based network retained more water that is a beneficial feature for a "green" hydrogel. Introducing ZnO nanoparticles into the BMg-poly(AA) hydrogel further enhanced the swelling capacity up to an optimum (~515% swelling) at 0.2 g ZnO content. This improvement is attributed to ZnO's hydrophilicity and its interaction with the polymer (via hydrogen bonding and electrostatic interactions), which promoted additional water uptake. However, excess ZnO (beyond the optimal loading) caused some aggregation and network stiffening, resulting in reduced swelling. Thus, an optimal nanofiller content was identified that maximized swelling. Overall, the green nanocomposite hydrogel (ZnO–BM-g-poly(AA)) exhibited the highest swelling, combining the natural polymer's affinity for water with the nanoparticle-induced network expansion. Such a highly swollen, porous structure increases the diffusion of dye molecules into the hydrogel matrix and exposes abundant binding sites, which is advantageous for adsorption applications.

Finally, the adsorption studies demonstrated the efficacy of these hydrogels in removing toxic anionic dyes from aqueous solutions, fulfilling the primary environmental application objective. Two model pollutants, Amaranth (AR) and Methyl Orange (MO) dyes were used to investigate the dye removal performance of the base hydrogel versus its nanocomposite. The results showed that the ZnO-BM-g-poly (AA) hydrogel nanocomposite consistently outperformed the BM-g-poly (AA) hydrogel in both adsorption capacity and rate of removal. For instance, in the case of Amaranth (10 mg/L initial concentration), the BM-g-poly(AA) hydrogel gradually

reached ~74.5% removal after 6 hours, whereas the ZnO-hydrogel nanocomposite achieved about 88.9% removal in the same time. Notably, the nanocomposite adsorbed dye much faster, attaining over 84% removal within the first 3 hours, compared to the slower uptake by the hydrogel. This enhanced kinetics is attributed to the presence of ZnO, which provides additional active sites (surface hydroxyl groups) and possibly facilitates electron-transfer interactions with the dye's sulfonate groups, thereby accelerating adsorption. The adsorbent dosage effect further confirmed the nanocomposite's superior capacity as the amount of adsorbent increased, both materials showed higher removal, but the nanocomposite achieved higher efficacy at each dosage and nearly complete dye removal at the highest dose, due to its greater density of binding sites and reinforced structure. Similarly, the nanocomposite was more effective across a range of pH conditions, maintaining high performance where the hydrogel's efficiency dropped. Both adsorbents performed best around neutral pH (pH 7), at which the hydrogel removed ~73.2% of Amaranth while the nanocomposite removed about 88.0%. The decline in removal at pH >7 for both is explained by electrostatic repulsion (as the deprotonated hydrogel and the anionic dye repel each other), but the nanocomposite's removal remained higher at each pH tested. Additionally, the nanocomposite proved more resilient to increasing initial dye concentrations: the BMg-poly(AA) hydrogel reached a plateau at ~77% removal for Amaranth as concentration rose (saturating its active sites), whereas the ZnO-hydrogel maintained about 87% removal even at 14 mg/L, reflecting its larger adsorption capacity. Methyl Orange adsorption showed analogous trends. Under optimal conditions, the hydrogel removed about 84% of MO at pH 7, while the ZnO nanocomposite reached ~89.8% removal. The nanocomposite also exhibited faster uptake of MO and higher efficiency across varying pH and dosages, underscoring its broad applicability. These results clearly demonstrate that embedding ZnO nanoparticles in the hydrogel significantly enhances dye removal efficiency and capacity, validating the approach of creating a nanocomposite for environmental pollutant remediation. The desorption studies showed that ZnO-BM-g-poly(AA) could effectively release previously adsorbed AR and MO, with desorption efficiencies consistently approaching ~80% across the tested concentrations, as evidenced by the tabulated (q.des) and percentage values. Solvent screening further revealed that mildly alkaline conditions (0.05 N NaOH) provided the

highest desorption efficiencies while preserving the structural integrity of the hydrogel nanocomposite, whereas acidic media, organic solvents and water were markedly less effective. Collectively, these findings demonstrate that the ZnO-BM-g-poly(AA) system is not only an efficient adsorbent but also readily regenerable, supporting its practical applicability in repeated dye removal cycles.

In conclusion, the green hydrogel nanocomposites developed in this work have shown excellent performance in both physicochemical properties and practical dye adsorption. The microwave-assisted synthesis was identified as the best route, yielding hydrogels with superior swelling (up to ~450% for natural gum-based hydrogel) and enabling the successful incorporation of nanofillers. The natural polymer-based hydrogel (BM-gpoly(AA)) outperformed the synthetic PEG-based hydrogel and its nanocomposite in water absorbency, highlighting the advantage of using renewable biopolymers for highswelling materials. The addition of ZnO nanoparticles further conferred notable advantages: it increased the hydrogel's swelling capacity and provided additional active sites, which together led to faster and more effective uptake of toxic dye molecules from solution. The optimized ZnO-BM-g-poly(AA) nanocomposite could remove around 85–90% of model anionic dyes under optimum conditions, versus ~70–80% for the non-composite hydrogel, and it sustained high removal efficiency even under less favorable conditions (e.g. higher pollutant loads or varying pH). These findings confirm that the formulated nanocomposite hydrogel is a robust and efficient adsorbent for toxic dye pollutants, merging the inherent high swelling and functional group-rich nature of grafted hydrogels with the reactivity and stability of inorganic nanoparticles. This work therefore contributes a promising sustainable material for environmental remediation and detection of these dyes that are also illegal adulterants, and the BM-based nanocomposite hydrogel emerges as a potent candidate for real-world wastewater treatment targeting hazardous dye contaminants and for forensic applications.

BIBLIOGRAPHY

Abdi, G., Jain, M., Patil, N., Tariq, M., Choudhary, S., Kumar, P., ... & Uthappa, U. T. (2024). Tragacanth gum-based hydrogels for drug delivery and tissue engineering applications. *Frontiers in Materials*, 11, 1296399.

Abdollahi, M., Andalib, S., Ghorbani, R., Afshar, D., Gholinejad, M., Abdollahi, H., ... & Nikfarjam, N. (2024). Polydopamine contained hydrogel nanocomposites with combined antimicrobial and antioxidant properties for accelerated wound healing. *International Journal of Biological Macromolecules*, 268, 131700.

Akhtar, M. S., Ali, S., & Zaman, W. (2024). Innovative adsorbents for pollutant removal: Exploring the latest research and applications. *Molecules*, 29(18), 4317.

Aljeboree, A. M., & Alkaim, A. F. (2024). Studying removal of anionic dye by prepared highly adsorbent surface hydrogel nanocomposite as an applicable for aqueous solution. *Scientific Reports*, 14(1), 9102.

Aljeboree, A. M., Alkaim, A. F., Alsultany, F. H., & Issa, S. K. (2025). Highly reusable nano adsorbent based on clay-incorporated hydrogel nanocomposite for cationic dye adsorption. *Journal of Inorganic and Organometallic Polymers and Materials*, 35(2), 1165-1186.

Amaral, M. A., Yasin, S., Gibson, A. P., & Morgan, R. M. (2020). Sampling of explosive residues: The use of a gelatine-based medium for the recovery of ammonium nitrate. *Science & Justice*, 60(6), 531-537.

Andersen, T., Auk-Emblem, P., & Dornish, M. (2015). 3D cell culture in alginate hydrogels. *Microarrays*, 4(2), 133-161.

Archana, P., Janarthanan, B., Bhuvana, S., Rajiv, P., & Sharmila, S. (2022). Concert of zinc oxide nanoparticles synthesized using Cucumis melo by green synthesis and the antibacterial activity on pathogenic bacteria. *Inorganic Chemistry Communications*, 137, 109255.

Bacsik, Z., Mink, J., & Keresztury, G. (2004). FTIR spectroscopy of the atmosphere. I. Principles and methods. *Applied spectroscopy reviews*, *39*(3), 295-363.

Bakhshi, V., Poursadegh, H., Amini-Fazl, M. S., Salari, D., & Javanbakht, S. (2024). Synthesis and characterization of bio-nanocomposite hydrogel beads based on magnetic hydroxyapatite and chitosan: a pH-sensitive drug delivery system for potential implantable anticancer platform. *Polymer Bulletin*, 81(8), 7499-7518.

Bakshi, M. I., Nazir, S., Restu, W. K., Rajamanickam, R., Selvasembian, R., Hua, L. S., ... & Fatriasari, W. (2024). Recent advances in lignin from forest residue for hydrogel application. *Biomass Conversion and Biorefinery*, 1-17.

Barrett-Catton, E., Ross, M. L., & Asuri, P. (2021). Multifunctional hydrogel nanocomposites for biomedical applications. *Polymers*, 13(6), 856.

Batouti, M. E., Sadik, W., Eldemerdash, A. G., Hanafy, E., & Fetouh, H. A. (2023). New and innovative microwave-assisted technology for synthesis of guar gum-grafted acrylamide hydrogel superabsorbent for the removal of acid red 8 dye from industrial wastewater. *Polymer Bulletin*, 80(5), 4965-4989.

Benhalima, T., Allali, F. Z., Roumane, N., & Ferfera-Harrar, H. (2023). Enhanced adsorptive removal of hazardous methyl violet 2B and methyl orange dyes by Algerian diatomite-loaded polysaccharide-based hydrogel beads. *Journal of Molecular Liquids*, 383, 122150.

Blachnio, M., & Zienkiewicz-Strzalka, M. (2024). Evaluation of the Dye Extraction Using Designed Hydrogels for Further Applications towards Water Treatment. *Gels*, 10(3), 159.

Cha, G. D., Lee, W. H., Lim, C., Choi, M. K., & Kim, D. H. (2020). Materials engineering, processing, and device application of hydrogel nanocomposites. *Nanoscale*, 12(19), 10456-10473.

Chauhan, S., Kumar, P., Chauhan, G. S., Ranote, S., Jamwal, P., & Kumar, K. (2025). Kinetic and thermodynamic evaluation of sulfonated guar gum-based hydrogels for

effective and rapid adsorption of cationic dyes. *Journal of Dispersion Science and Technology*, 46(2), 244-262.

Choudhary, S., Sharma, K., Bhatti, M. S., Sharma, V., & Kumar, V. (2022). DOE-based synthesis of gellan gum-acrylic acid-based biodegradable hydrogels: screening of significant process variables and in situ field studies. *RSC advances*, *12*(8), 4780-4794.

Choudhary, S., Sharma, K., Kumar, V., Bhatia, J. K., Sharma, S., & Sharma, V. (2020). Microwave-assisted synthesis of gum gellan-cl-poly (acrylic-co-methacrylic acid) hydrogel for cationic dyes removal. *Polymer Bulletin*, 77, 4917-4935.

Cooksey, C. J. (2016). Quirks of dye nomenclature. 6. Malachite green. *Biotechnic & Histochemistry*, *91*(6), 438-444.

Deng, Z., Yu, R., & Guo, B. (2021). Stimuli-responsive conductive hydrogels: design, properties, and applications. *Materials Chemistry Frontiers*, *5*(5), 2092-2123.

Drápalová, E., Michlovská, L., Poštulková, H., Chamradová, I., Lipový, B., Holoubek, J., ... & Vojtová, L. (2023). Antimicrobial cost-effective transparent hydrogel films from renewable gum karaya/chitosan polysaccharides for modern wound dressings. *ACS Applied Polymer Materials*, *5*(4), 2774-2786.

Dutta, S., Gupta, R. S., Pathan, S., & Bose, S. (2023). Interpenetrating polymer networks for desalination and water remediation: A comprehensive review of research trends and prospects. *RSC advances*, *13*(9), 6087-6107.

El-saied, H. A. A., & El-Fawal, E. M. (2021). Green superabsorbent nanocomposite hydrogels for high-efficiency adsorption and photo-degradation/reduction of toxic pollutants from waste water. *Polymer Testing*, 97, 107134.

Elsayed, M. M. (2019). Hydrogel preparation technologies: relevance kinetics, thermodynamics and scaling up aspects. *Journal of Polymers and the Environment*, 27(4), 871-891.

Epp, J. (2016). X-ray diffraction (XRD) techniques for materials characterization. In *Materials characterization using nondestructive evaluation (NDE) methods* (pp. 81-124). Woodhead Publishing.

Ferfera-Harrar, H., Benhalima, T., & Sadi, A. (2022). Development of functional chitosan-based superabsorbent hydrogel nanocomposites for adsorptive removal of Basic Red 46 textile dye. *Polymer Bulletin*, 79(8), 6141-6172.

Gaharwar, A. K., Peppas, N. A., & Khademhosseini, A. (2014). Nanocomposite hydrogels for biomedical applications. *Biotechnology and bioengineering*, 111(3), 441-453.

Gao, H., Jiang, J., Huang, Y., Wang, H., Sun, J., Jin, Z., ... & Zhang, J. (2022). Synthesis of hydrogels for adsorption of anionic and cationic dyes in water: Ionic liquid as a crosslinking agent. *SN Applied Sciences*, 4(4), 118.

García Schejtman, S. D., Mercadal, P. A., Picchio, M. L., Veglia, A. V., & Coronado, E. A. (2022). In Situ Preparation of Plasmonic Gold Nanoparticle-Supramolecular Hydrogel Nanocomposites with Tunable Optical Properties: Correlating Theory and Experiments. *The Journal of Physical Chemistry C*, *126*(23), 9979-9988.

Ge, H., Ding, K., Guo, F., Wu, X., Zhai, N., & Wang, W. (2022). Green and superior adsorbents derived from natural plant gums for removal of contaminants: a review. *Materials*, 16(1), 179.

Ghosh, T., Das, T., & Purwar, R. (2021). Review of electrospun hydrogel nanofiber system: Synthesis, Properties and Applications. *Polymer Engineering & Science*, 61(7), 1887-1911.

Gong, Z., Wang, C., Pu, S., Wang, C., Cheng, F., Wang, Y., & Fan, M. (2016). Rapid and direct detection of illicit dyes on tainted fruit peel using a PVA hydrogel surface enhanced Raman scattering substrate. *Analytical Methods*, 8(24), 4816-4820.

Gray, K. M., Walker, M. J., Burn, M. J. S., Mazur, M., Niedzwiedzka, K., Liszka, K., & Burns, D. T. (2016). Illegal dyes in food and spices—A 2006 LGC LC-UV/visible method reviewed and updated for 19 dyes. *J. Assoc. Public Anal*, *44*, 18-39.

Gyles, D. A., Castro, L. D., Silva Jr, J. O. C., & Ribeiro-Costa, R. M. (2017). A review of the designs and prominent biomedical advances of natural and synthetic hydrogel formulations. *European Polymer Journal*, 88, 373-392.

Haraguchi, K., & Takehisa, T. (2002). Nanocomposite hydrogels: A unique organic—inorganic network structure with extraordinary mechanical, optical, and swelling/deswelling properties. *Advanced materials*, *14*(16), 1120-1124.

Haraguchi, K., & Takehisa, T. (2005, January). Novel manufacturing process of nanocomposite hydrogel for bio-applications. In *ASME International Mechanical Engineering Congress and Exposition* (Vol. 42231, pp. 119-126).

He, C., Sun, Z., Xing, M., Lei, J., Ye, Z., Wang, L., & Zhang, J. (2024). Hydrogel Network: A Dynamic Solution for Reversible Metal Ion Valence Switching. *Chemistry of Materials*, *36*(7), 3316-3325.

Hidayah, N., Bakar, F. A., Mahyudin, N. A., Faridah, S., Nur-Azura, M. S., & Zaman, M. Z. (2013). Detection of malachite green and leuco-malachite green in fishery industry. *International Food Research Journal*, 20(4), 1511.

Hocine, S., Ghemati, D., & Aliouche, D. (2023). Synthesis, characterization and swelling behavior of pH-sensitive polyvinylalcohol grafted poly (acrylic acid-co-2-acrylamido-2-methylpropane sulfonic acid) hydrogels for protein delivery. *Polymer Bulletin*, 1-27.

Hoogenboom, L. A. P. (2016). Scientific opinion: Malachite green in food. *EFSA Journal*, 14(7), e04530.

Hou, X., Mu, L., Chen, F., & Hu, X. (2018). Emerging investigator series: design of hydrogel nanocomposites for the detection and removal of pollutants: from nanosheets, network structures, and biocompatibility to machine-learning-assisted design. *Environmental Science: Nano*, 5(10), 2216-2240.

Huang, X., Hu, B., Zhang, X., Fan, P., Chen, Z., & Wang, S. (2024). Recent advances in the application of clay-containing hydrogels for hemostasis and wound healing. *Expert Opinion on Drug Delivery*, 21(3), 457-477.

Hussain, S., Salman, M., Youngblood, J. P., Farooq, U., Yasmeen, S., Al-Ahmary, K. M., & Ahmed, M. (2024). Enhanced adsorption of Congo red dye by CS/PEG/ZnO composite hydrogel: Synthesis, characterization, and performance evaluation. *Journal of Molecular Liquids*, 411, 125704.

Hwang, U., Moon, H., Park, J., & Jung, H. W. (2024). Crosslinking and Swelling Properties of pH-Responsive Poly (Ethylene Glycol)/Poly (Acrylic Acid) Interpenetrating Polymer Network Hydrogels. *Polymers*, *16*(15), 2149.

Inobeme, A., Mathew, J. T., Adetunji, C. O., Agbugui, M. O., Inobeme, J., Enerijiofi, K. E., ... & Daniel, O. (2024). Understanding Dye Pollution and Its Impact on the Environment. In *Dye Pollution from Textile Industry: Challenges and Opportunities for Sustainable Development* (pp. 3-15). Singapore: Springer Nature Singapore.

Ivanov, A. S., Pershina, L. V., Nikolaev, K. G., & Skorb, E. V. (2021). Recent progress of layer-by-layer assembly, free-standing film and hydrogel based on polyelectrolytes. *Macromolecular bioscience*, *21*(10), 2100117.

Jabir, L., El-Hammi, H., Mohammed, N., Jilal, I., El Idrissi, A., Amhamdi, H., ... & Laatikainen, K. (2022). Cellulose based pH-sensitive hydrogel for highly efficient dye removal in water treatment: kinetic, thermodynamic, theoretical and computational studies. *Cellulose*, 29(8), 4539-4564.

Jeong, J. H., Schmidt, J. J., Cha, C., & Kong, H. (2010). Tuning responsiveness and structural integrity of a pH responsive hydrogel using a poly (ethylene glycol) cross-linker. *Soft Matter*, 6(16), 3930-3938.

Ji, X., Wang, Q., Yu, M., Hadi, M. K., Liu, Y., Zhao, L., & Ran, F. (2021). All-in-one energy storage devices supported and interfacially cross-linked by gel polymeric electrolyte. *Energy Storage Materials*, *37*, 587-597.

Kabiri, K., Omidian, H., Zohuriaan-Mehr, M. J., & Doroudiani, S. (2011). Superabsorbent hydrogel composites and nanocomposites: a review. *Polymer composites*, 32(2), 277-289.

Kaith, B. S., Jindal, R., Mittal, H., & Kumar, K. (2012). Synthesis, characterization, and swelling behavior evaluation of hydrogels based on gum ghatti and acrylamide for selective absorption of saline from different petroleum fraction–saline emulsions. *Journal of applied polymer science*, 124(3), 2037-2047.

Kant, R. (2011). Textile dyeing industry an environmental hazard.

Karchoubi, F., Ghotli, R. A., Pahlevani, H., & Salehi, M. B. (2024). New insights into nanocomposite hydrogels; a review on recent advances in characteristics and applications. *Advanced Industrial and Engineering Polymer Research*, 7(1), 54-78.

Khan, A., Zaman, M., Waqar, M. A., Mahmood, A., Shaheer, T., Sarfraz, R. M., ... & Papadakis, M. (2024). Sustained release delivery of favipiravir through statistically optimized, chemically cross-linked, pH-sensitive, swellable hydrogel. *BMC Pharmacology and Toxicology*, 25(1), 31.

Khanam, S., Ray, S. K., Bhuiyan, R. H., Sultana, S., Sharmin, N., & Ehsan, Q. (2025). Advancing nutrient management in agriculture: Rice straw to nitrogen, phosphorus and potassium-containing hydrogel as slow-release fertilizer. *Industrial Crops and Products*, 224, 120380.

Kopecek, J. (2009). Hydrogels: From soft contact lenses and implants to self-assembled nanomaterials. *Journal of Polymer Science Part A: Polymer Chemistry*, 47(22), 5929-5946.

Kumar, N., Gusain, R., Pandey, S., & Ray, S. S. (2023). Hydrogel nanocomposite adsorbents and photocatalysts for sustainable water purification. *Advanced Materials Interfaces*, 10(2), 2201375.

Li, Q., Shen, H. X., Liu, C., Wang, C. F., Zhu, L., & Chen, S. (2022). Advances in frontal polymerization strategy: From fundamentals to applications. *Progress in Polymer Science*, 127, 101514.

Li, X., & Xiong, Y. (2022). Application of "click" chemistry in biomedical hydrogels. *ACS omega*, 7(42), 36918-36928.

Liu, Y. (2006). Some consideration on the Langmuir isotherm equation. *Colloids and Surfaces A: Physicochemical and Engineering Aspects*, 274(1-3), 34-36.

Madduma-Bandarage, U. S., & Madihally, S. V. (2021). Synthetic hydrogels: Synthesis, novel trends, and applications. *Journal of Applied Polymer Science*, *138*(19), 50376.

Makhado, E., Motshabi, B. R., Allouss, D., Ramohlola, K. E., Modibane, K. D., Hato, M. J., ... & Pandey, S. (2022). Development of a ghatti gum/poly (acrylic acid)/TiO2 hydrogel nanocomposite for malachite green adsorption from aqueous media: Statistical optimization using response surface methodology. *Chemosphere*, 306, 135524.

Mankotia, P., Choudhary, S., Sharma, K., Kumar, V., Bhatia, J. K., Parmar, A., ... & Sharma, V. (2020). Neem gum based pH responsive hydrogel matrix: A new pharmaceutical excipient for the sustained release of anticancer drug. *International journal of biological macromolecules*, 142, 742-755.

Mohammad, S., & Suzylawati, I. (2020). Study of the adsorption/desorption of MB dye solution using bentonite adsorbent coating. *Journal of Water Process Engineering*, 34, 101155.

Moharrami, P., & Motamedi, E. (2020). Application of cellulose nanocrystals prepared from agricultural wastes for synthesis of starch-based hydrogel nanocomposites: Efficient and selective nanoadsorbent for removal of cationic dyes from water. *Bioresource technology*, 313, 123661.

More, A. P., & Chapekar, S. (2024). Irradiation assisted synthesis of hydrogel: A Review. *Polymer Bulletin*, 81(7), 5839-5908.

Nasution, H., Harahap, H., Dalimunthe, N. F., Ginting, M. H. S., Jaafar, M., Tan, O. O., ... & Herfananda, A. L. (2022). Hydrogel and effects of crosslinking agent on cellulose-based hydrogels: A review. *Gels*, 8(9), 568.

Nath, J., Kumar, S., & Kumar, V. (2023). Response surface methodology-based modeling and optimization of fenugreek gum-based hydrogel for efficient removal of malachite green dye. *Journal of Molecular Structure*, *1293*, 136234.

Neas, E. D. (1988). Introduction on microwave sample preparation. *Professional Refference Book*, 7.

Nguyen, H. T., Ngwabebhoh, F. A., Saha, N., Saha, T., & Saha, P. (2022). Gellan gum/bacterial cellulose hydrogel crosslinked with citric acid as an eco-friendly green adsorbent for safranin and crystal violet dye removal. *International Journal of Biological Macromolecules*, 222, 77-89.

Njuguna, D. G., & Schönherr, H. (2021). Xanthan gum hydrogels as high-capacity adsorbents for dye removal. *ACS Applied Polymer Materials*, *3*(6), 3142-3152.

Pereira, K. A., Aguiar, K. L., Oliveira, P. F., Vicente, B. M., Pedroni, L. G., & Mansur, C. R. (2020). Synthesis of hydrogel nanocomposites based on partially hydrolyzed polyacrylamide, polyethyleneimine, and modified clay. *ACS omega*, *5*(10), 4759-4769.

Periyasamy, A. P. (2024). Recent advances in the remediation of textile-dye-containing wastewater: prioritizing human health and sustainable wastewater treatment. *Sustainability*, 16(2), 495.

Prabhu, R. S., Priyanka, R., Vijay, M., & Vikashini, G. K. (2021). Field emission scanning electron microscopy (fesem) with a very big future in pharmaceutical research. *International Journal of Pharmacy and Biological Sciences*, 11(2), 183-187.

Priya, Sharma, A. K., Kaith, B. S., Chandel, K., & Singh, A. (2020). Chemically modified chitosan-sodium alginate as chemo-sensor adsorbent for the detection of picric acid and removal of biebrich scarlet. *International Journal of Biological Macromolecules*, 147, 582-594.

Priyadarshi, R., Kumar, B., & Rhim, J. W. (2020). Green and facile synthesis of carboxymethylcellulose/ZnO nanocomposite hydrogels crosslinked with Zn2+ions. *International Journal of Biological Macromolecules*, *162*, 229-235.

Qin, S., Niu, Y., Zhang, Y., Wang, W., Zhou, J., Bai, Y., & Ma, G. (2024). Metal ion-containing hydrogels: synthesis, properties, and applications in bone tissue engineering. *Biomacromolecules*, 25(6), 3217-3248.

Radia, N. D., Aljeboree, A. M., & Mhammed, A. A. A. (2024). Enhanced removal of crystal violet from aqueous solution using carrageenan hydrogel nanocomposite/MWCNTs. *Inorganic Chemistry Communications*, 112803.

Rana, H., Anamika, Sareen, D., & Goswami, S. (2024). Nanocellulose-Based Ecofriendly Nanocomposite for Effective wastewater Remediation: A study on its process optimization, improved swelling, adsorption, and thermal and mechanical behavior. *ACS omega*, *9*(8), 8904-8922.

Rando, G., Scalone, E., Sfameni, S., & Plutino, M. R. (2024). Functional bio-based polymeric hydrogels for wastewater treatment: from remediation to sensing applications. *Gels*, 10(8), 498.

Rose, K. A., Lee, D., & Composto, R. J. (2021). pH-Mediated nanoparticle dynamics in hydrogel nanocomposites. *Soft Matter*, *17*(10), 2765-2774.

Rosendo, L. M., Antunes, M., Simão, A. Y., Brinca, A. T., Catarro, G., Pelixo, R., ... & Gallardo, E. (2023). Sensors in the Detection of Abused Substances in Forensic Contexts: A Comprehensive Review. *Micromachines*, *14*(12), 2249.

Saadatkhah, N., Carillo Garcia, A., Ackermann, S., Leclerc, P., Latifi, M., Samih, S., ... & Chaouki, J. (2020). Experimental methods in chemical engineering: Thermogravimetric analysis—TGA. *The Canadian Journal of Chemical Engineering*, 98(1), 34-43.

Saidi, M., Dabbaghi, A., & Rahmani, S. (2020). Swelling and drug delivery kinetics of click-synthesized hydrogels based on various combinations of PEG and star-shaped PCL: influence of network parameters on swelling and release behavior. *Polymer Bulletin*, 77(8), 3989-4010.

Sandhu, A., & Bhatia, T. (2023). Hydrogels: From Design to Applications in Forensic Investigations. *ChemistrySelect*, 8(8), e202204228

Sandhu, A., Pandey, V., & Pandey, T. (2023). Polar moiety functionalized, controlled gelation to obtain highly efficient hydrogel nanocomposite: an expansion of green synthetic strategy. *New Journal of Chemistry*, 47(45), 20976-20986.

Santoso, S. P., Angkawijaya, A. E., Bundjaja, V., Hsieh, C. W., Go, A. W., Yuliana, M., ... & Ismadji, S. (2021). TiO2/guar gum hydrogel composite for adsorption and photodegradation of methylene blue. *International journal of biological macromolecules*, 193, 721-733.

Schexnailder, P., & Schmidt, G. (2009). Nanocomposite polymer hydrogels. *Colloid and Polymer Science*, 287, 1-11.

Sethi, S., Singh, A., Medha, Thakur, S., Kaith, B. S., & Khullar, S. (2023). Natural polymer-based nanocomposite hydrogels as environmental remediation devices. In *Handbook of Green and Sustainable Nanotechnology: Fundamentals, Developments and Applications* (pp. 407-441). Cham: Springer International Publishing.

Shabalina, A. V., Kozlov, V. A., Popov, I. A., & Gudkov, S. V. (2024). A Review on Recently Developed Antibacterial Composites of Inorganic Nanoparticles and Non-Hydrogel Polymers for Biomedical Applications. *Nanomaterials*, *14*(21), 1753.

Shao, X. H., Yang, X., Zhou, Y., Xia, Q. C., Lu, Y. P., Yan, X., ... & Gao, S. Z. (2022). Antibacterial, wearable, transparent tannic acid—thioctic acid—phytic acid hydrogel for adhesive bandages. *Soft Matter*, *18*(14), 2814-2828.

Sharma, A. K., Priya, & Kaith, B. S. (2021). Polymer nanocomposite matrices: classification, synthesis methods, and applications. In *Handbook of polymer and ceramic nanotechnology* (pp. 403-428). Cham: Springer International Publishing.

Sharma, G., Kumar, A., Naushad, M., García-Peñas, A., Al-Muhtaseb, A. A. H., Ghfar, A. A., ... & Stadler, F. J. (2018). Fabrication and characterization of Gum arabic-cl-poly (acrylamide) nanohydrogel for effective adsorption of crystal violet dye. *Carbohydrate polymers*, 202, 444-453.

Sharma, K., Kaith, B. S., Kumar, V., Kalia, S., Kumar, V., & Swart, H. C. (2014). Water retention and dye adsorption behavior of Gg-cl-poly (acrylic acid-aniline) based conductive hydrogels. *Geoderma*, 232, 45-55.

Shi, J., Yu, L., & Ding, J. (2021). PEG-based thermosensitive and biodegradable hydrogels. *Acta biomaterialia*, *128*, 42-59.

Shi, J., Zhang, J., Zhang, Y., Zhang, L., Yang, Y. B., Manor, O., & You, J. (2022). Crystallinity dependence of PLLA hydrophilic modification during alkali hydrolysis. *Polymers*, *15*(1), 75.

Shi, Y., Chang, Q., Zhang, T., Song, G., Sun, Y., & Ding, G. (2022). A review on selective dye adsorption by different mechanisms. *Journal of Environmental Chemical Engineering*, 10(6), 108639.

Shin, M., Lim, J., Park, Y., Lee, J. Y., Yoon, J., & Choi, J. W. (2024). Carbon-based nanocomposites for biomedical applications. *RSC advances*, *14*(10), 7142-7156.

Singh, A., Kaith, B. S., Mehra, R., Sreejay, C. S., Lohan, B., & Bhatti, M. S. (2022). Synergistic effect of bio-inspired Psyllium/Okra hybrid backbone based hydrogel using RSM optimization for efficient removal of toxic malachite green dye and sequestration of uranium (VI) ions from water.

Śmigiel-Kamińska, D., Pośpiech, J., Makowska, J., Stepnowski, P., Wąs-Gubała, J., & Kumirska, J. (2019). The identification of polyester fibers dyed with disperse dyes for forensic purposes. *Molecules*, 24(3), 613.

Sofini, S. P., Balasubramanian, D., Girigoswami, A., & Girigoswami, K. (2024). Biomedical applications of natural and synthetic polymer based nanocomposites. *Journal of Biomaterials Science--Polymer Edition*, *35*(2).

Soleymani Eil Bakhtiari, S., Bakhsheshi-Rad, H. R., Karbasi, S., Razzaghi, M., Tavakoli, M., Ismail, A. F., ... & Berto, F. (2021). 3-dimensional printing of hydrogel-based nanocomposites: a comprehensive review on the technology description, properties, and applications. *Advanced Engineering Materials*, 23(10), 2100477.

Sukri, Siti Nur Amalina Mohamad, Kamyar Shameli, Magdelyn Mei-Theng Wong, Sin-Yeang Teow, Jactty Chew, and Nur Afini Ismail. "Cytotoxicity and antibacterial activities of plant-mediated synthesized zinc oxide (ZnO) nanoparticles using Punica granatum (pomegranate) fruit peels extract." *Journal of Molecular Structure* 1189 (2019): 57-65.

Terán, J. E., Millbern, Z., Shao, D., Sui, X., Liu, Y., Demmler, M., & Vinueza, N. R. (2021). Characterization of synthetic dyes for environmental and forensic assessments: A chromatography and mass spectrometry approach. *Journal of Separation Science*, 44(1), 387-402.

Thakur, B., Sharma, G., Kumar, A., Sharma, S., Naushad, M., Iqbal, J., & Stadler, F. J. (2020). Designing of bentonite based nanocomposite hydrogel for the adsorptive removal and controlled release of ampicillin. *Journal of Molecular Liquids*, 319, 114166.

Thakur, S., Chaudhary, J., Thakur, A., Gunduz, O., Alsanie, W. F., Makatsoris, C., & Thakur, V. K. (2022). Highly efficient poly (acrylic acid-co-aniline) grafted itaconic acid hydrogel: Application in water retention and adsorption of rhodamine B dye for a sustainable environment. *Chemosphere*, *303*, 134917.

Tipa, C., Cidade, M. T., Vieira, T., Silva, J. C., Soares, P. I. P., & Borges, J. P. (2020). A New Long-Term Composite Drug Delivery System Based on Thermo-Responsive Hydrogel and Nanoclay. *Nanomaterials* 2021, 11, 25.

Ullah, F., Othman, M. B. H., Javed, F., Ahmad, Z., & Akil, H. M. (2015). Classification, processing and application of hydrogels: A review. *Materials Science and Engineering: C*, 57, 414-433.

Upstone, S., & Seer Green, U. K. (2012). Validating UV/visible spectrophotometers. *PerkinElmer*.

Vakili, M. R., Mohammed-Saeid, W., Aljasser, A., Hopwood-Raja, J., Ahvazi, B., Hrynets, Y., ... & Lavasanifar, A. (2021). Development of mucoadhesive hydrogels

based on polyacrylic acid grafted cellulose nanocrystals for local cisplatin delivery. *Carbohydrate Polymers*, 255, 117332.

van Helmond, W., O'Brien, V., de Jong, R., van Esch, J., Oldenhof, S., & de Puit, M. (2019). Non-marking collection of amino acids from fingerprints using hydrogels. *Amino Acid Analysis: Methods and Protocols*, 429-438.

Varaprasad, K., Raghavendra, G. M., Jayaramudu, T., Yallapu, M. M., & Sadiku, R. (2017). A mini review on hydrogels classification and recent developments in miscellaneous applications. *Materials Science and Engineering: C*, 79, 958-971.

Virk, K., Sharma, K., Kapil, S., Kumar, V., Sharma, V., Pandey, S., & Kumar, V. (2022). Synthesis of gum acacia-silver nanoparticles based hydrogel composites and their comparative anti-bacterial activity. *Journal of Polymer Research*, 29(4), 118.

Wang, Z., Ye, Q., Yu, S., & Akhavan, B. (2023). Poly ethylene glycol (PEG)-based hydrogels for drug delivery in cancer therapy: a comprehensive review. *Advanced healthcare materials*, 12(18), 2300105.

Wichterle, O., & Lim, D. (1960). Hydrophilic gels for biological use. *Nature*, 185(4706), 117-118.

Wu, D., Xu, J., Chen, Y., Yi, M., & Wang, Q. (2018). Gum Arabic: A promising candidate for the construction of physical hydrogels exhibiting highly stretchable, self-healing and tensility reinforcing performances. *Carbohydrate polymers*, 181, 167-174.

Xiang, L., & Cui, W. (2021). Biomedical application of photo-crosslinked gelatin hydrogels. *Journal of Leather Science and Engineering*, *3*, 1-24.

Xiong, H., Zeng, Z., Du, J., & Zhao, L. (2023). Fabrication of 3-diethylaminopropylamine modified bamboo fiber prepared by radiation technique and its efficient and recycle adsorption for methyl orange. *Desalination and Water Treatment*, 316, 281-289.

Xue, H., Gao, X., Seliem, M. K., Mobarak, M., Dong, R., Wang, X., ... & Li, Z. (2023). Efficient adsorption of anionic azo dyes on porous heterostructured MXene/biomass

activated carbon composites: Experiments, characterization, and theoretical analysis via advanced statistical physics models. *Chemical Engineering Journal*, 451, 138735.

Yang, H. J., Lim, S., Lee, D. H., Yun, C. I., & Kim, Y. J. (2024). Validation and measurement uncertainty of analytical methods for various azo dye adulterants in Curcuma longa L. *Journal of Food Science*, 89(9), 5993-6004.

Yu, Y., Liu, Z., & Zhao, Q. (2023). Inorganic Ionic Oligomers Induced Organic-Inorganic Synergistic Toughening Enabling Mechanical Robust and Recyclable Nanocomposite Hydrogels. *Advanced Functional Materials*, 2213699.

Zhang, Y., Wei, H., Hua, B., Hu, C., & Zhang, W. (2024). Preparation and application of the thermo-/pH-/ion-sensitive semi-IPN hydrogel based on chitosan. *International Journal of Biological Macromolecules*, *258*, 128968.

Zhao, Y., Lo, C. Y., Ruan, L., Pi, C. H., Kim, C., Alsaid, Y., ... & He, X. (2021). Somatosensory actuator based on stretchable conductive photothermally responsive hydrogel. *Science Robotics*, 6(53), eabd5483.

APPENDICES

LIST OF ABBREVIATIONS

BM- Butea monosperma

PEG- Polyethylene glycol

AA- Acrylic acid

ZnO- Zinc oxide

BM-g-poly(AA)- Butea monosperma grafted poly(acrylic acid)

PEG-g-poly(AA)- Polyethylene glycol grafted poly(acrylic acid)

Ps- Percentage swelling

FTIR- Fourier transform infrared

XRD- X-Ray diffraction

FE-SEM- Field emission scanning electron microscopy

AR- Amaranth

MO- Methyl Orange

PHEMA- poly(2-hydroxyethyl methacrylate)

PAAm- poly(acrylamide)

PVA- poly(vinyl alcohol) (PVA)

PAA- poly(acrylic acid)

Ag- silver

Au- gold

TiO₂- titanium dioxide

GO- graphene oxide

CNTs- Carbon nanotubes

CNFs- cellulose nanofibers

CNCs- Cellulose nanocrystals

APS- ammonium persulfate

KPS- potassium persulfate

MBA- N,N'-methylenebisacrylamide

MB- methylene blue

LC-MS- liquid chromatography-mass spectroscopy

DNA- deoxyribose nucleic acid

HPLC- high performance liquid chromatography

UV-Vis- Ultra violet-Visible

MS- Mass Spectroscopy

TLC- Thin layer chromatography

TGA- Thermogravimetric analysis

dH₂O- Distilled water

KBr- Potassium bromide

Cu- Copper

OH- hydroxyl group

SO₄⁻ - sulfate ion radicals

COOH- carboxyl group

FeSO₄ - Ferrous sulfate

RESEARCH PUBLICATIONS AND CONFERENCES

RESEARCH PUBLICATIONS

1. TITLE: Polar moiety functionalized, controlled gelation to obtain highly efficient hydrogel nanocomposite: an expansion of green synthetic strategy

REFERENCE: Sandhu, A., Pandey, V., & Pandey, T. (2023). Polar moiety functionalized, controlled gelation to obtain highly efficient hydrogel nanocomposite: an expansion of green synthetic strategy. New Journal of Chemistry, 47(45), 20976-20986.

NJC



PAPER



Polar moiety functionalized, controlled gelation to obtain highly efficient hydrogel nanocomposite: an expansion of green synthetic strategy†

Anuradha Sandhu,^a Vivek Pandey^b and Tejasvi Pandey 100 ***

Hydrogels have attracted worldwide attention in the era of sustainable development, nanocomposite hydrogels have proven their efficient role as smart materials because of their stable behaviour and expanded surface area. These materials with high swelling ability and large volume-tosurface ratio can be used in retaining aqueous solvent or solvent systems for a long time with larger volume capability compared to other materials of similar size, weight and shape. This study aims to synthesize a hydrogel nanocomposite by utilizing Butea monosperma and ZnO nanoparticles via a green synthetic approach. Graft co-polymerisation was performed under microwave irradiation. The optimized BM-g-poly (AA) hydrogel and ZnO nanoparticles was a green studies, where they displayed 448% and 515% swelling properties, respectively. The polarity of the nanocomposite increased with the attachment of ZnO nanoparticles to the hydrogel, showing greater swelling properties. This controlled green synthetic route for hydrogel nanocomposite synthesis will be beneficial for researchers in the future to obtain smart materials for various applications,

Received 28th July 2023, Accepted 24th October 2023 DOI: 10.1039/d3nj03529h

rsc.li/njc

Introduction

The combination of nanotechnology with other fields of science has attracted increasing attention in recent decades. There have been numerous approaches to incorporate nano-scale methods with conventional methods toward manufacturing improved materials. Nanocomposite hydrogels are one example improved materials. Nanocomposite hydrogets are one example of such a combination of nanotechnology and biomaterial science. By adding various kinds of nanoparticles or nanostructures to the hydrogel network, nanocomposite hydrogels were created to improve the problems associated with the hydrogels. Hydrogel nanocomposites are hybrid materials that combine the unique properties of hydrogels and nanoparticles. Three-dimensional network structures, termed hydrogels are hydrogels and problems associated with the combine the unique properties of hydrogels and nanoparticles. gels, can absorb an immense amount of water. Owing to cross-links created either chemically or physically, and chain entan-glements, hydrogels often do not disintegrate.^{2,3} Nanoparticles are nanometer-scale particles that exhibit unique optical,

mechanical, and electronic properties that are not present in bulk materials.

Combining these two subject matters results in an advanced category of materials that exhibit enhanced properties compared to hydrogels or nanoparticles alone. Hydrogel nanocom-posites are designed to show specific responses to external stimuli, such as pH, or the concentration of specific chemicals and temperature.⁵ This responsiveness can be exploited in various domains, such as biosensing, tissue engineering, drug delivery, and waste-water treatment.⁶⁻⁹ The synthesis of hydrodelivery, and waste-water treatment. 6-9 The synthesis of hydrogel nanocomposites involves the incorporation of nanoparticles into the hydrogel matrix. The nanoparticles can be added during the synthesis process or physically mixed with the hydrogel after their formation. 10 Alternatively, templating methods can be used, in which the nanoparticles act as a template to create a porous hydrogel structure. This method can result in materials with an increased surface area, which is helpful in catalysis and other applications.

A flexible and extensively researched synthetic polymer called poly(actylic acid) (PAA) is well recognised for its outstanding qualities, which make it appropriate for grafting in hydrogels. Because of its distinctive properties, PAA, a watersoluble polymer comprising repeating acrylic acid monomer

soluble polymer comprising repeating acrylic acid monomer units, is a prime option for use in a wide range of hydrogel chemistry and biomaterial research applications. ^{11,12} A high level of hydrophilicity is present in poly(acrylic acid) owing to

20976 | New J. Chem., 2023, 47, 20976-20986 | This journal is © The Royal Society of Chemistry and the Centre National de la Recherche Scientifique 2023

^a Department of Forensk Science, School of Bioengineering and Biosciences, Lovely Professional University, Phagwara, 144411, India. E-mail: sejasvi2.5999@fpu.co.in
^b Department of Chemistry, School of Physical and Chemical Engineering, Lovely Professional University, Phagwara, 144411, India
† Electronic supplementary in formation (ESI) available. See DOI: https://doi.org/10.1039/d3nj03529h

2. TITLE: Hydrogels: From Design to Applications in Forensic Investigations.

REFERENCE: Sandhu, A., & Bhatia, T. (2023). Hydrogels: From Design to Applications in Forensic Investigations. *ChemistrySelect*, 8(8), e202204228.

Review doi.org/10.1002/slct.202204228

ChemistrySelect

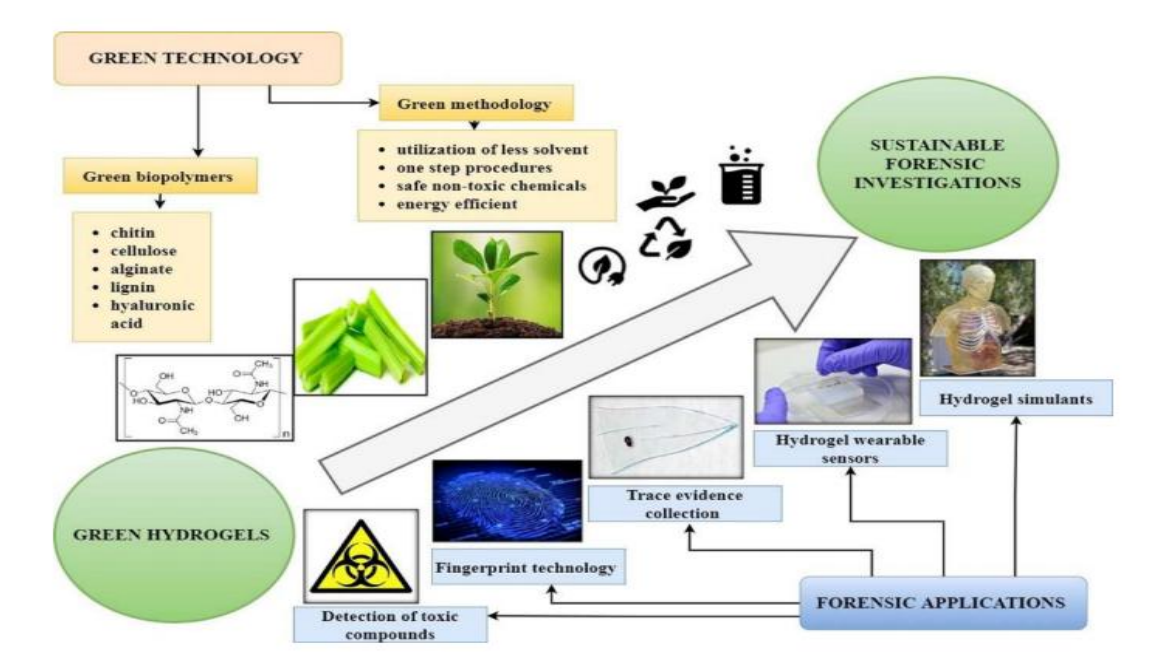
Review doi.org/10.1002/slct.202204228

ChemistrySelect

www.chemistryselect.org

Hydrogels: From Design to Applications in Forensic Investigations

Anuradha Sandhu and Tejasvi Bhatia*[a]



Chemistry Select 2023, e202204228 (1 of 16)

© 2023 Wiley-VCH GmbH

3. TITLE: Novel nanomaterials in forensic investigations: A review

REEFERENCE: Anuradha, & Bhatia, Tejasvi. (2021). Novel nanomaterials in investigations: review. **Materials Today:** Proceedings. forensic A 10.1016/j.matpr.2021.07.466.

Materials Today: Proceedings xxx (xxxx) xxx



Contents lists available at ScienceDirect

Materials Today: Proceedings

journal homepage: www.elsevier.com/locate/matpr



Novel nanomaterials in forensic investigations: A review

Anuradha, Tejasvi Bhatia*

Department of Forensic Science, School of Bioengineering and Biosciences, Lovely Professional University, Phagwara, Punjab 144001, India

ARTICLE INFO

Article history: Received 4 May 2021 Received in revised form 22 June 2021 Accepted 26 July 2021 Available online xxxx

Keywords: Material science Forensic investigations Functional polymers prensic polymers lanomaterials race evidence detection

ABSTRACT

A B S T R A C T

Material science has interdisciplinary nature that incorporates various fields of science and technology, it offers society innovative materials that are utilized to design further advanced devices. Novel nanomaterials are the new emerging polymers that can provide sustainable and functional solutions to the existing problems. Forensic investigations revolve around the identification and detection of evidence obtained at the crime scene. Advancements in material science offer a better understanding, design, identification, and detection of the polymers which is needed in forensics. Developing novel polymers and nanomaterials, accompanied by advanced instrumentation, has provided a sustainable approach to various forensic problems. The synthesis of nanomaterials like nanosensors, nano-codes, nano-films, nano-coatings, quantum dots, and composites has been augmented owing to their distinctive characteristics. It led to on-spot detection, fast analysis, and nano-scale level trace detection, which curtail the chances of error and save a detection from a proposition of time for analysis at the crime scene. This review is a culmination of the concept of novel nano polymers and nanomaterials provided by material science. It elucidates the various forensics areas that have been benefitted by employing innovative materials, functional polymers, and nanomaterials and hadditionally, current significant challenges and future perspectives related to the development of novel nano polymers and nanomaterials for crime prevention are discussed.

Copyright © 2021 Elsevier Ltd. All rights reserved.

Selection and peer-review under responsibility of the scientific committee of the 2nd International Conference on Functional Material, Manufacturing and Performances

Material science has emerged as a revolutionary field by developing various novel polymer materials, nanomaterials being a crucial part of them. New materials with advanced functions and properties have proven their applications to society from time to time [1]. Nanotechnology utilizes different biology, physics, and chemistry areas to synthesize, create, design, manipulate, and study the event or matter on a nanometre scale (1 nm- 100 nm). Many areas such as biomedical sciences, physical sciences, material sciences, and electronic engineering have utilized nanomaterials for different purposes [2,3]. Forensic studies generally utilize the finding, gathering, inspection, and analysis of the evidence obtained at the crime scene using specific techniques and methods. The evidence obtained at the crime scene can be either a natural The evidence obtained at the crime scene can be either a natural polymer (hair, DNA, protein, nail) or synthetic polymers (paint, fibers, minerals, plastics, tapes, etc.). The establishment of nanomaterials and nanotechnology in forensic science has enhanced the investigation process by making it more time-efficient, accu-

rate, selective, and sensitive [4]. Advanced nanomaterials and polyrate, selective, and sensitive [4]. Advanced nanomaterials and polymers are utilized in various instrumentation techniques that help analyze and detect the trace evidence or sample at a nano-scale level that was priorly unachievable. Latest nanomaterials provide novel solutions to collect and detect evidence like DNA from fingerprints, heavy metals, explosives, and gunshot residues (GSR) [5]. The synthesis of novel nanomaterials resulted in idiosyncratic mechanical, electric, optical, chemical, and magnetic properties. Nanomaticles carbon panotubes quantum dots supramolecules Nanoparticles, carbon nanotubes, quantum dots, supramolecules, Nanoparticles, carbon nanotubes, quantum dots, supramolecules, nanorods, and nanofibers are prominent examples of nanomaterials. Nano dimensions of these materials provide a high surface area which contributes to molecular interactions as there is high availability of active sites for the reaction [1,6–8]. Nanodevices have also gained significance owing to high selectivity and sensitivity. Nanochips, nano-bio sensors, and nanoprobes are highly used by researchers in different fields like metal detection, disease diagnosis, and hybridization assays [3].

The discoveries occurring due to material science have boosted the researcher's capabilities to link material based on its structure.

the researcher's capabilities to link material based on its structure with its functioning Nanomaterials are the trailblazing field in material science that proves their worth as sustainable and func-tional polymer. These are widely utilized in various fields, but this

https://doi.org/10.1016/j.matpr.2021.07.466
2214-7853/Copyright © 2021 Elsevier Ltd. All rights reserved.
Selection and peer-review under responsibility of the scientific committee of the 2nd International Conference on Functional Material, Manufacturing and Performances

Please cite this article as: Anuradha and T. Bhatia, Novel nanomaterials in forensic investigations: A review, Materials Today: Proceedings, https://doi.org/

^{*} Corresponding author. E-mail address: tejasvi.25999@lpu.co.in (T. Bhatia).

4. TITLE: Controlled polymerization in microfluidics: Advancement in nanogel synthesis

REFERENCE: Pandey, T., Sharma, A., Sandhu, A., & Pandey, V. (2024). Controlled polymerization in microfluidics: Advancement in nanogel synthesis. *SPE Polymers*, 5(2), 113-126.

Received: 27 November 2023

Revised: 11 December 2023

Accepted: 15 December 2023

DOI: 10.1002/pls2.10116

REVIEW ARTICLE





Controlled polymerization in microfluidics: Advancement in nanogel synthesis

Tejasvi Pandey | Aditi Sharma | Anuradha Sandhu | Vivek Pandey 0

Correspondence

Vivek Pandey, Department of Chemistry, School for Chemical Engineering and Physical Sciences, Lovely Professional University, Jalandhar, India. Email: vivekpandey11sep@gmail.com

Abstract

This comprehensive review provides a detailed examination of controlled polymerization in the development of nanogels-based microfluidic devices. Here, we have explored the integration of atom transfer radical polymerization (ATRP) and reversible addition-fragmentation chain transfer (RAFT) techniques within microfluidic platforms for the synthesis of nanogels. The synergistic combination of ATRP and RAFT with microfluidics has emerged as a powerful tool for precise control over polymerization reactions, enabling the fabrication of well-defined, multifunctional nanogels with tailored properties. The review begins with a thorough introduction to the principles of ATRP and RAFT, highlighting their respective advantages in controlled radical polymerization. Subsequently, it elucidates the principles of microfluidics and its profound impact on polymerization processes. The merging of these techniques enables precise control over reaction kinetics, monomer conversions, and molecular weight distributions, facilitating the synthesis of nanogels with unprecedented precision and reproducibility. Furthermore, this review delves into the chemical mechanisms

¹Department of Forensic Sciences, School for Bioengineering and Biosciences Sciences, Lovely Professional University, Jalandhar, India

²Department of Chemistry, School for Chemical Engineering and Physical Sciences, Lovely Professional University, Jalandhar, India

5. TITLE: Recent advances in applications of sonication and microwave.

REFERENCE: Pandey, T., Sandhu, A., Sharma, A., & Ansari, M. J. (2023). Recent advances in applications of sonication and microwave. *Ultrasound and Microwave for Food Processing*, 441-470.



CONFERENCES

- 1. Poster presentation in International Conference on Recent Advances in Fundamental and Applied Sciences (RAFAS-2021), L.P.U, Phagwara, India.
- 2. Paper presentation in 2nd International conference on Functional materials, manufacturing and performances (ICFMMP-2021), L.PU. Phagwara, India
- 3. Paper presentation in International Conference on Materials science and spectroscopy, Maharishi university of information technology Lucknow, Uttar Pradesh, India.
- 4. Paper presentation in 25th All India Forensic Science Conference, N.F.S.U, Gandhinagar, Gujarat, India.
- 5. Paper presentation in 15th IASR International conference on Forensic Science, International association of scientists and researchers, Delhi, India
- 6. Participation in 5th International Conference on Recent Advances in Fundamental and Applied Sciences (RAFAS-2024), L.P.U, Phagwara, India.



Poster presentation in International Conference on Recent Advances in Fundamental and Applied Sciences (RAFAS-2021), L.P.U, Phagwara, India.

[Under the Aegis of Lovely P	Professional University, Jalandhar-Delhi	G.T. Road, Phagwara (Punjab)]
		Certificate No. 233383
Cei	rtificate of Presenta	ntion
This is to certify that Dr./Mr./Ms	Anuradha novel nanomaterials in forensic investi	has Authored/Presented
AND PARTY OF A CANADAST AND	on Functional Materials, Manufacturing a	
held on 17th to 18th September 2021	organized by School of Mechanical Engine	eering at Lovely Professional University,
Punjab.		
Date of Issue: 01-10-2021 Place of Issue: Phagwara (India)		
	Jen	VXSV
	K 342.	

Paper presentation in 2nd International conference on Functional materials, manufacturing and performances (ICFMMP-2021), L.PU. Phagwara, India



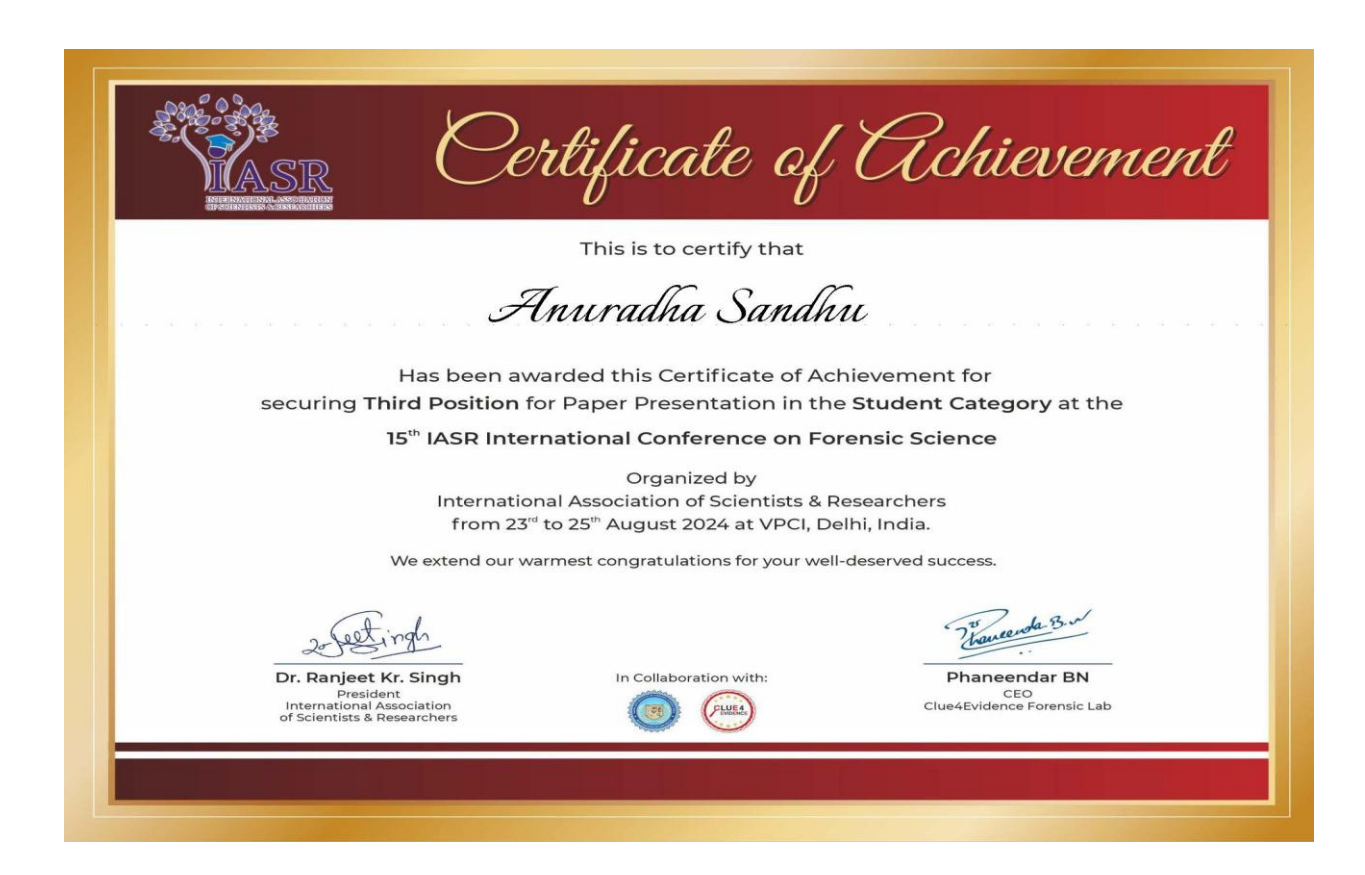
Oral presentation in International Conference on Materials science and spectroscopy, Maharishi university of information technology Lucknow, Uttar Pradesh, India.



Paper presentation in 25th All India Forensic Science Conference, N.F.S.U, Gandhinagar, Gujarat, India.



Participation in 5th International Conference on Recent Advances in Fundamental and Applied Sciences (RAFAS-2024), L.P.U, Phagwara, India.





Paper presentation in 15th IASR International conference on Forensic Science, International association of scientists and researchers, Delhi, India

WORKSHOPS

- 1. National workshop on Research methodology and Data analysis using SPSS, L.P.U, Phagwara, India.
- 2. Short term course on Emerging trends and modelling in advanced functional materials and devices, N.I.T, Jalandhar, Punjab.
- 3. 3 day- National Workshop on X-ray Diffraction and Particle size analyzer, L.P.U, Phagwara, India.

HUMAN RESOURCE DEVELOPMENT CENTER

[Under the Aegis of Lovely Professional University, Jalandhar-Delhi G.T Road, Phagwara (Punjab)]

Certificate No. 220574

Certificate of Participation

This is to certify that Ms. Anuradha D/o Sh. Ramanjit participated in National Workshop on Research Methodology and Data Analysis using SPSS organized by Lovely Professional University w.e.f. April 26, 2021 to May 1, 2021 (6 days) and obtained "A" Grade.

Date of Issue : 01-05-2021 Place : Phagwara (Punjab), India

Prepared by (Administrative Officer-Records)

Checked By Program Coordinator

Head Human Resource Development Center

National workshop on Research methodology and Data analysis using SPSS, L.P.U, Phagwara, India.



Short term course on Emerging trends and modelling in advanced functional materials and devices, N.I.T, Jalandhar, Punjab



3 day- National Workshop on X-ray Diffraction and Particle size analyzer, L.P.U, Phagwara, India.